# REEXAMINATION OF GAIN THEORY FOR PHOTOCONDUCTIVE DEVICES

by

Nenad Vrucinic

A dissertation submitted to the faculty of
The University of North Carolina at Charlotte
in partial fulfillment of the requirements
for the degree of Doctor of Philosophy in
Optical Science and Engineering

Charlotte

2024

Approved by:

_____
Dr. Yong Zhang

_____
Dr. Glenn Boreman

_____
Dr. Abasifreke Ebong

_____
Dr. Yasin Raja

# ABSTRACT

NENAD VRUCINIC. Reexamination of gain theory for photoconductive devices.
(Under the direction of DR. YONG ZHANG)

Photoconductive detectors are semiconductor optoelectronic devices that absorb optical energy and convert it to electrical signal. However, photoconductive gain or quantum efficiency ($QE$) theory of photodetector exhibits considerable controversy in optoelectronics literature. Gain is generally defined as the ratio of the number of photogenerated charge carriers collected by the electrodes and the number of photons absorbed in the semiconducting photoconductor. This gain is often expressed as the ratio of the carrier's lifetime over the carrier's transit time, where the lifetime is the average time before an electron recombines with a hole, and the transit time is the time needed for photogenerated carriers to travel from one electrode to another under an applied voltage. This simple theory implies that it is possible to obtain high gain by reducing the transit time.

In this dissertation, the gain theory of photoconductive detector with an intrinsic (undoped) semiconductor is reexamined by assuming primary photoconductivity. In contrast to the widely adopted gain formula as a ratio of the carrier lifetime to transit time, allowing for a value much greater than unity, it is shown that this ratio can only be used as $QE$ under the low-drift limit, but has been inappropriately generalized in the literature. The analytic results for photocarrier density, photocurrent, and $QE$ in terms of normalized drift and diffusion lengths are obtained, which indicates that $QE$ is limited to unity for arbitrary drift and diffusion parameters. A distinction between the two $QE$ definitions used in the literature, but not explicitly distinguished, is discussed. The accumulative quantum

efficiency ($QE_{acc}$) includes the contributions of the flow of all photocarriers, regardless of whether they reach the electrodes, whilst the apparent quantum efficiency ($QE_{app}$) is based on the photocurrent at the electrodes. In general, $QE_{acc} > QE_{app}$; however, they approach the same unity limit for the strong drift. Furthermore, it is shown that the photocurrent in the photoconductive channel is in general spatially nonuniform and that the presence of diffusion tends to reduce the photocurrent. As one form of secondary photoconductivity, it is confirmed that doping in a photoconductive device can yield a gain, limited by the ratio of the mobilities of majority and minority carriers. Based on the simulation results, new analytic results that show good agreement with simulated results are proposed.

This work lays the ground for understanding mechanisms of experimentally observed, above-unity photoconductivity gains. Moreover, these findings should offer new insights into photoconductivity and semiconductor device physics and may potentially lead to novel applications.

# DEDICATION

I dedicate this dissertation to father Nikola, mother Gordana, sister Dragana, grandfather Sava, late grandmothers Savka and Leposava, uncles Dragan and Aleksandar, aunts Ana and Slavica and their families.

# ACKNOWLEDGEMENTS

I would like to express sincere gratitude to my advisor, Dr. Yong Zhang, for his guidance and incredible patience during my work on this dissertation. Finishing this dissertation would certainly not be possible without his support and help. I want to thank my committee member, Dr. Glenn Boreman, for his understanding and great support during this journey, as well as to other committee members, Dr. Abasifreke Ebong and Dr. Yasin Raja. Administrative help from Mrs. Renee Johnson and retired Mr. Mark Clayton is appreciated.

I would also like to express my gratitude to people from Rochester Institute of Technology for their help while I was student there: Dr. Drew Maywar and Dr. Nenad Nenadic, as well as to people from Center for Imaging Science: Dr. John Kerekes, Dr. Charles Bachmann, Dr. David Messinger, Dr. Zoran Ninkov, and Mrs. Elizabeth Lockwood. Additionally, I want to thank people from my previous schools for their impact on my education: Dr. Goran Poparic and late Dr. Ivan Anicin from Faculty of Physics at University of Belgrade, Dr. Zeljen Trpovski and Dr. Vladimir Vujicic from Faculty of Technical Sciences at University of Novi Sad, as well as to my high school physics teacher Mr. Vladimir Kovac. I want to extend my thanks to friends from the Optical Science and Engineering program at UNC Charlotte: Dr. Arash Shiri, Dr. Ana Hiza Ramirez-Andrade, Dr. Rui Qi and Trailokya, as well as to Dr. Zhang's group members: Dr. Antardipan Pal, Wanseok, Austin, Hasan, Javad and Ismatul. Last, but not least, I want to thank my family for their endless support during the work on this dissertation.

This work was supported by UNC Charlotte's Graduate School and GASP, teaching assistantships and tuition funding provided by Department of Physics and Optical

Science, research assistantships and Bissell Distinguished Professor Tuition Award provided by Dr. Zhang and U.S. Department of Defense (DOD) grant W911NF-23-1-0215.

TABLE OF CONTENTS

LIST OF FIGURES ix

LIST OF ABBREVIATIONS xiii

CHAPTER 1: INTRODUCTION 1

1.1. Types of electrical contacts 1

1.2. Photoconductivity of insulating crystals 9

CHAPTER 2: REVIEW OF THE EXISTING PHOTOCONDUCTIVE GAIN THEORY 13

2.1. Derivation of photoconductive gain formula 13

2.2. Quantum efficiency of drifting charge carriers–analytic results 17

CHAPTER 3: A NEW PHOTOCONDUCTIVE GAIN THEORY 27

3.1. Assumptions and key findings 27

3.2. Quantum efficiency of drift-diffusion charge carriers–analytic results 29

CHAPTER 4: QUANTUM EFFICIENCY OF DRIFT-DIFFUSION CHARGE CARRIERS – NUMERICAL RESULTS 45

CHAPTER 5: QUANTUM EFFICIENCY OF DRIFT-DIFFUSION CHARGE CARRIERS – SIMULATION RESULTS 54

CHAPTER 6: QUANTUM EFFICIENCY OF DOPED PHOTOCONDUCTIVE DEVICE – SIMULATION RESULTS 62

CHAPTER 7: CONCLUSIONS 69

7.1. Summary 69

7.2. Further work 71

REFERENCES 74

# LIST OF FIGURES

Figure 1: Energy level diagrams for neutral contact between metal electrode and semiconductor in MSM system: (a) $q\phi_{m1} = q\phi_{m2} = q\phi$; (b) $q\phi_{m1} < q\phi < q\phi_{m2}$ 3

Figure 2: An intrinsic blocking MS system before contact (left) and after contact (right): (a) an electron blocking contact; (b) a hole blocking contact 5

Figure 3: An intrinsic Ohmic MS system: (a) before contact; (b) after contact; and (c) after contact with bias 5

Figure 4: A doped MS system, without and with a bias: (a) *n*-type injecting Ohmic or *p*-type blocking contact; (b) *n*-type blocking or *p*-type injecting Ohmic contact 7

Figure 5: An experimental setup for the measurement of the primary photocurrent 9

Figure 6: Schematic representation of charge carriers for a primary photocurrent: (a) at low electric field (left); (b) at high electric field (right) 12

Figure 7: Spatial distribution of photogenerated electrons (dashed lines) and holes (solid lines) for $V = 0.1\ V, 0.5\ V, 1.0\ V, 2.0\ V$: (a) $\mu = 10\ cm^2V^{-1}s^{-1}$; (b) $\mu = 100\ cm^2V^{-1}s^{-1}$ 23

Figure 8: $QE_{acc}$ (solid lines) and $QE_{app}$ (dashed lines) vs. applied voltage on logarithmic scale for: (a) different mobilities; (b) different lifetimes; and (c) different channel lengths. The green lines represent the maximum quantum efficiency $QE_{max} = 1$. 26

Figure 9: Normalized spatial distributions of photogenerated holes for different combinations of diffusion and drift parameters, $l_{di} = (0, 0.1, 0.2, 0.4, 0.6)$: (a) $l_{dr} = 0.1$; (b) $l_{dr} = 0.5$; (c) $l_{dr} = 1.0$; and (d) $l_{dr} = 5.0$ 34

Figure 10: Normalized spatial dependencies of hole photocurrent densities for different combinations of diffusion and drift parameters, $l_{di} = (0, 0.1, 0.2, 0.4, 0.6)$: (a) $l_{dr} = 0.1$; (b) $l_{dr} = 0.5$; (c) $l_{dr} = 1.0$; and (d) $l_{dr} = 5.0$ 37

Figure 11: (a) Quantum efficiencies $QE_{acc}$ (solid lines) and $QE_{app}$ (dashed lines)

vs. normalized drift length $l_{dr}$ for $l_{di} = (0, 0.2, 0.4, 0.6)$; (b) $QE_{acc}$ (solid lines) with low $l_{dr}$ approximation (dashed lines); and (c) $QE_{app}$ (solid lines) with low $l_{dr}$ approximation (dashed lines). The green line represents the maximum quantum efficiency $QE_{max} = 1$. 39

Figure 12: The total normalized photocurrent density $j(\xi)$, electron component $j_n(\xi)$ and hole component $j_p(\xi)$ vs. normalized distance $\xi$, compared to the average photocurrent density $j_{avg}$ for three different $(l_{dr}, l_{di})$ combinations: (a) low field: $(l_{dr}, l_{di}) = (0.2, 0.2)$; (b) medium field: $(l_{dr}, l_{di}) = (1.0, 0.2)$; and (c) high field: $(l_{dr}, l_{di}) = (5.0, 0.2)$ 41

Figure 13: (a) Normalized electron concentration $\delta n(\xi)$ vs. normalized distance $\xi$ for different $(l_{dr}, l_{di})$ combinations; (b) Normalized hole concentration $\delta p(\xi)$ vs. normalized distance $\xi$ for different $(l_{dr}, l_{di})$ combinations; and (c) Normalized photocurrent density $j(\xi)$ vs. normalized distance $\xi$ for different $(l_{dr}, l_{di})$ combinations 49

Figure 14: (a) Normalized photocurrent density $j(\xi)$ vs. normalized distance $\xi$ for different normalized Debye lengths $l_D = (0.1, 0.2, 0.3, 0.4)$ and for $(l_{dr}, l_{di}) = (0.2, 0.1)$; (b) $QE_{acc}$ vs. normalized Debye length $l_D$ for $(l_{dr}, l_{di}) = (0.2, 0.1)$; and (c) $QE_{app}$ vs. normalized Debye length $l_D$ for $(l_{dr}, l_{di}) = (0.2, 0.1)$ 51

Figure 15: The total normalized photocurrent density $j(\xi)$, electron component $j_n(\xi)$ and hole component $j_p(\xi)$ vs. normalized distance $\xi$, compared to the average photocurrent density $j_{avg}$ for two different $(l_{dr}, l_{di})$ combinations: (a) low field $(0.2, 0.2)$; and (b) medium field $(1.0, 0.2)$. Dashed lines represent $j(\xi)$ for $k = 0$, whilst the solid lines represent $j(\xi)$ for $k = 1$ after 10 iterations. 52

Figure 16: Comparison of spatial distributions of photogenerated carriers $\Delta n(x)$ and $\Delta p(x)$, respectively, for two applied voltages, 0.1 V and 1.0 V: (a) and (b) for $(\mu_n, \mu_p) = (1, 1)\ cm^2V^{-1}s^{-1}$; (c) and (d) for $(\mu_n, \mu_p) = (10, 10)\ cm^2V^{-1}s^{-1}$ 55

Figure 17: Photocurrent density $J$ vs. applied voltage $V$ for comparison of the simulated results $J_{sim}$ (black curves) and analytic results: $J_{acc}$ (red curves)

and $J_{app}$ (blue curves), for different combinations of mobility parameters $(\mu_n, \mu_p)$: (a) $(1,1)\ cm^2V^{-1}s^{-1}$; (b) $(10,10)\ cm^2V^{-1}s^{-1}$; and (c) $J_{sim}$ for $(1,1)\ cm^2V^{-1}s^{-1}$, $(10,1)\ cm^2V^{-1}s^{-1}$, and $(10,10)\ cm^2V^{-1}s^{-1}$, respectively. The green lines represent the maximum photocurrent density $J_{max} = qgL = 4.8\ mAcm^{-2}$. 56

Figure 18: Spatial variations of the photocurrent density $J(x)$ for mobility parameters $(\mu_n, \mu_p) = (10,10)\ cm^2V^{-1}s^{-1}$ and different voltages: (a) 0.1 V; (b) 1.0 V and 2.0 V. Spatial variations of the photocurrent densities $J(x)$ (blue curves), $J_{dr}(x)$ (black curves), $J_{di}(x)$ (red curves), for mobility parameters $(\mu_n, \mu_p) = (10,10)\ cm^2V^{-1}s^{-1}$ and for different voltages: (c) 0.1 V; (d) 1.0 V. Solid lines represent simulated results, dashed lines represent analytic results, whilst the green lines represent the maximum photocurrent density $J_{max} = qgL = 4.8\ mAcm^{-2}$. 59

Figure 19: Spatial distributions of photogenerated minority (electron) carrier concentrations $\Delta n(x)$ under *p*-type doping concentration of $10^{17}cm^{-3}$, for different levels of applied voltages $0.1\ V, 0.5\ V, 1.0\ V, 2.0\ V$ and for different combinations of mobility parameters: (a) $(\mu_n, \mu_p) = (337,875)\ cm^2V^{-1}s^{-1}$; (b) $(\mu_n, \mu_p) = (875,875)\ cm^2V^{-1}s^{-1}$; (c) $(\mu_n, \mu_p) = (1700,875)\ cm^2V^{-1}s^{-1}$; and (d) $(\mu_n, \mu_p) = (2700,875)\ cm^2V^{-1}s^{-1}$. Simulated results of minority carriers (electrons) are represented by solid lines, simulated results of majority carriers (holes) are represented by yellow dashed lines, whilst analytic results are represented by dash-dotted lines. 63

Figure 20: Photocurrent density $J_{ph}$ vs. applied voltage $V$ for $\mu_n > \mu_p$ (black curve), $\mu_n = \mu_p$ (red curve), and $\mu_n < \mu_p$ (blue and magenta curves) for *p*-type doping concentration of $10^{17}cm^{-3}$. The green line represents the maximum photocurrent density $J_{max} = qgL = 8\ Acm^{-2}$ for $\mu_n = \mu_p$. 65

Figure 21: Photocurrent density $J_{acc}$ vs. applied voltage $V$ curves under *p*-type doping concentration of $10^{17}cm^{-3}$ for comparison of the simulated results $J_{sim}$ (black curves) and analytic results: $J_{acc}$ (red curves) and

$J_{app}$ (blue curves), for different combinations of mobility parameters $(\mu_n, \mu_p)$: (a) $\mu_n > \mu_p$; (b) $\mu_n = \mu_p$; (c) and (d) $\mu_n < \mu_p$. The green lines represent the maximum photocurrent densities $J_{max} = qgL$ for different combinations of mobility parameters $(\mu_n, \mu_p)$. 67

Figure 22: Analytic photocurrent densities $J_{acc}$ and $J_{app}$, and three simulated photocurrent densities $J_{sim}$ under *n*-type of doping for different levels of *n*-type doping concentrations $10^{15}cm^{-3}$ (red curves), $10^{16}cm^{-3}$ (magenta curves), and $10^{17}cm^{-3}$ (cyan curves) vs. applied voltage $V$: (a) $\mu_n < \mu_p$; (b) $\mu_n = \mu_p$; (c) and (d) $\mu_n > \mu_p$. The green lines represent the maximum photocurrent densities $J_{max} = qgL$ for different combinations of mobility parameters $(\mu_n, \mu_p)$. 68

# LIST OF ABBREVIATIONS

| | |
|---|---|
| BC | boundary condition |
| G | gain |
| MS | metal-semiconductor |
| MSM | metal-semiconductor-metal |
| QE | quantum efficiency |
| QEacc | accumulative quantum efficiency |
| QEapp | apparent quantum efficiency |
| SCLC | space-charge-limited current |
| SRH | Shockley-Read-Hall |

# CHAPTER 1: INTRODUCTION

## 1.1. Types of electrical contacts

A photoconductive device is a special type of photodetector that consists of a metal-semiconductor-metal (MSM) structure [1-5]. To make measurements of the electrical conductivity or the photoconductivity in a semiconductor or an insulator, it is necessary to make electrical contact to the material, which is usually done with metallic contacts. Here, two identical metallic electrodes at MSM systems are assumed for the metallic contact. The most common types of contacts between the metal and semiconductor are blocking (rectifying or Schottky) contacts, neutral or flat-band contacts, and injecting Ohmic contacts [1, 6-9]. One of the properties of Ohmic contacts is the ability to replenish carriers to maintain charge neutrality in the material, if carriers are drawn out of the opposite contact by an electric field [7]. The blocking contacts are non-injecting and thus, they are unable to replenish carriers created by photoexcitation when they are drawn out of the material by an applied electric field. A neutral contact is defined as one in which the carrier concentration at the contact is equal to that in the bulk of the semiconductor and they can replenish carriers created by photoexcitation when they are drawn out of the material by an applied electric field. Electrical neutrality condition further implies that there is no space charge and no band bending within the semiconductor. In this case the conduction and the valence band edges will be flat right up to the interface and thus, this type of contact is sometimes referred to as the flat band. Therefore, regions adjacent to the contact on both sides are electrically neutral. There are three possibilities in forming neutral contacts [7, 8]. In the first case, the metal and the semiconductor are brought together into contact as shown in Fig. 1(a), where the work function of metal $q\phi_m$ and the work function of semiconductor $q\phi_s$ are the same, i.e., $q\phi_{m1} = q\phi_{m2} = q\phi_{ms}$, and $q$ is unit charge of electrons. The work function of metal is defined as the energy

difference between the vacuum energy level $E_{vac}$ and Fermi energy level $E_F$ in the material, i.e. $q\phi_m = E_{vac} - E_F$ , whilst the work function of semiconductor is defined by $q\phi_s = \chi + (E_C - E_F)$, where $E_C$ denotes conduction band energy level and $\chi$ represents the electron affinity of semiconductor defined as the energy required for an electron to be removed from the bottom edge of the conduction band at the surface to a point in the vacuum just outside the material. The probability that the electrons will flow from the metal to the semiconductor is equal to the probability that the electrons will flow in the reverse direction. Therefore, there is no net flow, and no space charge formed near the interface. Apparently, after the contacts have been made, the differences between metal work functions and electron affinity will be equal, i.e., $q\phi_{b1} = q\phi_{b2}$, whilst $q\phi_{b1} = q\phi_{m1} - \chi$ and $q\phi_{b2} = q\phi_{m2} - \chi$. In another case, the contact can be neutral because the trapped space charge is too small to cause significant band bending [10]. The condition which needs to be fulfilled is $q\phi_m \neq q\phi_s$ ($q\phi_m > q\phi_s$ or $q\phi_m < q\phi_s$), at low temperatures or with an electron trapping level at a distance sufficiently above $E_F$ (or the hole trapping level below $E_F$) [8]. The case when the work functions of electrode 1, electrode 2, and the semiconductor are related as $q\phi_{m1} < q\phi_s < q\phi_{m2}$ is shown in Fig. 1(b), where the potential difference (contact potential) across the semiconductor is given as $V_{12} = q(\phi_{m2} - q\phi_1)$ and represents the difference in the work functions of the two materials when they are brought into the intimate contact. After the contacts have been made, differences between metal work functions and electron affinity are not equal, i.e., $q\phi_{b1} < q\phi_{b2}$, since $q\phi_{m1} < q\phi_{m2}$.

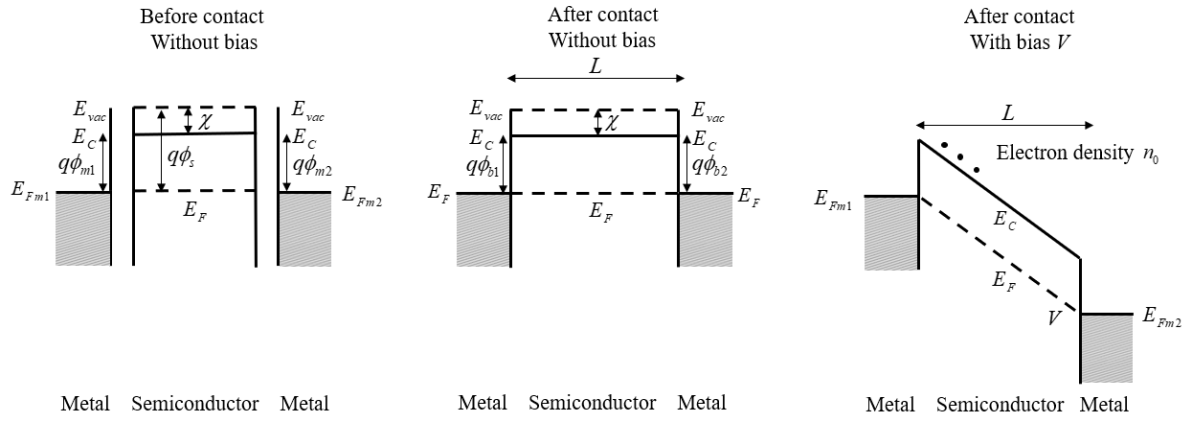


(a)

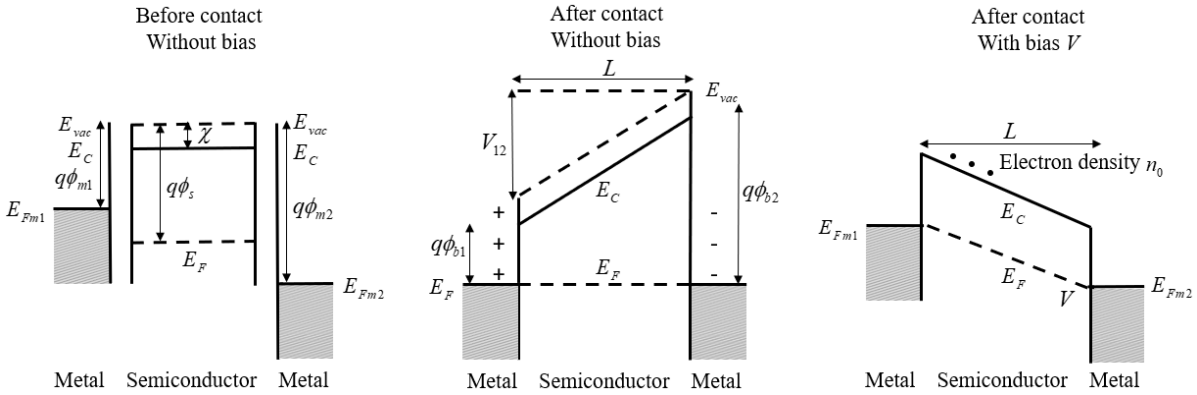


(b)

Figure 1: Energy level diagrams for neutral contact between metal electrode and semiconductor in MSM system: (a) $q\phi_{m1} = q\phi_{m2} = q\phi$; (b) $q\phi_{m1} < q\phi < q\phi_{m2}$ [8]

Semiconductors can be distinguished as intrinsic (undoped) vs. extrinsic (doped), where extrinsic semiconductors are doped by impurity atoms, for the purpose of modulating their electrical or optical properties. There are two types of doped semiconductors: *n*-type, where electrons are majority carriers, and *p*-type, where holes are majority carriers [2, 7, 8]. In the case of an *n*-type semiconductor, material is doped with atoms that can donate electrons, which increases its conductivity. Conversely, in the case of a *p*-type semiconductor, material is doped with atoms that can accept electrons, but which increases conductivity as well. In the case of doped

materials, the carrier concentrations obey the relationship $np = n_i^2$, where $n_i$ is the intrinsic carrier concentration, and $n$ and $p$ are electron and hole carrier concentrations, respectively, whilst in case of intrinsic materials $n = p = n_i$.

In the case of rectifying contacts, electrons can flow from the semiconductor to the metal under forward bias. However, the electrons available over the Schottky barrier can limit the flow of electrons from the metal under reverse bias. Fig. 2 shows energy level diagrams before and after contact, for an electron and hole blocking contact respectively, in a metal-semiconductor (MS) system. For an intrinsic MS, the condition for an electron blocking contact is $q\phi_m > q\phi_s$, as shown in Fig. 2(a). Conversely, the condition for a hole blocking contact, seen by electrons from semiconductor side or by holes from metal side, is $q\phi_s > q\phi_m$, as shown in Fig. 2(b). When carriers created by photoexcitation are drawn out of the material by an applied electric field, a blocking contact is unable to replenish carriers. In this case the photocurrent varies linearly with an applied electric field and become saturated at high electric fields. This type of photocurrent, called the primary photocurrent, was found in early experiments [7, 11-15]. When the photoconductor is illuminated, one absorbed photon can create at most one electron-hole pair and thus, the maximum gain is limited to unity in the context of primary photocurrent [1, 2, 14]. On the other hand, Ohmic contacts promote linear, Ohmic photocurrent at low voltages through the device [6, 16-18]. Furthermore, with Ohmic contacts at the electrodes, the space-charge can be injected and volume-distributed or spatially localized near the potential minimum at the contact [6]. This is the reason why Ohmic contacts are also called injecting contacts. Similarly, Figs. 3(a)-(c) shows the energy level diagrams for an Ohmic contact between metal and intrinsic semiconductor.

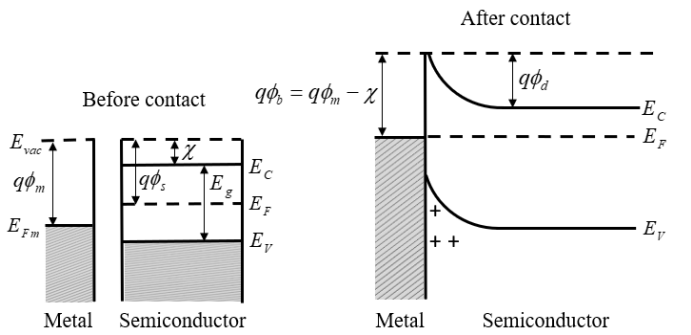


(a)

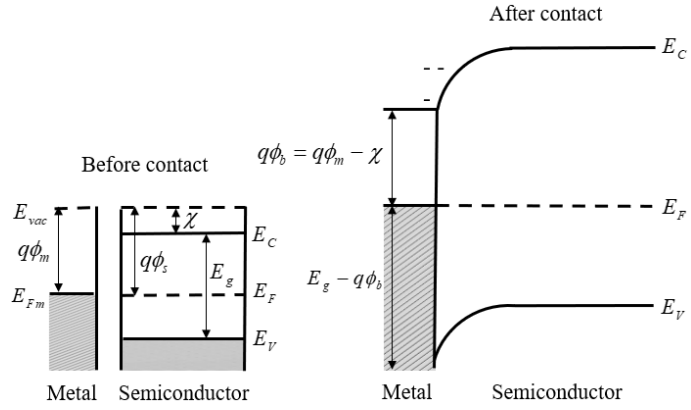


(b)

Figure 2: An intrinsic blocking MS system before contact (left) and after contact (right): (a) an electron blocking contact; (b) a hole blocking contact [8]

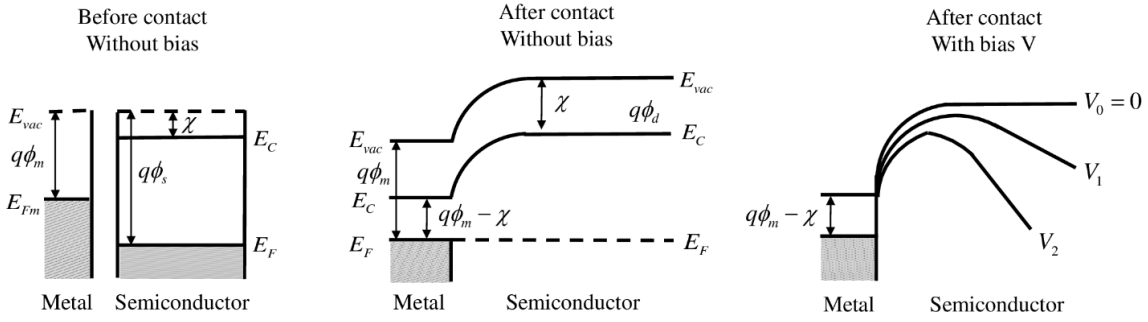


(a) (b) (c)

Figure 3: An intrinsic Ohmic MS system: (a) before contact; (b) after contact; and (c) after contact with bias [8]

A distinction between blocking contact and injecting Ohmic contact can be made under condition that effects of surface states are neglected and based on the relative magnitude of the metal work function $q\phi_m$ and the semiconductor work functions $q\phi_s$. In Fig. 4(a) on the left, it is shown the *n*-type of an Ohmic injecting contact (or *p*-type blocking contact) without an applied electric field. On the right side of the same figure, it is shown the *n*-type of an Ohmic injecting contact (or *p*-type blocking contact) with an applied electric field, where $q\phi_d$, which represents a diffusion potential, is the difference between $q\phi_s$ and $q\phi_m$, i.e., $q\phi_d = q\phi_s - q\phi_m$ and $q\phi_m < q\phi_s$. Here, in the downward-bending region, there is a reservoir of free electrons available for injection into the bulk of the insulator at the contact. If an applied electric field is high enough, this reservoir can deliver an excess electron current, known as space-charge-limited current (SCLC), into the conduction band. Furthermore, there is a potential minimum or energy maximum in the insulator under an applied voltage and near the contact interface, shown as position $P$. Therefore, if carriers created by photoexcitation are drawn out of the material by an electric field, an Ohmic injecting contacts have ability to replenish carriers to maintain charge neutrality in the material. In this case the contacts contribute negligible electrical resistance, and the photocurrent flow is controlled by the resistance of the bulk semiconductor.

A typical blocking contact to an *n*-type semiconductor (or *p*-type injecting Ohmic contact) without an applied electric field is shown in Fig. 4(b) on the left, and with an applied electric field in figure on the right, where $q\phi_d = q\phi_m - q\phi_s$ and $q\phi_m > q\phi_s$. While moving from the metal to the semiconductor, the electron faces barrier height $V_b$, which is larger than $q\phi_d$ by the amount $E_C - E_F$, i.e., $V_b = q\phi_d + (E_C - E_F)$, and can be also written by using an electron affinity $\chi$ as $V_b = q\phi_m - \chi$.

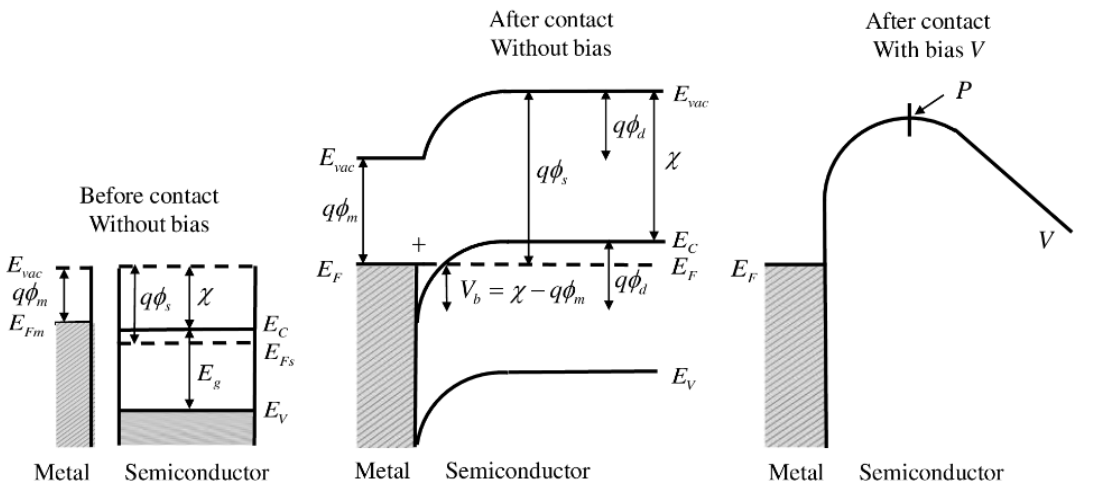


(a)

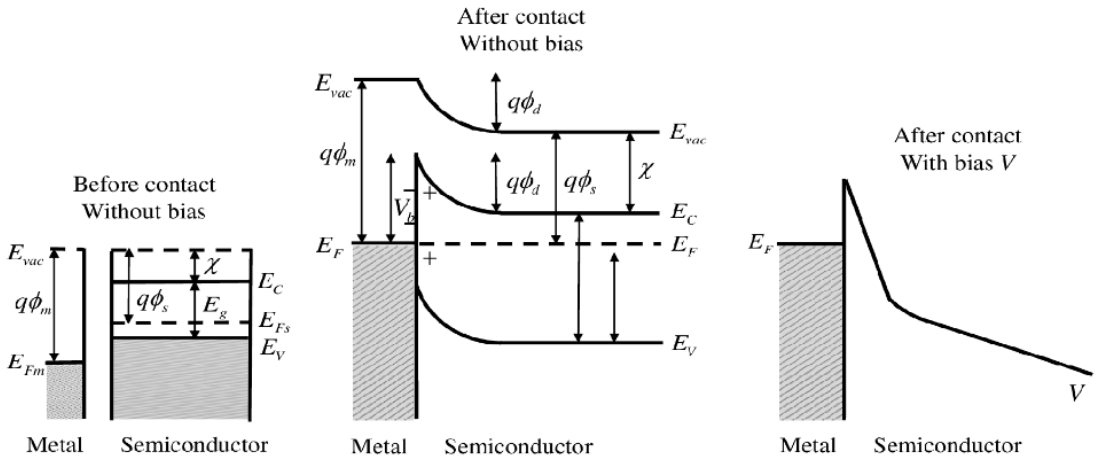


(b)

Figure 4: A doped MS system, without and with a bias: (a) *n*-type injecting Ohmic or *p*-type blocking contact; (b) *n*-type blocking or *p*-type injecting Ohmic contact [7, 8]

If the semiconductor is *n*-type injecting Ohmic contact, as shown in Fig. 4(a), then electrons are transferred from the semiconductor to the metal upon contact and $V_b = \chi - q\phi_m$, which leaves a depletion layer in the semiconductor. The condition for blocking contact, seen by holes from the metal side or by electrons from the opposite side is $q\phi_m < q\phi_s$, for a metal *p*-type semiconductor

junction. Thus, this kind of contact blocks the hole emission from the metal. On the other hand, the *n*-type of an Ohmic injecting contact will be formed if electrons transferred from the metal to the semiconductor upon contact produce an accumulation layer in the semiconductor, i.e., $q\phi_m < q\phi_s$. For the *p*-type of an Ohmic injection contact, the relationship is reversed, i.e., $q\phi_m > q\phi_s$.

Under photoexcitation of the semiconductor, the injecting Ohmic contact may be converted into a neutral contact or even a blocking contact. Likewise, the neutral contact may be converted into a blocking contact. If an electric field $E$ is applied between two electrodes, the first electrode (cathode) can supply a maximum electron density $n_0$ through a thermionic emission process to maintain the current flow in the insulator. The current density $J$ recorded at the second electrode (anode) is then given by $J = qn_0\mu E$, which is well-known Ohm's law, and it depends linearly on electric field $E$, where $q$ is the unit charge and $\mu$ carrier mobility. The contact can be considered as an Ohmic if the next three conditions are met: 1) for a given applied voltage $V$, the electric field $E$ is constant throughout the insulator, i.e., there is no band bending; 2) the current density $J$ should be small enough to avoid the change of mobility $\mu$ with an electric field $E$ through the effect of Joule heating, so the electron mobility $\mu$ is independent of electric field $E$; and 3) the current density drawn through the insulator is less than the saturated thermionic emission current density from the cathode. The current density $J$ is proportional to the electric field $E$, until it becomes equal to the saturated thermionic emission current density. With the further increasing of an electric field, the thermionic emission current density is no longer capable of replacing the electrons drawn out at the anode. Under such conditions, the contact ceases to be an Ohmic and tends to become a blocking, whilst the conduction becomes electrode limited. In the case of an Ohmic injecting contacts and at low applied electric field, the photocurrent varies linearly with the field, whereas under high applied electric field, the charge carriers injected from a contact produce a net space

charge in the solid. This net space charge produces the secondary photocurrent, earlier introduced as SCLC, which has nonlinear variation with the applied field [1, 2, 6-8, 16-19]. Therefore, a distinction between blocking and neutral contacts vs. injecting Ohmic contacts regarding the type of the produced photocurrent and regarding the photoconductive gain is very important. With blocking or neutral contacts, provided there is no impact ionization, the maximum photoconductive gain is limited to unity since there is no replenishment of carriers at the electrodes. However, with the injecting Ohmic contacts between metal and semiconductor (insulator), there is possibility of the carrier replenishment at the electrodes, which allows for high photoconductive gain due to the electrically injected carriers from contacts.

## 1.2. Photoconductivity of insulating crystals

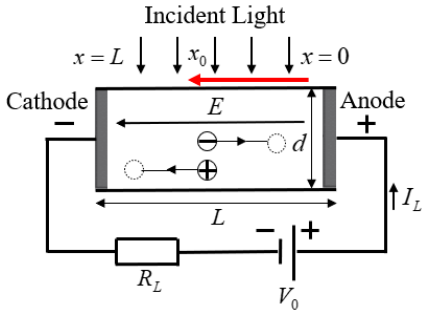


Figure 5: An experimental setup for the measurement of the primary photocurrent in the insulating crystals

The photoconductivity of insulating crystals is well-described in classical textbooks [1, 2]. Here, it is assumed that the insulating crystal is mounted between two electrodes (cathode and anode) and illuminated in a small slice or throughout its volume, as shown in Fig. 5, where $R_L$ is load resistance required to convert the photocurrent $I_L$ into an output voltage under bias voltage $V_0$, $E$ is the applied electric field, $d$ is the thickness, and $L$ is distance between electrodes. When an insulating crystal is placed between metal electrodes, there is no current flow in dark because

the conduction levels are empty. Also, electrons in the cathode do not have sufficient energy to pass into the conduction band of the insulator. However, if an insulating crystal or its part is illuminated with the light of suitable wavelength, electrons are raised to the conduction band and can move toward the anode. At the same time, the holes may be mobile and drawn towards the cathode. The motion of photogenerated electrons and holes constitutes the primary photoelectric current, which is a direct photoelectric current. When the primary photocurrent is flowing, electrons are not able to enter the crystal from the cathode, unless they can neutralize holes drawn by the electric field. In early work, Gudden and Pohl studied photoconductivity processes and the nature of the charge carriers in crystals [11-13]. Also, they examined how photoconductivity depended on the applied electric field, the light intensity and wavelength, and time. They specified four characteristics of the primary photocurrent: (1) the photocurrent $I_{ph}$ is described as

$$I_{ph} = I - I_{dark} = \frac{Fq(X_+ + X_-)}{L}, \quad (1)$$

where $I$ is the total current, $I_{dark}$ is dark current of thermally generated carriers, $F$ is the rate at which free carriers (electrons and holes) are being generated by light, $X_+$ is the distance in the direction of the electric field traveled by the freed positive carrier before it is trapped, $X_-$ is the distance in the direction opposite to the electric field traveled by the freed negative carrier before it is trapped, and $L$ is the distance between electrodes with which the electric field is applied; (2) the photocurrent is proportional to the light intensity; (3) the photocurrent is proportional to the applied electric field at the small electric field values and saturates with increasing the applied electric field to high values; and (4) the rise of the photocurrent at the beginning of excitation and the decay of the photocurrent when the excitation is removed is both essentially instantaneous. The behavior of the primary photocurrents was found in different kinds of materials, such as mercuric sulfide, zinc sulfide, diamond, and to a lesser extent in antimony sulfide, sulfur, and red selenium.

In the investigated materials, it has been found that the primary photocurrent could be separated into two portions: (1) a normal photocurrent produced under illumination due to the motion of the charge carriers under the applied electric field; and (2) the photocurrent in the reverse direction produced under illumination when the external electric field is removed, and the crystal is electrically short-circuited. The ratio of the number of charges passing between electrodes to the number of absorbed photons for a given time interval is called the quantum efficiency $(QE)$ or the gain $(G)$. Eq. (1) shows that the number of electronic charges passing between the electrodes for each photon absorbed is at most unity, since the maximum value of $X_+ + X_-$ is equal to the distance between electrodes $L$. If either the positive or the negative carrier freed by light is trapped and immobilized in the crystal before it reaches the electrode, the gain could be even less than unity. At a low applied electric field both carriers have been trapped in real crystals before they have reached electrodes. The traveling distance of carriers before being trapped is increased linearly with an applied electric field. Therefore, the photocurrent is proportional to the electric field at low electric fields, as shown in Fig. 6(a), and the photoconductive gain has been much less than unity. When the electric field is increased, more mobile carriers arrive at the electrode before being trapped and the photocurrent starts to saturate with the applied field. When the electric field is high enough to draw both carriers out of the crystal before they have been trapped, the photocurrent saturates at the constant value, as shown in Fig. 6(b), and the photoconductive gain approaches to unity, which is the maximum value. It should be noted that the present discussion is applicable when the contacts on electrodes are blocking. It means that holes or electrons cannot be injected from electrodes to maintain charge neutrality within the crystal, thus, the holes cannot enter the crystal from the positive electrode when the holes excited by light pass out into the negative electrode, and the electrons cannot enter the crystal from the negative electrode when the

electrons excited by light have passed out into the positive electrode. On the other hand, if the contacts between metal and insulator or semiconductor are injecting (Ohmic), an injection of carriers from the electrodes is possible and the gains much greater than unity may be obtained. Since at low applied electric fields excited carriers could be possibly trapped by crystal imperfections before they reach the electrodes, and if the saturation of the photocurrent with an applied electric field occurs at lower field, then the crystal could be considered as "more perfect".

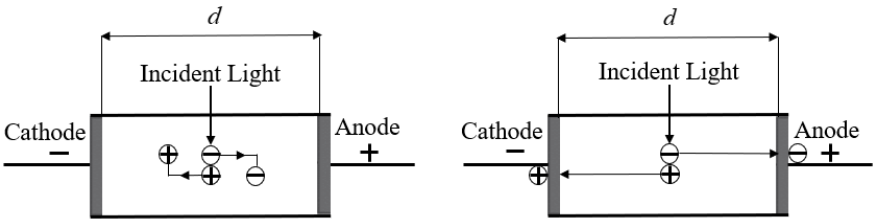


Figure 6: Schematic representation of charge carriers for a primary photocurrent: (a) low electric field (left); (b) high electric field (right) [2]

# CHAPTER 2: REVIEW OF THE EXISTING PHOTOCONDUCTIVE GAIN THEORY

## 2.1. Derivation of photoconductive gain formula

The photoconductive gain of a photodetector based on a semiconductor has been observed for over 150 years in a wide variety of materials [2, 20-24]. However, the photoconductive gain theory still exhibits considerable controversy and ambiguity in the literature. The gain $G$ is commonly expressed as the ratio of the carrier recombination lifetime $\tau_c$ to the carrier transit time $\tau_t$ over the conductive channel [2, 21-28]

$$G = \frac{\tau_c}{\tau_t}. \quad (2)$$

This simplistic equation implies that $G$ can be obtained by increasing $\tau_c$ and/or decreasing $\tau_t$. Since its initial appearance [25], Eq. (2) has been widely used to explain the observed gains: due to a long recombination lifetime [22, 26, 27], a short transit time by having a high carrier mobility [26] or by increasing applied voltage [29], or by shortening channel length of the device [21, 22, 26, 29]. Additionally, carrier trapping within the photoconductive channel (e.g., on the surface), thought to increase $\tau_c$, is often used as the mechanism for the high gain [22]. According to the existing photoconductive gain theory [23, 24, 26, 27], the photogenerated carriers may circulate multiple times throughout the circuit before they recombine, and based on this, they can generate a larger photocurrent and consequently photoconductive gain. This theory is also known as "recycling gain mechanism", since it only leads to increased number of the collected carriers, while the concentration of the excess carriers does not increase [5]. The problem with the existing theory is that it assumes spatially uniform distribution of photogenerated carriers and their independence on the electric field [2, 7].

To find an expression for a traditional definition of the photoconductive gain of the photoconductor $G$ given by Eq. (2), it is necessary to start from a definition of *QE*, which is the

ratio of the number of photogenerated charge carriers collected by the electrodes $N_c$ and the number of photons absorbed in the semiconducting photoconductor $N_{ph}$ [22]

$$G = \frac{N_c}{N_{ph}}. \quad (3)$$

In general, when the carrier diffusion is neglected, the total current density $J$ is determined only by its drift component and can be expressed as

$$J = qE(\mu_n n + \mu_p p) \quad (4)$$

where $\mu_n$ and $\mu_p$ are mobilities of electrons and holes, whilst $n$ and $p$ are the total electron and hole concentrations, respectively. When the photoconductor is uniformly illuminated, the total electron and hole concentrations can be written as $n = n_0 + \Delta n$ and $p = p_0 + \Delta p$, where $n_0$ and $p_0$ are concentrations of the thermally generated electron and hole concentrations, whilst $\Delta n$ and $\Delta p$ are the photogenerated electron and hole concentrations, respectively. If optical carrier concentrations due to illumination of the photoconductor are much larger than the thermally generated carrier concentrations, i.e., $\Delta n \gg n_0$ and $\Delta p \gg p_0$, it is justified to neglect a dark background carrier concentrations and currents at room temperature, which is typically a usual assumption in literature [2, 7, 30]. The photocurrent density, $J_{ph}$ can be written as

$$J_{ph} = \frac{I_{ph}}{A} = J - J_{dark} = qE(\mu_n \Delta n + \mu_p \Delta p), \quad (5)$$

where $A$ is the cross-sectional area of the photoconductive device, and $J_{dark} = qE(\mu_n n_0 + \mu_p p_0)$ is the dark current density. In general, the photogenerated concentrations of electrons and holes are considered to be given by $\Delta n = g\tau_n$ and $\Delta p = g\tau_p$, where $\tau_n$ and $\tau_p$ are recombination lifetime of electrons and holes, respectively, and $g$ is the generation rate of electron-hole pairs or the number of absorbed photons per unit volume per second [2, 7]. This is valid under the assumption of the small photocurrent which does not affect the carrier lifetime. The maximum

photocurrent density is defined as $J_{max} = qgL$, and, thus, gain can be also written as ratio of $J_{ph}$ and $J_{max}$

$$G = \frac{J_{ph}}{J_{max}} = \frac{qE(\mu_n \Delta n + \mu_p \Delta p)}{qgL} = \frac{E(\mu_n \tau_n + \mu_p \tau_p)}{L} = \frac{V(\mu_n \tau_n + \mu_p \tau_p)}{L^2}, \quad (6)$$

where $V = EL$ is the applied voltage. The transit times of electrons and holes can be further expressed as $\tau_{t,n} = L^2 \mu_n^{-1} V^{-1}$ and $\tau_{t,p} = L^2 \mu_p^{-1} V^{-1}$, respectively, and by substituting them into Eq. (6), the total photoconductive gain can be expressed as

$$G = \frac{\tau_n}{\tau_{t,n}} + \frac{\tau_p}{\tau_{t,p}}. \quad (7)$$

Eq. (7) considers both types of carriers and is generally adopted as a definition of photoconductive gain in the literature [2, 26, 27].

However, this formula is obtained under two problematic assumptions: (1) all carriers, no matter where they are generated (i.e., at any location relative to the electrodes), contribute equally to the photocurrent; (2) the carrier distribution under an applied voltage remains uniform as in the zero-bias, when the detector is uniformly illuminated. The first assumption would be valid if the current of one carrier type alone could close the circuit without loss (e.g., electrons exiting the anode could all return to the conduction band through the cathode). However, this assumption is inconsistent with the primary photoconductivity, where in a steady state an electron and a hole are needed together to close the circuit, which implicitly assumes that a conduction band electron exiting from the anode can only return to the photoconductor through the cathode to the valence band, i.e., no carrier recycling within the same band. In this case, since electrons generated at a distance away from the collection electrode (i.e., anode) will decay in number while drifting toward the electrode, those generated at different distances from the electrode will contribute differently to the photocurrent. Specifically, for the carriers that either can or cannot reach the electrode, their contributions to the photocurrent are given by the ratio of their travel lengths

toward the collecting electrode to the channel length of the device [1, 14, 31]. The second assumption is invalid when more realistic boundary conditions (BCs), such as a vanishing BC, are applied to the semiconductor-metal contacts or electrodes in solving the drift-diffusion equation. For instance, the vanishing BCs correspond to the Ohmic injecting contacts of *n*-type or *p*-type doped semiconductors [3, 5, 32], as given in Fig. 4 and described in Ch. 1.1.

There were a lot of attempts to explain the photoconductive gain theory in the literature, as well as to offer analytic solutions for the high photoconductive gain. The various interpretations have been adopted [5, 22, 33-37], however, they often fall back to the general consideration of Eq. (2), by seeking to prolong the carrier lifetime $\tau_c$. For instance, Dan et al. [5] modeled photoconductive high photoconductive gain as the ratio of majority photogenerated carriers (holes) and minority photogenerated carriers (electrons), where electrons are localized by trapping effect of defects, surface states, and surface depletion region. Soci et al. [22] pointed out that the extremely high photoconductive gain is attributed to the presence of oxygen-related hole-trap states at the NW surface, which prevents charge-carrier recombination and prolongs the photocarrier lifetime. Matsuo et al. [33] proposed a model which includes spatial separation of photogenerated electron-hole pairs and their recombination at the surface. Papaionau [34] concluded that photoconductive gain depends on the photocarrier injection mechanisms from the surface and the substrate. Zardas et al. [35] claimed that the minority carrier lifetime is longer because of the separation of electron-hole pairs by the depletion region near the semiconductor surfaces. Konstantanos et al. [36] simply replaced the short minority carrier lifetime with the long trap lifetime to explain the phenomena. Grunwald and Schreck [37] derived analytical solutions for the gain as a function of impurity concentration, crystal thickness, and excitation density.

## 2.2. Quantum efficiency of drifting charge carriers–analytic results

In the literature, two subtly different $QE$ definitions are used, but without being explicitly distinguished. One definition, here referred to as an accumulative quantum efficiency ($QE_{acc}$), assumes uniform absorption of light across the photoconductive device and includes all photocurrents that ever flow in the device, regardless of whether they reach the electrodes, as used in some literature [1, 3, 14, 31, 38, 39]. The other definition, here referred to as an apparent quantum efficiency ($QE_{app}$), corresponds to all the light being absorbed at the anode or cathode and evaluates the photocurrent collected at the anode or cathode. The latter is perhaps the one typically or often implicitly adopted in literature [5, 14, 15, 39]. However, these two definitions are not equivalent in general, which has not been recognized in literature, at least not explicitly. The necessity to distinguish them lies in that when the photogenerated carrier density distributions are nonuniform, the total photocurrent in the photoconductive channel, equal to the sum of the electron and hole currents, can be nonuniform as well. The spatial nonuniformity of photocurrent contradicts with the common wisdom that the current should be constant throughout a circuit.

Another form of $QE$, different than from Eq. (2) and based on accumulated charges that have ever travelled in the channel, including those that do not actually reach the electrode, can be found in [1, 14, 39]. Hecht [14] found that when a slice of the crystal is illuminated, as shown in Fig. 5, electrons released by a flash of the light were drawn by an applied electric field from the cathode into an unilluminated portion. One might expect that irrespective of the voltage all electrons would eventually reach the anode, as if they were in a vacuum tube. However, photocurrents did not behave in this way in any type of crystal, because of inevitable inter-band recombination. At low applied electric fields, the photocurrent was not independent on the voltage, instead, it was always roughly proportional to it. In every case, after drifting a certain distance, the

photogenerated electrons could get stuck in the crystal. Two types of electrons were considered under a weak electric field applied to the crystal. The first type of electrons was trapped at points lying towards the cathode from the point where they were released due to the diffusion, whilst the second type of electrons were trapped at points lying towards the anode from the point where they were released due to the drift and diffusion. An effect observed on the galvanometer has shown that in any field the number of the latter was greater than the number of the former. A deflection of the galvanometer has had the same value as it would have if all the photoelectrons would drift down the field a certain small drifting distance $L_{dr,n}$, called "Schubweg", or mean travel range of the photoelectrons in this field [1, 14, 15, 39]. If electrons released by the light traveled a certain distance before being trapped or before they reached the anode, the first thing which should have been considered is the charge that has passed through the circuit as illustrated in Fig. 5. If an electron traveled only a distance $x$, the charge measured by the electrometer or by the galvanometer was given as $Q = qxL^{-1}$. Clearly, the total measured charge would have been equal to the elementary electronic charge for an electron travelled right across the crystal. It was supposed that the crystal was illuminated in a section at a distance $x_0$ from the anode as shown in Fig. 5. For a weak electric fields, the mean distance $x$ travelled by the electron was equal to $L_{dr,n}$, and the measured photocurrent was proportional to the electric field $E$. However, when $L_{dr,n}$ became comparable with the distance $x_0$, it was expected that the measured photocurrent would show a saturation value. The maximum charge obtained during a given illumination by increasing the applied field indefinitely was given as $Q_{max} = nqx_0L^{-1}$, where $n$ is the number of the released electrons. If the crystal was illuminated uniformly between the two electrodes, then the maximum obtained charge was given as $Q_{max} = nq/2$. If electrons and positive holes have moved freely, then in either case the maximum obtained charge was doubled, i.e., $Q_{max} = nq$. To find a

theoretical expression for the mean drifting range $L_{dr,n}$, it was assumed that an electron remains in the free state for a time $\tau$ before it has been captured, where $\tau$ was independent on the electric field $E$ [1, 14]. Then, the range $L_{dr,n}$ was given as $L_{dr,n} = E\mu_n\tau_n$, where $\mu_n$ is the mobility or drift velocity in unit field of an electron in the free state in the crystal, and $\tau_n$ is a lifetime of an electron. Apparently, the mean drifting range of electron $L_{dr,n}$ was proportional to the applied electric field $E$. If an electron was in the free state, it was assumed that the probability per time $dt$ that it was captured was equal to $dt/\tau$. If $n_0$ electrons were freed at a given instant of time, after a time $t$ a number of electrons equal to $n = n_0 exp(-t/\tau)$ has remained. As earlier, it was assumed that $n_0$ electrons have been released at a distance $x_0$ from the anode. There were $n = n_0 exp(-x/L_{dr,n})$ electrons left after travelling a distance $x$ in the direction of the electric field. The number which has ended their path in the range $dx$ was equal to $-(dn/dx)dx = (n_0/L_{dr,n})exp(-x/L_{dr,n})dx$. The total distance drifted by particles was made up of two terms: a distance drifted by particles which did not reach the anode, and a distance drifted by particles which reached the anode. A distance drifted by particles which did not reach the anode was $\int_0^{x_0} x(dn/dx)dx = (n_0/L_{dr,n}) \int_0^{x_0} x\, exp(-x/L_{dr,n})dx$ , which was further reduced to $n_0\{L_{dr,n}[1 - exp(-x_0/L_{dr,n})] - x_0 exp(-x_0/L_{dr,n})\}$. The distance drifted by $n_0 exp(-x_0/L_{dr,n})$ particles which reached the anode was equal to $n_0 x_0 exp(-x_0/L_{dr,n})$. By summing up these two terms and diving it by $n_0$, the mean distance drifted by an electron was expressed as $\bar{x} = L_{dr,n}[1 - exp(-x_0/L_{dr,n})]$. For the whole channel length of the crystal $L$, the collection efficiency of electrons $QE_{acc,n}$, determined as the ratio of the released charge $n_0 q$ and the charge passing through the galvanometer $(qn_0\bar{x})/L$, was written as $QE_{acc,n} = (L_{dr,n}/L)[1 - exp(-x_0/L_{dr,n})]$. The average collection efficiency of electrons for the uniformly illuminated crystal $\overline{\eta_n}$ was

obtained by averaging over all $x_0$ from 0 to $L$. Similarly, the equivalent expression can be found for holes. In that case, the mean drifting range $L_{dr,p}$ could be expressed as $L_{dr,p} = E\mu_p\tau_p$, where $\mu_p$ is the mobility of holes in the free state in the crystal and $\tau_p$ is the lifetime of holes. Thus, it can be written

$$QE_{acc,n} = \frac{L_{dr,n}}{L}\left\{1 - \frac{L_{dr,n}}{L}\left[1 - \exp\left(-\frac{L}{L_{dr,n}}\right)\right]\right\}, \quad (8a)$$

$$QE_{acc,p} = \frac{L_{dr,p}}{L}\left\{1 - \frac{L_{dr,p}}{L}\left[1 - \exp\left(-\frac{L}{L_{dr,p}}\right)\right]\right\}. \quad (8b)$$

Therefore, the total average quantum collection efficiency of drifting particles can be written as a sum of the average collection efficiency of both type of carriers

$$QE_{acc} = \frac{L_{dr,n}}{L}\left\{1 - \frac{L_{dr,n}}{L}\left[1 - \exp\left(-\frac{L}{L_{dr,n}}\right)\right]\right\} + \frac{L_{dr,p}}{L}\left\{1 - \frac{L_{dr,p}}{L}\left[1 - \exp\left(-\frac{L}{L_{dr,p}}\right)\right]\right\}. \quad (8c)$$

Only in the limiting case of $L_{dr,n} \ll L$, one finds $QE_{acc,n} \approx L_{dr,n}/L = \tau_c/\tau_t$. On the other hand, when $L_{dr,n} \gg L$, one has $QE_{acc,n} \to ½$. Therefore, if only the primary conductivity is considered, Eq. (2) is an inappropriately generalized low conductivity limit result of Eq. (8a) and the total $QE_{acc}$ is limited to unity. If both types of carriers have the same mobility and lifetime, or a mobility-lifetime product, they contribute equally to the total $QE_{acc}$. This result is appropriate for the primary photoconductivity, defined as that induced by the photogenerated carriers within the photodetector, without the participation of either externally injected or internally preexisted carriers and without the recycling effect [1, 2, 11-14]. In early literature, blocking electrodes were used to suppress recycling and disallow replenishment of carriers on electrodes [11-15]. To achieve the same effect and improve performance in modern day optoelectronic devices (e.g., photodetectors, solar cells, and light-emitting devices), an additional layer is typically inserted between the electrode and active layer to block selectively either the electron or the hole current in one electrode [40-42].

To find an expression for the nonuniform photogenerated concentration of carriers, it is necessary to solve the continuity equation for electrons and holes. By neglecting diffusion, one can express the continuity equations and the photocurrent density equations for electrons and holes, respectively, as

$$\frac{\partial(\Delta n(x))}{\partial t} = g - \frac{\Delta n(x)}{\tau_n} + \frac{1}{q}\frac{\partial J_n(x)}{\partial x} = 0, \tag{9a}$$

$$\frac{\partial(\Delta p(x))}{\partial t} = g - \frac{\Delta p(x)}{\tau_p} - \frac{1}{q}\frac{\partial J_p(x)}{\partial x} = 0, \tag{9b}$$

where $J_n(x) = J_{dr,n}(x) = qE\mu_n\Delta n(x)$ and $J_p(x) = J_{dr,p}(x) = qE\mu_p\Delta p(x)$ are the photocurrent densities of electrons and holes, respectively. Under the steady state, and by neglecting the effect of diffusion, the continuity equations for electrons and holes can be further written respectively as

$$g\tau_n - \Delta n(x) + L_{dr,n}\frac{\partial(\Delta n(x))}{\partial x} + \mu_n\tau_n\Delta n(x)\frac{\partial E(x)}{\partial x} = 0, \tag{10a}$$

$$g\tau_p - \Delta p(x) - L_{dr,p}\frac{\partial(\Delta p(x))}{\partial x} - \mu_p\tau_p\Delta p(x)\frac{\partial E(x)}{\partial x} = 0. \tag{10b}$$

Due to the absence of space-charge effects, the electric field is considered constant, which eliminates the $\partial E(x)/\partial x$ term in Eqs. (10). Furthermore, under an assumption that $\Delta n(x)$ and $\Delta p(x)$ have spatially uniform distributions, i.e., $\partial(\Delta n(x))/\partial x = 0$ and $\partial(\Delta p(x))/\partial x = 0$, these concentrations could be determined solely by $\Delta n(x) = g\tau_n$ and $\Delta p(x) = g\tau_p$, which incorrectly leads to "recycling gain mechanism" [5].

Depending on the assumption of the nature of the MS contacts, different BCs have been used in literature. For instance, when diffusion is neglected, and by assuming a blocking contact for the hole current at the anode, BC given as $\Delta p(x = 0) = 0$ is used to ensure that the hole current is zero at the anode, i.e., $J_p(x = 0) = 0$ [15]. Similarly, for electrons at the cathode, one has $\Delta n(x = L) = 0$ and $J_n(x = L) = 0$. In this case, even under uniform illumination, the continuity condition for the photocurrent yields a nonuniform carrier distribution.

Despite Eqs. (10) can be solved independently when $\partial E/\partial x = 0$, it should be noted that if the mobility-lifetime products of electrons and holes are different, i.e., $\mu_n\tau_n \neq \mu_p\tau_p$ , photocurrents at the anode (mostly the electron current) and the cathode (mostly the hole current) will be different, which would disrupt the basic requirement of the current continuity in the external circuit. Moreover, solutions for the carrier densities would not satisfy the overall charge neutrality within the photoconductive channel. Since the focus is to determine the limiting value of the gain, another assumption of equal mobility-lifetime product of electrons and holes, i.e., $\mu_n\tau_n = \mu_p\tau_p$ is adopted. Although the mobility-lifetime product is different in the most materials, $\mu_n\tau_n = \mu_p\tau_p$ is not an unphysical assumption. Additionally, when $\partial E/\partial x = 0$ and the vanishing BCs are used, it is the only case that can have meaningful analytic solutions for both electrons and holes. Furthermore, since $\mu_n\tau_n \neq \mu_p\tau_p$ tends to reduce the gain through the polarization effect, this additional constrain does not affect the conclusion regarding the maximum gain value.

The solutions of Eq. (10), for an excess concentration of electrons and holes respectively, could be written as

$$\Delta n(x) = g\tau_n\left[1 - exp\left(-\frac{L-x}{L_{dr,n}}\right)\right], \tag{11a}$$

$$\Delta p(x) = g\tau_p\left[1 - exp\left(-\frac{x}{L_{dr,p}}\right)\right]. \tag{11b}$$

The plots of spatial distributions of photogenerated carrier concentrations $\Delta c(x)$ are shown in Fig. 7 for four different applied voltages $V = \ 0.1\,V, 0.5\,V, 1.0\,V, 2.0\,V$ and two different mobilities $\mu = 10\ cm^2V^{-1}s^{-1}, 100\ cm^2V^{-1}s^{-1}$. Carrier distributions given by Eqs. (11) can be further used to calculate the photocurrent by averaging (integrating) the carrier density over the channel length [15]

$$J_{acc,n} = \frac{qE\mu_n}{L}\int_0^L \Delta n(x)dx = qgL_{dr,n}\left\{1 - \frac{L_{dr,n}}{L}\left[1 - exp\left(-\frac{L}{L_{dr,n}}\right)\right]\right\}, \tag{12a}$$

$$J_{acc,p} = \frac{qE\mu_p}{L}\int_0^L \Delta p(x)dx = qgL_{dr,p}\left\{1 - \frac{L_{dr,p}}{L}\left[1 - exp\left(-\frac{L}{L_{dr,p}}\right)\right]\right\}, \quad (12b)$$

whilst the total drift photocurrent can be expressed as sum of both, electron and holes photocurrents

$$J_{acc} = qg\left\{L_{dr,n}\left\{1 - \frac{L_{dr,n}}{L}\left[1 - exp\left(-\frac{L}{L_{dr,n}}\right)\right]\right\} + L_{dr,p}\left\{1 - \frac{L_{dr,p}}{L}\left[1 - exp\left(-\frac{L}{L_{dr,p}}\right)\right]\right\}\right\}. \quad (12c)$$

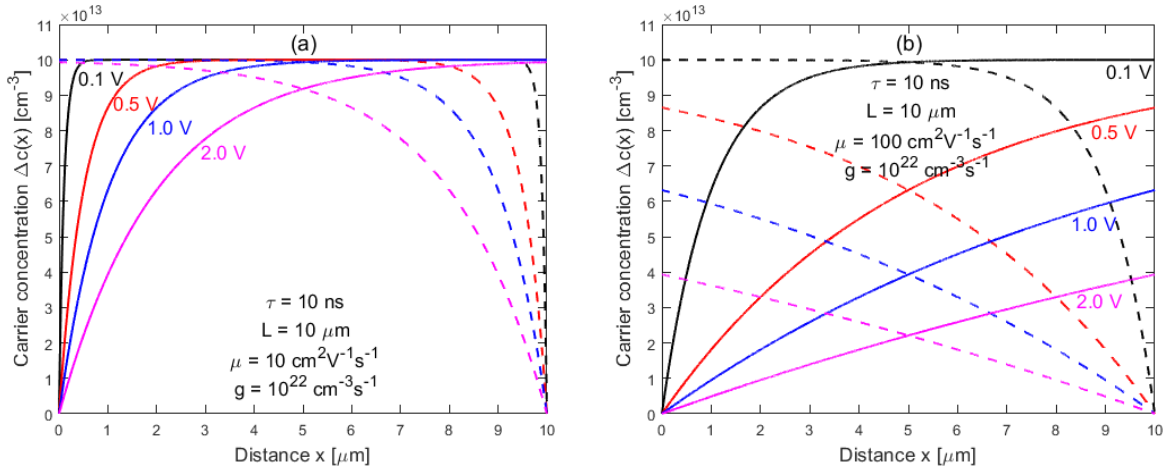


Figure 7: Spatial distribution of photogenerated electrons (dashed lines) and holes (solid lines) for $V = (0.1\ V, 0.5\ V, 1.0\ V, 2.0\ V)$: (a) $\mu = 10\ cm^2V^{-1}s^{-1}$; (b) $\mu = 100\ cm^2V^{-1}s^{-1}$

Thus, it can be concluded that photodetector has two operation regimes: a linear regime of "Ohmic photocurrent density" at low electric fields and the saturation regime, where the photocurrent density approaches to its maximum value at high electric fields [31]. Based on this, the photoconductive gain could be obtained by dividing Eq. (12c) by the maximum photocurrent density $J_{max} = qgL$ and the obtained expression is the same as is $QE_{acc}$ given by Eq. (8c). Therefore, it is shown that results found in [1, 14] and [15] are equivalent. This is an important conclusion since by using the same approach, a new analytic expression for photoconductive gain can be derived when the effect of diffusion is considered.

The $QE_{acc}$ given by Eq. (8c) includes all photocurrents that ever flow in the device, regardless of whether they reach the electrodes. However, some of these carriers recombine before reaching the electrode, thus, not contributing to the photocurrent flowing through the external circuit. One might wonder how $QE_{acc}$ differs from another one $QE$, which uses the current at the electrodes. Another definition, referred to as $QE_{app}$, evaluates the photocurrent collected at the electrode and is perhaps the one typically or often implicitly adopted in literature [5, 14, 15, 39]. However, it can be shown that $QE_{acc}$ and $QE_{app}$ are not equivalent in general. Thus, in the literature, two subtly different $QE$ definitions have been used, but without being explicitly distinguished. Evidently, by evaluating the drift current at $x = 0$ for electrons or at $x = L$ for holes, Eqs. (11) lead to $QE_{app}$ at electrodes, given by [15, 39]

$$QE_{app,n} = \frac{L_{dr,n}}{L}\left[1 - exp\left(-\frac{L}{L_{dr,n}}\right)\right], \tag{13a}$$

$$QE_{app,p} = \frac{L_{dr,p}}{L}\left[1 - exp\left(-\frac{L}{L_{dr,p}}\right)\right]. \tag{13b}$$

It should be noted that $QE_{app} = QE_{app,n}$ given by Eq. (13a) is solely due to contribution of electrons at $x = 0$, whilst the contribution of holes is equal to 0. On the other hand, from Eq. (13b), $QE_{app} = QE_{app,p}$ at $x = L$, whilst the contribution of electrons is equal to 0. This preserves equality of currents at both ends of the device under assumption $\mu_n\tau_n = \mu_p\tau_p$.

In Fig. 8(a)-(c), it is shown on the logarithmic scale how a drift-only $QE_{acc}$ and $QE_{app}$ change with an applied voltage for different carrier lifetimes, carrier mobilities and channel lengths of photoconductor. It can be shown that at low electric fields, the ratio of $QE_{acc}$, given by Eq. (8c) and $QE_{app}$, given by Eq. (13a) or Eq. (13b) is exactly 2. Thus, it can be concluded that both, $QE_{acc}$ and $QE_{app}$, have two limiting cases: 1) at low electric fields, $QE$ depends linearly on the applied electric field, whereas $QE_{acc} = L_{dr,n}/L + L_{dr,p}/L$ , whilst $QE_{app} = QE_{app,n}(x = 0) =$

$QE_{app,p}(x = L)$ and $QE_{acc}/QE_{app} \approx 2/1$, and 2) at high electric fields, when the traveled distance is much longer than the channel length of photoconductor and in both cases, the maximum gain is limited to unity, i.e., $QE_{acc} \to 1$ and $QE_{app} \to 1$. However, it is important to point out here that this difference between $QE_{acc}$ and $QE_{app}$ arises because constant carrier lifetimes are used, as it is the case in most literature [1-5, 7, 14, 15, 22-29, 31, 33-37, 39]. If, for instance, $\tau_n(x)$ and $\tau_p(x)$ are used instead of $\tau_n$ and $\tau_p$, it would be expected that the $QE$ evaluated on electrodes $QE_{app}$ is equal to the $QE_{acc}$, obtained by averaging all carriers across the channel length $L$, i.e., $QE_{app} = QE_{acc}$.

Nevertheless, increasing the carrier lifetime, the carrier mobility, or shortening the channel length means that photoconductor can only saturate faster, which makes it "more perfect", however, in all cases $QE$ approaches to the maximum, unity value. Therefore, when only drift of carriers is considered, under assumption of primary photoconductivity, an intrinsic photoconductor does not have $QE$ larger than unity, independently of size of any of its parameter: the carrier mobility, the carrier lifetime, or the channel length of the device.

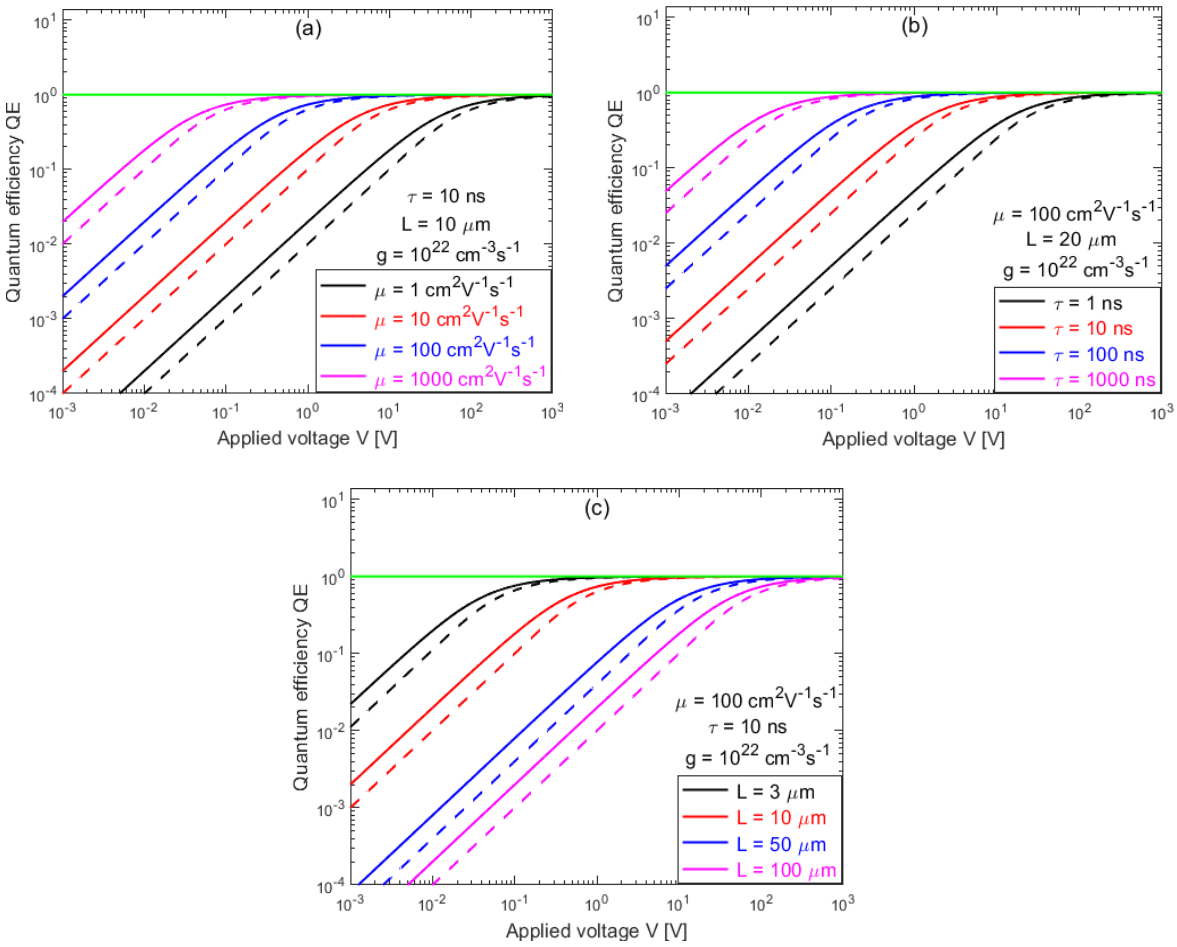


Figure 8: $QE_{acc}$ (solid lines) and $QE_{app}$ (dashed lines) vs. applied voltage on logarithmic scale for: (a) different mobilities; (b) different lifetimes; and (c) different channel lengths. The green lines represent the maximum quantum efficiency $QE_{max} = 1$.

# CHAPTER 3: A NEW PHOTOCONDUCTIVE GAIN THEORY

## 3.1. Assumptions and key findings

Many real-world photodetectors are *p*-*n* junction devices which use a vertical structure with planar contacts at the top and bottom, where the carriers are generated very close to the top contact. A *p*-*n* photodetector is known to not have a gain [3, 25]. However, most MSM type photoconductive devices often adopt a lateral structure, where the device is uniformly illuminated from the side, as those in the early literatures [1, 11-15, 31], as well as in many recent publications using nanowire type structures [22, 32, 43]. Thus, here is considered an undoped, lateral photoconductive device illuminated uniformly from the side.

Within the framework of the primary photoconductivity, the photoconductive gain theory for a MSM structure with an intrinsic (undoped) semiconductor is reexamined in this work, with the goal of laying the ground for understanding the mechanism(s) of the photoconductive gain. In this photoconductive theory, by applying a few physically sound applications, analytic solutions for the photocarriers and photocurrent can be obtained for arbitrary conditions of drift and diffusion. By assuming primary photoconductivity, it is shown that the gain formula given by Eq. (2) is only valid in the low-drift limit. Nevertheless, this seemingly oversimplified case reveals a few previously not well recognized aspects of photoconductivity.

The key assumptions related to the analytic model adopted here, as well as commonly adopted in the literature, are: (1) thermally generated carriers are negligible compared to photogenerated carriers and only photogenerated carriers within the photoconductive medium contribute to the photocurrent [1, 5, 14, 15, 39]; (2) the carrier velocity is proportional to the applied electric field [15]; (3) the carrier lifetime may include carrier trapping mechanisms, but the trapped carriers (e.g., by defect states) do not contribute to the photoconductivity; (4) there is

no surface recombination loss either at the MS contacts or the semiconductor surface [1, 5, 14, 39]; (5) $\partial \mathrm{E}/\partial \mathrm{x} = 0$ or polarization effect is negligible, since this is the only case where the continuity equations for drift-only and drift-drift diffusion currents can be solved analytically [1, 3, 5, 14, 15, 32, 39]; (6) constant mobilities and carrier lifetimes are assumed [1-5, 7, 14, 15, 22-29, 31, 33-37, 39]; and (7) assumption of equal mobility-lifetime product of electrons and holes is adopted in analytic model, since nonequal product would violate charge neutrality, and currents at the anode and cathode would be different, which is physically impossible.

Finally, the specific key findings and conclusions of this dissertation include: (1) By assuming negligible polarization effect, the general analytic results including drift and diffusion, for the electron and hole distributions and photocurrents, as well as $QE_{acc}$ and $QE_{app}$, are obtained in terms of normalized drift and diffusion lengths. Furthermore, it is shown that when diffusion is neglected, they recover the analytic results given in the literature for different limiting cases; (2) It is shown that by including both drift and diffusion, the intrinsic photoconductive gain, defined by either $QE_{acc}$ or $QE_{app}$, is always limited to unity, whilst in general $QE_{acc} > QE_{app}$; (3) The commonly adopted definition of photoconductive gain as the ratio of carrier lifetime to transit time given by Eq. (2), which allows a value much greater than unity, is only applicable in the low drift length region or low $QE$ limit, but has been inappropriately generalized in the literature; (4) Numerical simulations for an intrinsic device are performed to confirm that the presence of the polarization effect does not change the qualitative conclusions; (5) Analytical and numerical results show good agreement and confirm experimentally obtained gains limited to unity within the framework of primary photoconductivity, as found in the numerous literature [1, 2, 11-14, 44-46]; (6) Even though the individual photocarrier densities (i.e., electrons and holes) are expected to be nonuniform when the vanishing BCs are applied [3, 5, 15], the total photocurrent is often

implicitly assumed and sometimes explicitly stated to be uniform [3]. However, it is found that the photocurrent across the photoconductive channel is in general nonuniform, which is consequence of using constant $\tau$; (7) It is pointed out that within the framework of the intrinsic primary photoconductivity, carrier trapping does not lead to gain; (8) By performing numerical simulations, it is found that a modest gain is achievable if a doped semiconductor is used, as found in [5]. However, based on these results, new analytic solutions are proposed.

### 3.2. Quantum efficiency of drift-diffusion charge carriers–analytic results

Two basic transport mechanisms in a semiconducting or insulating crystals are drift, which is the movement of carriers due to an applied electric field, and diffusion, which is the process where carriers flow from a region of high concentration toward a region of low concentration due to the presence of a density gradients. In Ch. 2.2., where only drift of carriers was considered, it was shown that both, $QE_{acc}$ and $QE_{app}$, approaches unity even for increased carrier lifetime, carrier mobility or shortened channel length. The carrier diffusion is often omitted in the photoconductivity theory [1, 2, 14, 15, 21, 25-27, 31, 39, 47]. In a few cases, carrier diffusion is considered, for instance, in the low drift region [3, 38] and for the general conditions of drift and diffusion [3, 5, 32]. To examine potential impact on photocurrents, in this chapter a diffusion effect is included in analysis.

In steady state, for uniform generation, the electron and hole carrier densities, $\Delta n(x)$ and $\Delta p(x)$, respectively, can be obtained by solving drift-diffusion equations for electrons and holes [26, 27], and the corresponding photocurrent densities, $J_n(x)$ and $J_p(x)$ can be respectively calculated as below

$$J_n(x) = J_{dr,n}(x) + J_{di,n}(x) = q\mu_n E(x)\Delta n(x) + qD_n \frac{\partial(\Delta n(x))}{\partial x}, \quad (14a)$$

$$J_p(x) = J_{dr,p}(x) + J_{di,p}(x) = q\mu_p E(x)\Delta p(x) - qD_p \frac{\partial(\Delta p(x))}{\partial x}, \quad (14b)$$

where $D_n = (kT\mu_n)/q$ and $D_p = (kT\mu_p)/q$ are diffusion coefficients of electrons and holes, respectively, $k$ the Boltzmann's constant, and $T$ the temperature. Furthermore, the drift-diffusion equations, as well as a Poisson's equation that describes the photocarrier induced change in the internal electric field, can be respectively written as

$$L_{di,n}^2 \frac{\partial^2(\Delta n(x))}{\partial x^2} + L_{dr,n} \frac{\partial(\Delta n(x))}{\partial x} + \mu_n \tau_n \Delta n(x) \frac{\partial E}{\partial x} - \Delta n(x) + g\tau_n = 0, \quad (15a)$$

$$L_{di,p}^2 \frac{\partial^2(\Delta p(x))}{\partial x^2} - L_{dr,p} \frac{\partial(\Delta p(x))}{\partial x} - \mu_p \tau_p \Delta p(x) \frac{\partial E}{\partial x} - \Delta p(x) + g\tau_p = 0, \quad (15b)$$

$$\frac{\partial E}{\partial x} = \frac{q[\Delta p(x) - \Delta n(x)]}{\varepsilon \varepsilon_0}, \quad (15c)$$

where $L_{dr,n} = E\mu_n\tau_n$ and $L_{dr,p} = E\mu_p\tau_p$ are the drift lengths, $L_{di,n} = \sqrt{D_n\tau_n}$ and $L_{di,p} = \sqrt{D_p\tau_p}$ the diffusion lengths, $\varepsilon$ is the relative dielectric constant of the semiconductor, and $\varepsilon_0$ is the permittivity of the vacuum. In the standard forms of drift-diffusion equations, Eqs. (14) or (15), independent carrier lifetime $\tau_n$ and $\tau_p$ are used to describe the recombination of electrons and holes, respectively [26, 27]. A more thorough treatment should consider a kinetic model, such as the Shockley-Read-Hall (SRH) model, where the two processes are connected, as done in some literatures [26, 48-50]. Similarly to drift-only case, even if Eqs. (15) can be solved independently when $\partial E/\partial x = 0$, it should be noted that if the mobility-lifetime products of electrons and holes are different, i.e., $\mu_n\tau_n \neq \mu_p\tau_p$, photocurrents at the anode (mostly the electron current) and the cathode (mostly the hole current) will be different, which would disrupt the basic requirement of the current continuity in the external circuit. Furthermore, this would lead to violating the charge neutrality law for carrier distributions. Thus, the assumption of equal mobility-lifetime product of electrons and holes, i.e., $\mu_n\tau_n = \mu_p\tau_p$ is adopted again.

Qualitatively, the diffusion effect, which results in bidirectional motion of the carriers, tends to reduce the photocurrent, in contrast to the drift-only case where the carrier motion is

unidirectional under the applied field. The $\partial E/\partial x$ term $\propto \Delta p(x) - \Delta n(x)$ in the drift-diffusion equation describes a charge polarization effect associated with the relative displacement of the electron and hole distributions induced by the external bias. This effect resembles the ultrafast screening of an applied bias resulting from the space-charge field set up by the separating carriers in a GaAs THz device [51]. As earlier, assumption $\partial E/\partial x \approx 0$ is adopted, which means that the external field being much stronger than this perturbation. Under these approximations, Eqs. (15) can be solved analytically and independently. It can be seen from Eq. 15(c) that the impact of the $\partial E/\partial x$ term is inversely scaled by the square of a normalized Debye length $l_D = L_D/L$, where $L_D = \sqrt{\frac{\varepsilon\varepsilon_0 kT}{q^2 g\tau}}$ is Debye length and $\tau = \sqrt{\tau_n \tau_p}$. Therefore, for a small $g\tau$ value or a large $l_D$, the polarization effect is negligible.

Solving the drift-diffusion equation typically requires two BCs. Typically, the minority carrier densities at the electrodes are assumed to be equal to the thermal equilibrium value [3] or simply zero [5]. In the recent work including diffusion [5], BCs of $\Delta n(x = 0) = \Delta n(x = L) = 0$ for a *p*-type semiconductor are used for Ohmic contacts by arguing that no excess of electrons is generated in the metal and that the carrier density should be continuous from the metal to semiconductor. Here, it is assumed the perfect carrier extraction at the electrodes, i.e., all carriers that can reach the electrodes will flow through the external circuit, which is consistent with the consideration that leads to Eq. (8a) [1, 14, 31]. The carrier extraction by the electrode can be treated as equivalent to the surface recombination of the MS interface at the electrode, with standard BCs for electrons and holes [7], respectively,

$$D_n \frac{d(\Delta n(x=0))}{dx} = s\Delta n(x = 0), \tag{16a}$$

$$-D_n \frac{d(\Delta n(x=L))}{dx} = s\Delta n(x = L), \tag{16b}$$

where $s$ is the electrode extraction velocity (resembling the surface recombination velocity), taking the limit of $s \to \infty$ for perfect extraction. These BCs are appropriate for a Schottky junction, with the metal work function $q\phi$ significantly larger than the semiconductor electron affinity $\chi$, i.e., $q\phi - \chi \gg kT$, where the electrons encounter a "cliff" at the contacts [1]. Because the gradient is expected to be finite at the boundary, $s \to \infty$ implies that the carrier density goes to zero at the boundary. Thus, the solution will be the same as simply applying the vanishing BCs [5]. Again, the drift-diffusion equations can be solved analytically by assuming $\partial \mathrm{E}/\partial \mathrm{x} = 0$ [3, 5, 32]. By applying following BCs: $\Delta n(x = 0) = \Delta n(x = L) = 0$ and $\Delta p(x = 0) = \Delta p(x = L) = 0$, the photogenerated concentration of electrons and holes can be respectively expressed as

$$\Delta n(x) = g\tau_n[1 - c_1\, exp((x - L)\lambda_1) - c_2\, exp((x - L)\lambda_2)], \tag{17a}$$

$$\Delta p(x) = g\tau_n[1 - c_1\, exp(-x\lambda_1) - c_2\, exp(-x\lambda_2)], \tag{17b}$$

where $c_1 = \frac{exp(-L\lambda_2)-1}{exp(-L\lambda_2)-exp(-L\lambda_1)} > 0$, $c_2 = \frac{1-exp(-L\lambda_1)}{exp(-L\lambda_2)-exp(-L\lambda_1)} > 0$ and $\lambda_{1,2} = \frac{-L_{dr,p} \pm \sqrt{L_{dr,p}^2 + 4L_{di,p}^2}}{2L_{di,p}^2}$ [5, 32]. By combining and solving Eq. (16a) and Eq. (17a), it can be shown after lengthy calculations that solution which includes surface recombination velocity is given for electrons as

$$\Delta n(x, s) = g\tau_n \left\{1 - \frac{sc_1}{s - D_n\lambda_1} exp[(x - L)\lambda_1] - \frac{sc_2}{s - D_n\lambda_2} exp[(x - L)\lambda_2]\right\}. \tag{18a}$$

At $x = 0$ and $x = L$, it follows

$$\Delta n(x = 0, s) = g\tau_n \left[1 - \frac{sc_1\, exp(-L\lambda_1)}{s - D_n\lambda_1} - \frac{sc_2\, exp(-L\lambda_2)}{s - D_n\lambda_2}\right], \tag{18b}$$

$$\Delta n(x = L, s) = g\tau_n \left[1 - \frac{sc_1}{s - D_n\lambda_1} - \frac{sc_2}{s - D_n\lambda_2}\right]. \tag{18c}$$

Thus, carrier distributions also depend on surface recombination velocity. For instance, by neglecting surface recombination velocity, i.e., $s = 0$, the solution of Eq. (18a) would simply be spatially uniform and independent of an electric field, i.e., $\Delta n = g\tau_n$. However, it was earlier

shown that this is not the case under an applied electric field. On the other hand, if Ohmic contacts are ideal, the surface recombination velocity would approach to the infinity, i.e., $s \to \infty$, since the metal is equivalent to a very strong surface recombination [9]. In that case, $\lim_{s\to\infty} \Delta n(x,s)$ of Eq. (18a) reduces to Eq. (17a). In another case, when diffusion was considered [3], assuming Ohmic contacts for both electrodes, with the anode at $x = 0$ and cathode at $x = L$, a nonuniform carrier distribution for holes at zero field was found as

$$\Delta p(x) = g\tau_p \left[1 - \frac{\cosh\left(\frac{2x-1}{2L_{di,p}}\right)}{\cosh\left(\frac{L}{2L_{di,p}}\right)}\right]. \tag{19}$$

This solution is then used to calculate the photocurrent and gain by using the averaged carrier density over the channel length; however, not directly, but instead by introducing an effective carrier lifetime $\tau_{eff}$ such that $\Delta p_{avg} = g\,\tau_{eff}$.

Fig. 9 plots the normalized carrier density $\delta p(\xi) = \Delta p(\xi)/g\tau$, where $\Delta p(\xi)$ is determined by Eq. 17(b), for the following combinations of $(l_{dr}; l_{di})$: $(l_{dr} = 0.1, 0.5, 1.0, 5.0; l_{di} = 0, 0.2, 0.4, 0.6)$. Note that normalized carrier distributions only depend on two parameters: normalized drift length $l_{dr} = L_{dr}/L$ and normalized diffusion length $l_{di} = L_{di}/L$, when expressed in normalized coordinate $\xi = x/L$. Generally, $\Delta p(\xi)$ is highly nonuniform and asymmetric in the photoconductive channel and it is more symmetric as diffusion becomes more dominant. Evidently, only in the low drift and weak diffusion cases, $\delta p \to 1$ (i.e., $\Delta p \to g\tau$) on the cathode side (e.g., $l_{dr} = 0.1$ and $l_{di} = 0.1$ in Fig. 9(a)), which is in stark contrast to the common assumption of $\Delta p = g\tau$ throughout the channel for arbitrary $(l_{dr}, l_{di})$. As $l_{di} \to 0$, Eqs. (17) $\to$ Eqs. (11) in $[\xi L, L)$.

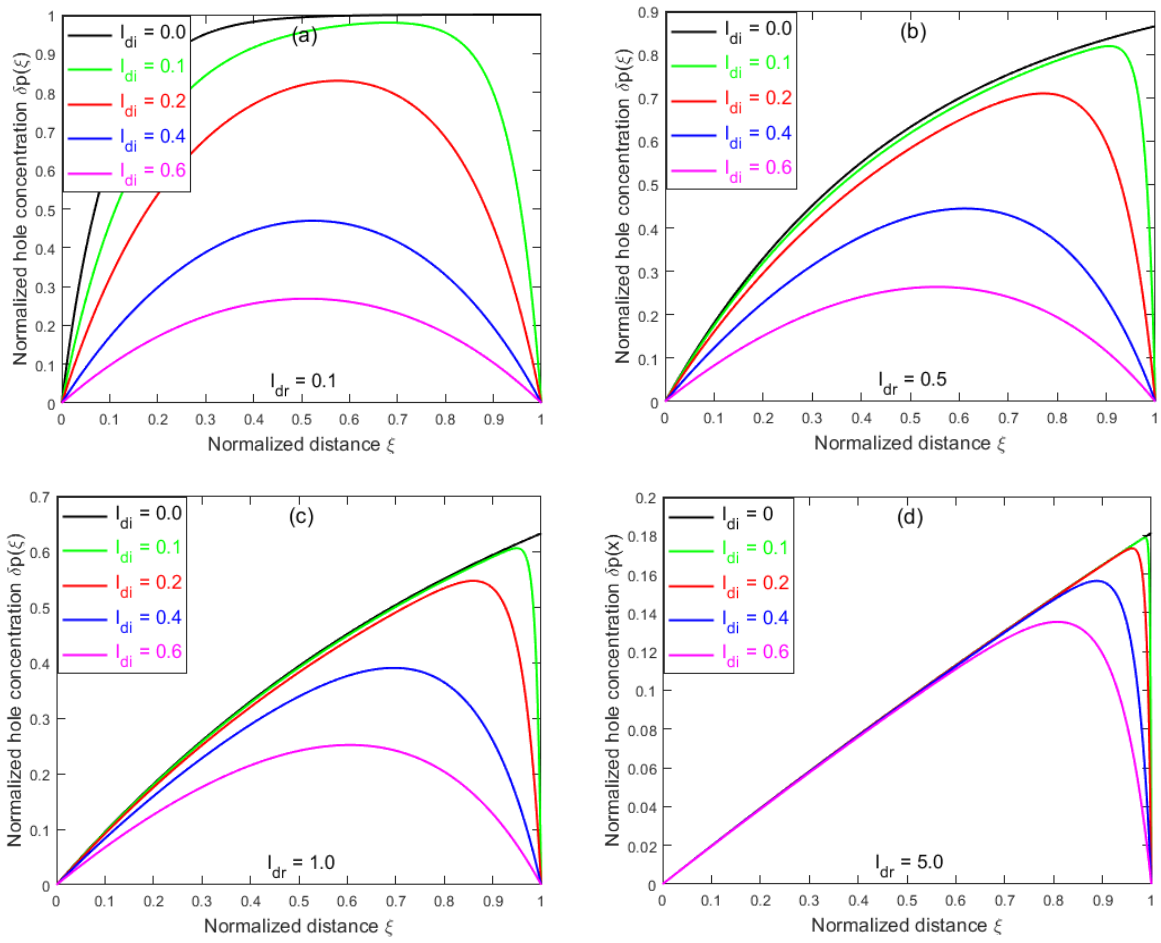


Figure 9: Normalized spatial distributions of photogenerated holes for different combinations of diffusion and drift parameters, $l_{di} = (0, 0.1, 0.2, 0.4, 0.6)$: (a) $l_{dr} = 0.1$; (b) $l_{dr} = 0.5$; (c) $l_{dr} = 1.0$; and (d) $l_{dr} = 5.0$

To find an accumulated drift-diffusion photocurrent density, it is necessary to find an average concentration of excess electrons and holes, as was the case with the drift-only photocurrent density. The average drift components of photocurrent density include the contribution of diffusion through $\lambda$ parameters and can be expressed as

$$J_{dr,n} = \frac{qE\mu_n}{L}\int_0^L \Delta n(x)dx = qgL_{dr,n}\left\{1 - \frac{1}{L}\left[\frac{1}{\lambda_1} - \frac{1}{\lambda_2}\right]\frac{[1-exp(-L\lambda_1)][1-exp(-L\lambda_2)]}{exp(-L\lambda_2)-exp(-L\lambda_1)}\right\}, \quad (20a)$$

$$J_{dr,p} = \frac{qE\mu_p}{L}\int_0^L \Delta p(x)dx = qgL_{dr,p}\left\{1 - \frac{1}{L}\left[\frac{1}{\lambda_3} - \frac{1}{\lambda_4}\right]\frac{[1-exp(-L\lambda_3)][1-exp(-L\lambda_4)]}{exp(-L\lambda_4)-exp(-L\lambda_3)}\right\}. \quad (20b)$$

On the other hand, the average diffusion photocurrent densities of electrons and holes are calculated as $J_{di,n} = \int_0^L \frac{\partial(\Delta n(x))}{\partial x}dx = 0$ and $J_{di,p} = \int_0^L \frac{\partial(\Delta p(x))}{\partial x}dx = 0$. Therefore, the average diffusion photocurrent density is equal to zero; however, diffusion still contributes to the total photocurrent density through $\lambda$ parameters, which can be written as a sum of Eqs. (20)

$$J_{acc} = qg\left\{\begin{matrix} L_{dr,n}\left\{1 - \frac{1}{L}\left[\frac{1}{\lambda_1} - \frac{1}{\lambda_2}\right]\frac{[1-exp(-L\lambda_1)][1-exp(-L\lambda_2)]}{exp(-L\lambda_2)-exp(-L\lambda_1)}\right\} \\ + \\ L_{dr,p}\left\{1 - \frac{1}{L}\left[\frac{1}{\lambda_3} - \frac{1}{\lambda_4}\right]\frac{[1-exp(-L\lambda_3)][1-exp(-L\lambda_4)]}{exp(-L\lambda_4)-exp(-L\lambda_3)}\right\} \end{matrix}\right\}. \quad (20c)$$

Similarly, the average photoconductive gain due to a drift-diffusion photocurrent density can be expressed as the ratio of eq. (20c) and the maximum photocurrent density $J_{max} = qgL$

$$QE_{acc} = \left\{\begin{matrix} l_{dr,n}\left\{1 - \frac{1}{L}\left[\frac{1}{\lambda_1} - \frac{1}{\lambda_2}\right]\frac{[1-exp(-L\lambda_1)][1-exp(-L\lambda_2)]}{exp(-L\lambda_2)-exp(-L\lambda_1)}\right\} \\ + \\ l_{dr,p}\left\{1 - \frac{1}{L}\left[\frac{1}{\lambda_3} - \frac{1}{\lambda_4}\right]\frac{[1-exp(-L\lambda_3)][1-exp(-L\lambda_4)]}{exp(-L\lambda_4)-exp(-L\lambda_3)}\right\} \end{matrix}\right\} \quad (21)$$

Another way to derive the equivalent expression is to normalize the photocurrent density of the holes to the maximum current $J_{max} = qgL$, by using Eq. (14b) and Eq. (17b) in normalized coordinate $\xi$, which can be written as

$$j_p(\xi) = j_{dr,p}(\xi) + j_{di,p}(\xi), \quad (22a)$$

where the first term is the drift current with diffusion, whilst the second term is the diffusion current with drift, respectively

$$j_{dr,p}(\xi) = l_{dr}[1 - c_1\, exp(-\xi L\lambda_1) - c_2\, exp(-\xi L\lambda_2)], \quad (22b)$$

$$j_{di,p}(\xi) = l_{di}^2[-c_1 L\,\lambda_1 exp(-\xi L\lambda_1) - c_2\, L\lambda_2 exp(-\xi L\lambda_2)]. \quad (22c)$$

Note that the spatial average of the diffusion term in Eq. (22a) is identically zero for any $l_{dr,p}$ and $l_{di,p}$. As $l_{di} \to 0$, it recovers the drift-only result in $[x, L)$ [15]. Fig. 10 plots $j_p(\xi)$ using the same

parameters (without $l_{di} = 0.1$) as in Fig. 9. With diffusion considered, the photocurrent is in opposite directions or signs toward the two electrodes, indicating loss in photocurrent due to the bidirectional nature of the carrier diffusion, but the diffusion effect is being suppressed with increasing drift length $l_{dr}$: for a fixed $l_{di}$, $j_p(\xi)$ increases with increasing $l_{dr}$ from Fig. 10(a) to Fig. 10(d). Again, the electron photocurrent density $j_n(\xi)$ can be obtained by substituting $\xi$ with $L(1-\xi)$ in Eq. (22a). Both, $j_p(\xi)$ and $j_n(\xi)$, are in general highly nonuniform. For small $l_{dr}$ and large $l_{di}$ (e.g., $l_{dr} = 0.1$ and $l_{di} = 0.6$ in Fig. 10(a)), $j_p(x)$ is close to be antisymmetric with respect to the center, thus, the average photocurrent is expected to be small (exactly zero for $l_{dr} = 0$), as expected for the diffusion dominated case. In contrast, for large $l_{dr}$ and small $l_{di}$ (e.g., $l_{dr} = 5.0$ and $l_{di} = 0.2$ in Fig. 10(d)), $j_p(\xi)$ is positive in almost the whole channel, and the average approaches ½, as expected for the drift-only case.

Adopting the same $QE$ definition as in [1, 3, 14, 15, 31, 39] and by calculating the spatially averaged photocurrent density with diffusion included, the $QE_{acc}$ for holes can be obtained as

$$QE_{acc,p} = l_{dr}\{1 - l_{dr}\alpha[\coth(\alpha\beta) - csch(\alpha\beta)\cosh(\beta)]\}, \quad (23)$$

where $\alpha = \sqrt{1 + 4\frac{l_{di}^2}{l_{dr}^2}}$ and $\beta = \frac{l_{dr}}{2l_{di}^2}$. Note that the spatial average of the diffusion term in Eq. (22a) is identically zero for any $l_{dr}$ and $l_{di}$. The total $QE_{acc}$ is given by $QE_{acc} = QE_{acc,n} + QE_{acc,p}$, with a unity limit. Fig. 11(a) plots $QE_{acc}$ vs. $l_{dr}$ for $l_{di} = 0, 0.2, 0.4$, and 0.6. For $l_{di} \ll l_{dr}$, when $l_{dr} \ll 1$, $QE_{acc,p} \approx l_{dr} \approx \tau_c/\tau_t$, the same as Eq. (2); when $l_{dr} \sim 1$, $QE_{acc,p}$ becomes Eq. (8b); and when $l_{dr} \gg 1$, $QE_{acc,p} \to$ ½. When $l_{dr} \ll 1$, $QE_{acc,p}$ can be expanded to the first order in $l_{dr}$, yielding

$$QE_{acc,p} \approx l_{dr}\left[1 - 2l_{di}\,tanh\left(\frac{1}{2l_{di}}\right)\right]. \quad (24)$$

This result is consistent with that of [3], where the zero-field carrier density distribution is used for the calculation. When $l_{di} \to 0$ and $l_{dr} \ll 1$, $QE_{acc} \approx 2l_{dr}$. It should be noted that the gain calculated by using Eq. (19) is equivalent to $QE_{acc}$.

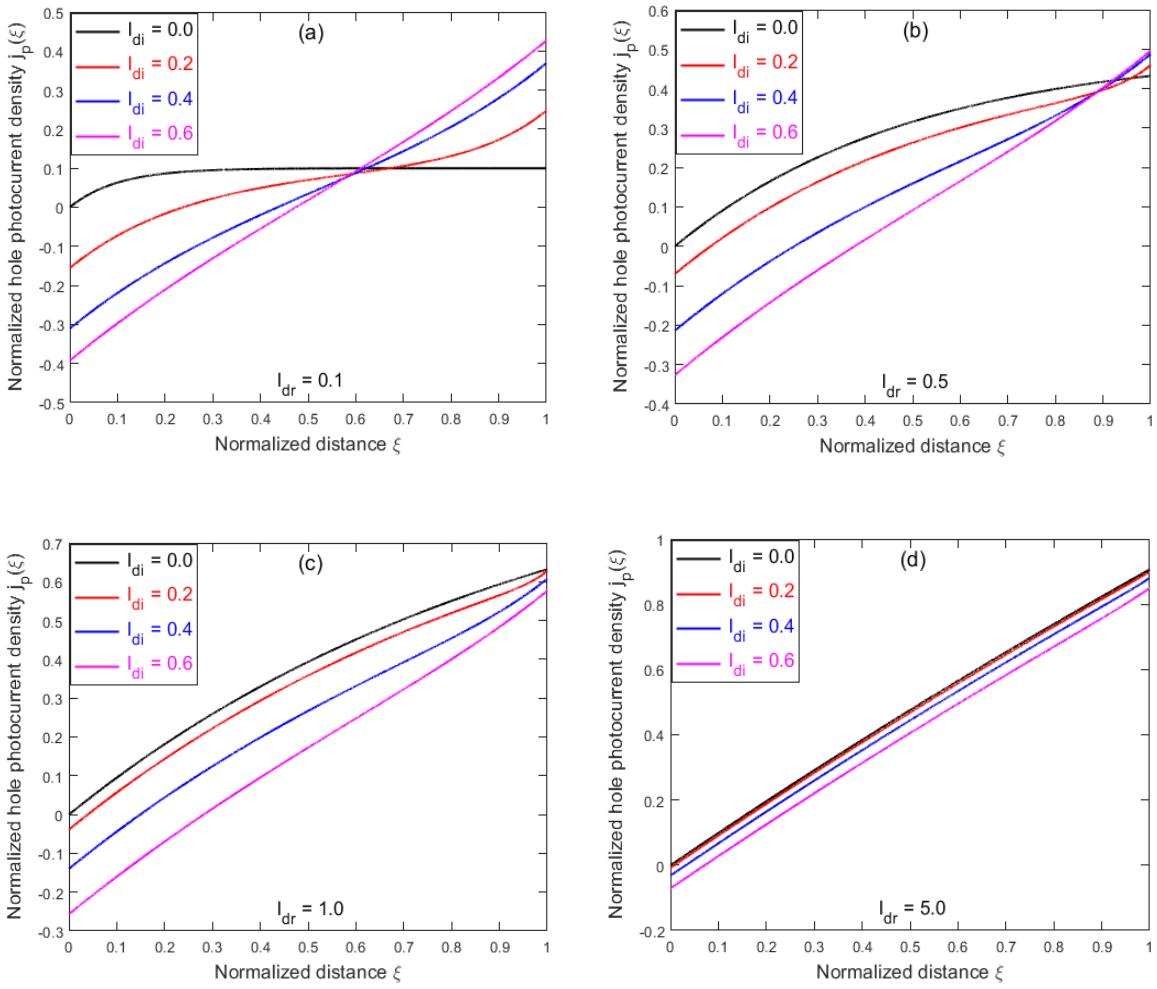


Figure 10: Normalized spatial dependencies of hole photocurrent densities for different combinations of diffusion and drift parameters, $l_{di} = (0, 0.1, 0.2, 0.4, 0.6)$: (a) $l_{dr} = 0.1$; (b) $l_{dr} = 0.5$; (c) $l_{dr} = 1.0$; and (d) $l_{dr} = 5.0$

Similarly, as with $QE_{acc}$, it is possible to find $QE_{app}$ with diffusion included. The total normalized photocurrent density, can be calculated as

$$j(\xi) = J(\xi)/(qgL) = j_n(\xi) + j_p(\xi) = j_{dr}(\xi) + j_{di}(\xi), \quad (25a)$$

with the drift term and diffusion terms, respectively

$$j_{dr}(\xi) = 2l_{dr}\left\{1 - c_1\, exp\left(-\frac{L\lambda_1}{2}\right) cosh\left[L\lambda_1\left(\xi - \frac{1}{2}\right)\right] - c_2\, exp\left(-\frac{L\lambda_2}{2}\right) cosh\left[L\lambda_2\left(\xi - \frac{1}{2}\right)\right]\right\}, \quad (25b)$$

$$j_{di}(\xi) = 2l_{di}^2 L\left\{-c_1\lambda_1\, exp\left(-\frac{L\lambda_1}{2}\right) cosh\left[L\lambda_1\left(\xi - \frac{1}{2}\right)\right] - c_2\,\lambda_2 exp\left(-\frac{L\lambda_2}{2}\right) cosh\left[L\lambda_2\left(\xi - \frac{1}{2}\right)\right]\right\}. \quad (25c)$$

The photocurrent density at the collecting electrodes, $j(\xi = 0)$ or $j(\xi = 1)$, respectively, at the anode or cathode, represents the actual photocurrent that goes through the external circuit and can be directly measured. A short-circuit condition is implicitly assumed in the calculation, thus, $j(\xi = 0) = j(\xi = 1)$ is expected, as implied by Eq. (25a). Therefore, $QE_{app} = j(\xi = 0) = j(\xi = 1)$ can be calculated as

$$QE_{app} = l_{di}^2 L\left\{\frac{\lambda_1[1+exp(-L\lambda_1)][1-exp(-L\lambda_2)]-\lambda_2[1-exp(-L\lambda_1)][1+exp(-L\lambda_2)]}{exp(-L\lambda_2)-exp(-L\lambda_1)}\right\}, \quad (26a)$$

which can be further simplified as

$$QE_{app} = l_{dr}[1 - \alpha csch(\alpha\beta) sinh(\beta)]. \quad (26b)$$

Note that Eq. (25a) yields $j_{dr}(\xi = 0) = j_{dr}(\xi = 1) = 0$ and, thus, $QE_{app} = j_{di}(\xi = 0) = j_{di}(\xi = 1)$. When $l_{di} \to 0$, $QE_{app}$ approaches Eqs. (8a) and (8b), because $j_{app,p}(\xi = 0) = j_{app,n}(\xi = 1) = 0$. When $l_{dr} \ll 1$, $QE_{app}$ can be expanded to the first order in $l_{dr}$ as

$$QE_{app} \approx l_{dr}\left[1 - \frac{1}{l_{di}} csch\left(\frac{1}{l_{di}}\right)\right]. \quad (27)$$

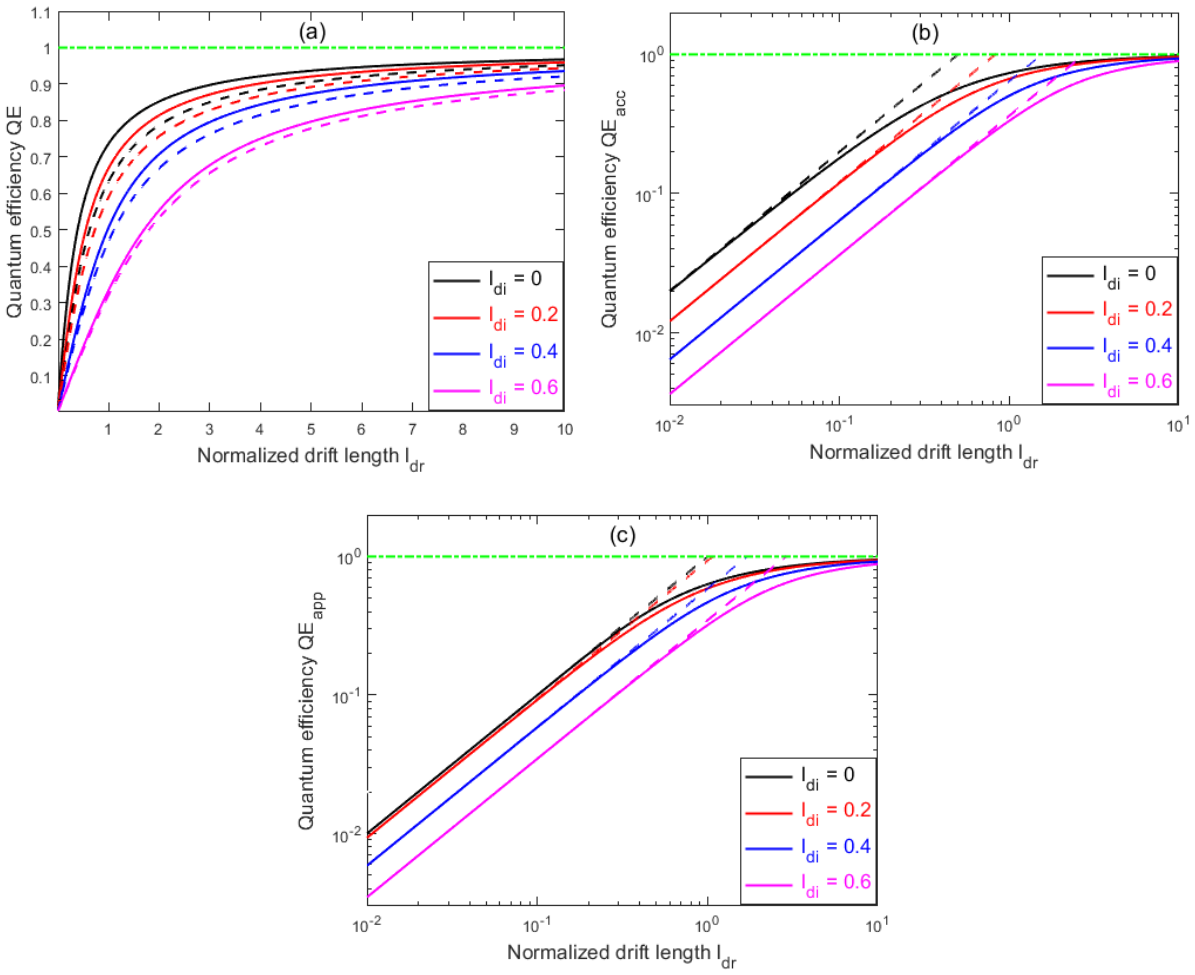


Figure 11: (a) Quantum efficiencies $QE_{acc}$ (solid lines) and $QE_{app}$ (dashed lines) vs. normalized drift length $l_{dr}$ for $l_{di} = (0, 0.2, 0.4, 0.6)$; (b) $QE_{acc}$ (solid lines) with low $l_{dr}$ approximation (dashed lines); and (c) $QE_{app}$ (solid lines) with low $l_{dr}$ approximation (dashed lines). The green line represents the maximum quantum efficiency $QE_{max} = 1$.

When $l_{di} \to 0$ and $l_{dr} \ll 1$, $QE_{app} \approx l_{dr}$, which is a factor of 2 smaller than $QE_{acc}$ in the same limit. Fig. 11(a) also plots $QE_{app}$ vs. $l_{dr}$ for $l_{di} = 0, 0.2, 0.4$, and $0.6$, to compare with the corresponding $QE_{acc}$ curves, showing $QE_{acc} > QE_{app}$ in general. Note that Eq. (26b) gives the

total $QE_{app}$, including the contributions either of electrons or holes on the opposite electrodes. For comparison, Figs. 11(b) and 11(c) plot $QE_{acc}$ and $QE_{app}$, respectively, vs. $l_{dr}$ in logarithmic scale, for $l_{di} = 0, 0.2, 0.4$, and 0.6, including the results of the low $l_{dr}$ limit, i.e., Eq. (24) and Eq. (27), respectively.

$QE_{app}$ given by Eq. (26), reflecting the total current at $\xi = 0$ or $\xi = 1$, is essentially the same as the minority-carrier photocurrent, for instance, $J_n$ for a *p*-type semiconductor [5], where $J_n$ seems to be evaluated from $J_n = J_n(x = 0) + J_n(x = L)$ from the solution of Eq. (15a). The reason that $J_n$ of doped device is in agreement with total current for an intrinsic device $J(x) = J_n(x) + J_p(x)$ at $x = 0$ or $x = L$ is because here it is considered an intrinsic semiconductor device with $\mu_n\tau_n = \mu_p\tau_p$, where $J_p(x = 0) = J_n(x = L)$ and $J_n(x = 0) = J_p(x = L)$. Thus, it can be written $J(x = 0) = J_n(x = 0) + J_p(x = 0) = J_n(x = 0) + J_n(x = L)$ or similarly $J(x = L) = J_n(x = L) + J_p(x = L) = J_p(x = 0) + J_p(x = L)$. However, it should be noted that it is not possible to solve the drift-diffusion equations for a *p*-type semiconductor for electrons and holes independently while ensuring $J(x = 0) = J(x = L)$.

Similarly, as in Ch. 2.2, when drift-only cases have been discussed, it should be pointed out that the difference between $QE_{acc}$ and $QE_{app}$ appears due to the assumption (6) using constant carrier lifetime $\tau$, instead of spatially dependent $\tau(\xi)$.

Furthermore, Figs. 12 compare $j_n(\xi)$, $j_p(\xi)$, and $j(\xi) = j_n(\xi) + j_p(\xi)$ with the spatially averaged value $j_{avg}$ for three representative $(l_{dr}, l_{di})$ combinations: low field $(0.2, 0.2)$, medium field $(1.0, 0.2)$, and high field $(5.0, 0.2)$, respectively, and illustrate how each type of carrier contributes to the total drift-diffusion photocurrent at different field strengths measured by $l_{dr}$. When diffusion is significant, as in Fig. 12(a), $j_n(\xi)$ and $j_p(\xi)$ tend to have opposite signs and partially cancel each other at the electrodes, yielding a smaller net photocurrent. However, when

drift is dominant, as in Fig. 12(c), one of $j_n(\xi)$ and $j_p(\xi)$ diminishes at the respective electrode, yielding a larger net photocurrent, approaching $j_{avg}$ or $QE_{acc}$.

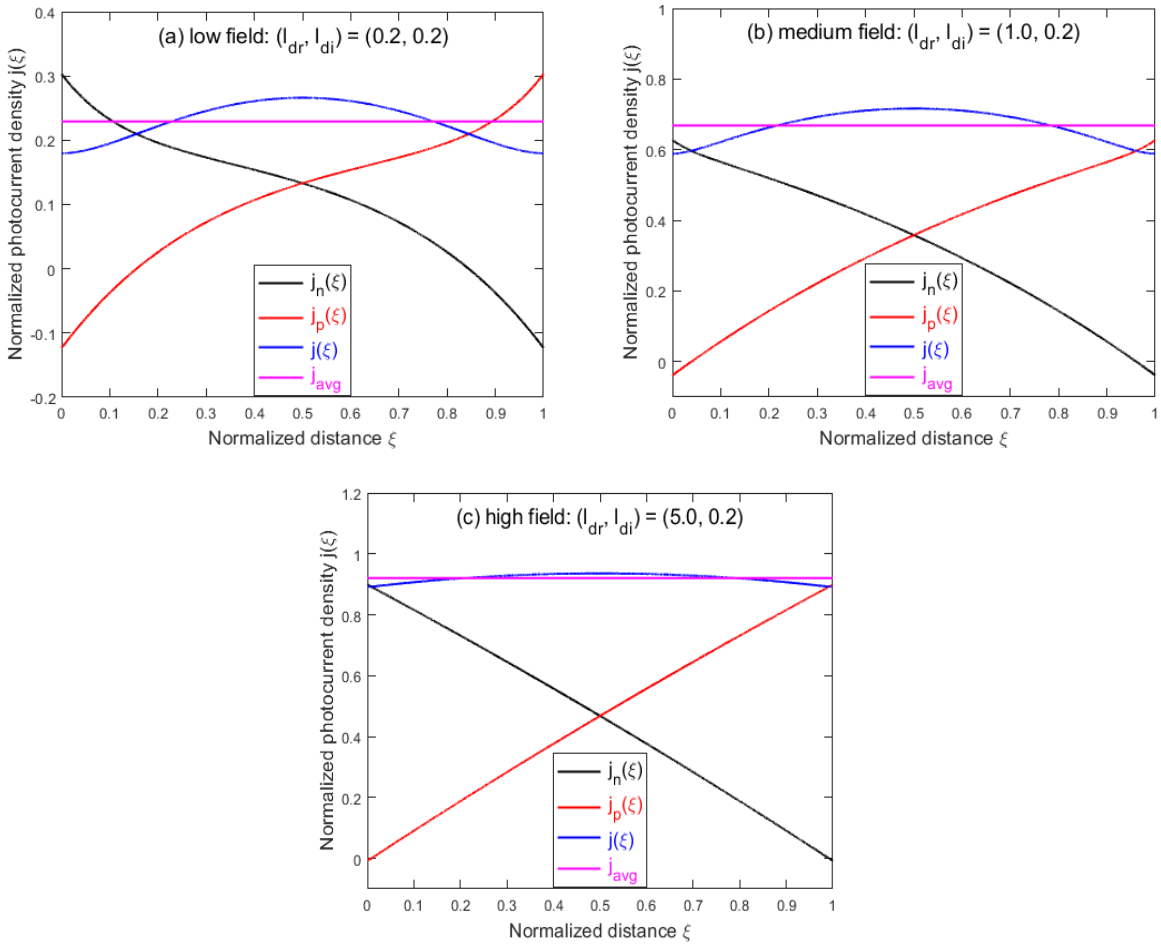


Figure 12: The total normalized photocurrent density $j(\xi)$, electron component $j_n(\xi)$ and hole component $j_p(\xi)$ vs. normalized distance $\xi$, compared to the average photocurrent density $j_{avg}$ for three different $(l_{dr}, l_{di})$ combinations: (a) low field: $(l_{dr}, l_{di}) = (0.2, 0.2)$; (b) medium field: $(l_{dr}, l_{di}) = (1.0, 0.2)$; and (c) high field: $(l_{dr}, l_{di}) = (5.0, 0.2)$

Physically, the cancellation of the $j_n(\xi = 0)$ and $j_p(\xi = 0)$ can be understood as that some electrons reaching the anode, instead of flowing through the external circuit, may go back to the valence band directly, which is equivalent to saying that some holes diffuse out from the anode. In the case with diminished diffusion, $\delta p \to 0$ and, thus, no empty state is available for the electrons to take. Thus, the whole electron current will flow through the external circuit and be the total current at the anode. Importantly, under the assumption of constant $\tau$, the total photocurrent $j(\xi)$ is typically nonuniform, which is more prominent in the case of low field as in Fig. 12(a). However, as the applied field increases, as shown in Figs. 12(b) and 12(c), it follows $j(\xi) \to j_{avg}$ since in this case the effect of recombination starts to diminish. This spatial nonuniformity of the current might sound inconsistent with the conventional wisdom that the current should be constant throughout the circuit under continuous and uniform illumination. In fact, not the entire amount of the electron or hole photocurrents can flow to the respective electrodes due to the interplay of generation, drift, and diffusion. Furthermore, the constant current within the photoconductive channel is not necessary to satisfy the current continuity in the external circuit, so long as the currents at the anode and cathode are equal, i.e., $j(\xi = 0) = j(\xi = 1)$. Mathematically, the current nonuniformity is due to the nonuniform distributions of the carrier densities, where the electrons are skewed to the anode and holes to the cathode, and the current at the anode is dominated by that of the electrons, whereas at the cathode by the holes, as well as due to using constant $\tau$ instead of $\tau(\xi)$. Under that assumption and from Eq. (14) and Eq. (15), it follows that $dJ(\xi)/d\xi = (q/\tau)[\Delta n(\xi) - \Delta p(\xi)] \neq 0$ under an applied bias. However, in the steady state, as in the earlier mentioned SRH model, it is expected to be $\Delta n(\xi)/\tau_n(\xi) - \Delta p(\xi)/\tau_p(\xi) = 0$. Otherwise, carriers would accumulate in the trap states until the balance is reached. Thus, a more general model should

be developed to treat this issue. Since $\mu_n\tau_n = \mu_p\tau_p$, the total current maximizes at the center, as described by the analytic result below

$$j(\xi = 1/2) = l_{dr}\left[2 - \alpha\, csch\left(\frac{\alpha\beta}{2}\right) sinh\left(\frac{\beta}{2}\right) - cosh\left(\frac{\beta}{2}\right) sech\left(\frac{\alpha\beta}{2}\right)\right]. \quad (28)$$

In general, $j(\xi = 1/2) > j(\xi = 0)$, whilst the small $l_{dr}$ and $l_{di}$ values favor a large ratio of $j(\xi = 1/2)/j(\xi = 0)$, with a limit of 2. Despite in general $QE_{acc} > QE_{app}$, they approach the same limit of 1 as $l_{dr} \gg 1$, which is true even as $l_{di} \to 0$, as shown in Fig. 11(a). In the limit of $l_{di} \to 0$ and $l_{dr} \ll 1$, $QE_{acc} \to 2l_{dr}$, whereas $QE_{app} \to l_{dr}$. Here, a factor of 2 difference is because of $j_p(\xi = 1) \to l_{dr}$, but $j_n(\xi = 1) \to 0$, whereas both $j_n(\xi)$ and $j_p(\xi)$ are averaged to $l_{dr}$. On the other hand, in the limit of $l_{dr} \gg 1$, $j_p(\xi = 1) \to 1$ and $j_n(\xi = 1) \to 0$, whilst $j_n(\xi = 0) \to 1$ and $j_p(\xi = 0) \to 0$, which contradicts the commonly accepted model, in which both the electron and hole photocurrents contribute equally at each electrode. The situation is like the short circuit current calculation in a solar cell, where only one type of carrier is considered, even though a uniform carrier distribution is assumed [52].

Apparently, as in the case of the drift-only photocurrent density, the drift-diffusion photocurrent density also has two limiting cases: 1) in low-drift limit, i.e., $l_{dr} \ll 1$, the average drift photocurrent density depends linearly on the applied electric field ("Ohmic photocurrent density") and the maximum $G$ or $QE$ is less than unity; and 2) in high-drift limit, i.e., $l_{dr} \gg 1$, the average drift photocurrent density saturates to its maximum value, and, thus, $G$ or $QE$ is limited to unity. As $l_{di} \to 0$, $QE_{acc}$ and $QE_{app}$ given by Eq. (23) and Eq. (26b), respectively reduce to Eq. (8b) and Eq. (13b), which confirms correctness of results when diffusion is included in analysis.

It is interesting to compare how including or excluding diffusion effect can affect analytic results for $QE$. For very short channel lengths, when diffusion length is comparable to the channel length, i.e., $l_{di} \sim 1$ or is much longer than the channel length, i.e., $l_{di} \gg 1$, the difference between

drift-only photocurrent density vs. drift-diffusion photocurrent density in the low drift region, i.e., $l_{dr} \ll 1$ can be easily few orders of magnitude. The difference becomes more noticeable when $\tau$ or $\mu$ is being increased, and particularly when $L$ is decreased. For instance, by using following parameters: $\tau = 100\ ns$, $\mu = 500\ cm^2V^{-1}s^{-1}$, $L = 5\ \mu m$, $g = 10^{22}cm^{-3}s^{-1}$, and $T = 300\ K$, the diffusion length can be calculated as $L_{di} = 11.374\ \mu m$ or $l_{di} = 2.275$. In this case, a drift-only photocurrent density given by Eq. (12c) is about 60 times larger than a drift-diffusion photocurrent density given by Eq. (20c) when $l_{dr} \ll 1$, although $l_{di} \sim 1$. With further reduction of the size of the photoconductive device, and, thus, with increased $l_{di}$, that difference would be even more prominent. Therefore, if $l_{di} \sim 1$ or if $l_{di} \gg 1$, then it is of great importance to include the effect of a diffusion into analysis for an accurate determination of $QE$ when $l_{dr} \ll 1$. On the other hand, neglecting diffusion photocurrent densities is justified if the channel length of device is much longer than the diffusion length, i.e., $l_{di} \ll 1$.

Clearly, if only the primary photoconductivity and intrinsic devices are considered, the photodetector cannot have $G$ or $QE$ above unity, independently of the values of the device parameters even when diffusion is included in analysis. Moreover, it was shown that the presence of diffusion effect tends to reduce $QE$, more significantly for small $l_{dr}$. It should be noted that the experimentally observed gains greater than unity are not disputed in this work, however, the widely accepted gain mechanism given by Eq. (2), appears to be a consequence of an inappropriately generalized low-field-limit result of Eq. (26), at least in the case of an intrinsic photoconductive device. Finally, even though some secondary photoconductivity effects could lead to $QE$ greater than unity, it is not mathematically feasible to have the gain expressed universally as in Eq. (2).

# CHAPTER 4: QUANTUM EFFICIENCY OF DRIFT-DIFFUSION CHARGE CARRIERS – NUMERICAL RESULTS

In the previous chapters it was shown that $QE$ of an intrinsic photoconductive device is limited to unity within the primary photoconductivity. Furthermore, to assure equality of photocurrent on both ends of the photoconductive device in an analytic approach, it was necessary to assume equal mobilities of electrons and holes, i.e., $\mu_n = \mu_p$. Since this is a very special case and, typically, for the most materials $\mu_n > \mu_p$, it is necessary to extend the analytic theory assuming nonequal mobilities, i.e. $\mu_n \neq \mu_p$. However, for simplicity, the assumption of equal carrier lifetime for electrons and holes, i.e., $\tau_n = \tau_p$, is still adopted. In this case, BCs used in an analytic approach, assuming $\mu_n\tau_n = \mu_p\tau_p$, given by $\Delta n(\xi = 0) = \Delta n(\xi = 1) = 0$ and $\Delta p(\xi = 0) = \Delta p(\xi = 1) = 0$ would lead to breakdown of the charge neutrality and consequently $j(\xi = 0) \neq j(\xi = 1)$, which is not physically meaningful. Thus, for the $\mu_n > \mu_p$, the finite, non-zero BCs for electron concentrations need to be introduced, i.e., $\Delta n(\xi = 0) \neq 0$ and $\Delta n(\xi = 1) \neq 0$, which do not necessarily need to be same, whilst those for hole concentrations can be kept as zeros, i.e., $\Delta p(\xi = 0) = \Delta p(\xi = 1) = 0$.

The problem can be now solved analytically and two parameters can be determined from the two conditions: (1) charge neutrality, i.e., equality of the total electrons and holes concentrations, $\Delta n_{tot} = \Delta p_{tot}$, which is equivalent to the $\overline{\Delta n} = \int_0^1 \Delta n(\xi) d\xi = \overline{\Delta p} \int_0^1 \Delta p(\xi) d\xi$; and (2) equality of currents at the cathode and anode, i.e., $j(\xi = 0) = j(\xi = 1)$. The condition $\overline{\Delta n} = \overline{\Delta p}$ implies $QE_{acc,n} = QE_{acc,p}$. Additionally, both conditions can be satisfied even if only one of BCs for electron concentrations is non-zero, for instance, $\Delta n(\xi = 0) \neq 0$. It can be shown that these two conditions are equivalent. To show this equivalency, normalized Eqs. (17) should be integrated and equalized to set for charge neutrality condition. Further, normalized

concentration from Eq. (17a) should be set as $\Delta n(\xi = 0) \neq 0$ and $\Delta n(\xi = 1) = 0$. To satisfy the second condition, the normalized Eqs. (14) should be equalized. After setting up these conditions and lengthy algebraic calculations, it can be shown that the condition of $j(\xi = 0) = j(\xi = 1)$ is indeed equivalent to the condition $\overline{\Delta n} = \overline{\Delta p}$.

To obtain the analytic solutions of drift-diffusion equations, another major approximation adopted in Ch. 3 was $\partial \mathrm{E}/\partial \mathrm{x} = 0$. Here, the effect of the inhomogeneity of the electric field caused by the relative displacement of the electron and hole distributions, i.e., $\Delta n(x) - \Delta p(x) \neq 0$ is examined, whilst a polarization effect is induced by the applied field $E_0 = V/L$. If the total field is written as $E(x) = E_0 + \delta E(x)$, the change in the $E$ field $\delta E(x)$ can be expressed in terms of a potential $\phi(x)$ through $\delta E(x) = -d\phi(x)/dx$. By using following BCs: $\Delta n(\xi = 0) \neq 0$, $\Delta n(\xi = 1) = 0$, $\Delta p(\xi = 0) = 0$, $\Delta p(\xi = 1) = 0$, $\phi(\xi = 0) = 0$, and $\phi(\xi = 1) = 0$, the following system of three equations can be solved

$$\frac{\partial^2(\Delta n(\xi))}{\partial \xi^2} + \frac{l_{dr,n,0}}{l_{di,n}^2}\frac{\partial(\Delta n(\xi))}{\partial \xi} - k\left(\frac{\partial(\Delta n(\xi))}{\partial \xi}\frac{\partial \phi(\xi)}{\partial \xi} + \Delta n(\xi)\frac{\partial^2 \phi(\xi)}{\partial \xi^2}\right) - \frac{\Delta n(\xi)}{l_{di,n}^2} + \frac{1}{l_{di,n}^2} = 0, \tag{29a}$$

$$\frac{\partial^2(\Delta p(\xi))}{\partial \xi^2} - \frac{l_{dr,p,0}}{l_{di,p}^2}\frac{\partial(\Delta p(\xi))}{\partial \xi} + k\left(\frac{\partial(\Delta p(\xi))}{\partial \xi}\frac{\partial \phi(\xi)}{\partial \xi} + \Delta p(\xi)\frac{\partial^2 \phi(\xi)}{\partial \xi^2}\right) - \frac{\Delta p(\xi)}{l_{di,p}^2} + \frac{1}{l_{di,p}^2} = 0, \tag{29b}$$

$$\frac{\partial^2(\phi(\xi))}{\partial \xi^2} - \frac{(\Delta n(\xi) - \Delta p(\xi))}{l_D^2} = 0, \tag{29c}$$

where $l_{dr,n,0}$ and $l_{dr,p,0}$ are, respectively, the drift lengths determined solely by the externally applied field, whilst $k = 0$ or $k = 1$ respectively indicates negligence or inclusion the polarization term $\partial \mathrm{E}/\partial \xi$. Evidently, the polarization effect is sensitive to the Debye length $l_D$ and diminishes when $l_D$ is very large. Solving coupled nonlinear equations for arbitrary $l_D$ is generally challenging. Here, the goal is to understand the potential impact of this effect by assuming a relatively large $l_D$ or small $g\tau$ value. The following system of equations can be solved by using an iterative approach for $k = 1$ or $\partial \mathrm{E}/\partial \xi \neq 0$

$$\frac{\partial^2(\Delta n_i(\xi))}{\partial \xi^2} + \frac{l_{dr,n}}{l_{di,n}^2}\frac{\partial(\Delta n_i(\xi))}{\partial \xi} - k\left(\frac{\partial(\Delta n_i(\xi))}{\partial \xi}\frac{\partial \phi_s(\xi)_{i-1}}{\partial \xi} + \Delta n_i(\xi)\frac{\partial^2 \phi_s(\xi)_{i-1}}{\partial \xi^2}\right) - \frac{\Delta n_i(\xi)}{l_{di,n}^2} + \frac{1}{l_{di,n}^2} = 0, \quad (30a)$$

$$\frac{\partial^2(\Delta p_i(\xi))}{\partial \xi^2} - \frac{l_{dr,p}}{l_{di,p}^2}\frac{\partial(\Delta p_i(\xi))}{\partial \xi} + k\left(\frac{\partial(\Delta p_i(\xi))}{\partial \xi}\frac{\partial \phi_s(\xi)_{i-1}}{\partial \xi} + \Delta p_i(\xi)\frac{\partial^2 \phi_s(\xi)_{i-1}}{\partial \xi^2}\right) - \frac{\Delta p_i(\xi)}{l_{di,p}^2} + \frac{1}{l_{di,p}^2} = 0, \quad (30b)$$

$$\frac{\partial^2(\phi_{s,i}(\xi))}{\partial \xi^2} - \frac{(\Delta n_{i-1}(\xi) - \Delta p_{i-1}(\xi))}{l_D^2} = 0, \quad (30c)$$

where $i$ represents the order of iterations. Thus, this system of equations is only possible to be solved numerically and iteratively, i.e., first using the zero-order carrier concentrations $\Delta n_0(\xi)$ and $\Delta p_0(\xi)$ to solve for the potential $\phi_0(\xi)$, then, using $\phi_0(\xi)$ to solve for $\Delta n_1(\xi)$ and $\Delta p_1(\xi)$, and repeating process until they converge. For the case of $\mu_n = \mu_p$ and $\tau_n = \tau_p$, the charge neutrality condition $\overline{\Delta n} = \overline{\Delta p}$ is satisfied automatically when the polarization effect is considered. However, for the case of $\mu_n \neq \mu_p$, $\Delta n(\xi = 0)$ needs to be adjusted in each iteration to maintain the charge neutrality $\overline{\Delta n} = \overline{\Delta p}$. Thus, firstly, by assuming $k = 0$, $\Delta n_0(\xi)$ and $\Delta p_0(\xi)$ are obtained with $\Delta n(\xi = 0)$ that satisfies $\overline{\Delta n_0} = \overline{\Delta p_0}$. Then, by using the $\Delta n(\xi)$ and $\Delta p(\xi)$ it is possible to solve for the potential $\phi_0(\xi)$; then solve for $\Delta n_1(\xi)$ and $\Delta p_1(\xi)$ by using the potential $\phi_0(\xi)$, but this yields $\overline{\Delta n_1} \neq \overline{\Delta p_1}$. However, $\Delta n(\xi = 0)$ can be adjusted such that a new $\Delta n(\xi = 0)$ is found to achieve $\overline{\Delta n_1} = \overline{\Delta p_1}$. This can be done by solving the equation with a few $\Delta n(\xi = 0)$ values, then perform linear interpolation to find the desirable $\Delta n(\xi = 0)$ value. The process can be repeated iteratively to reach the expected accuracy. By using this approach, Figs. 13(a) and 13(b) plot normalized electron and hole distributions $\delta n(\xi)$ and $\delta p(\xi)$, respectively, vs. normalized distance $\xi$, for different $(l_{dr}, l_{di})$ combinations. In Fig. 13(a), black and red curves represent solution for $k = 0$ and $k = 1$ after 10 iterations, respectively, for $(l_{dr,n}, l_{di,n}) = (0.40, 0.20)$ and $(l_{dr,p}, l_{di,p}) = (0.10, 0.10)$. The corresponding non-zero BCs at $\Delta n(\xi = 0)$ for black and red curves are 3.2774 and 3.1361, respectively. After increasing mobilities of electrons and holes both

by 10 times, $(l_{dr}, l_{di})$ combinations become $(l_{dr,n}, l_{di,n}) = (4.00, 0.63)$ and $(l_{dr,p}, l_{di,p}) = (1.00, 0.32)$. The corresponding non-zero BCs at $\Delta n(\xi = 0)$ are now 2.0385 and 1.9926, for $k = 0$ and $k = 1$ after 10 iterations, for blue and magenta curves, respectively. It should be noted that after normalization, the concentration of electrons can be above unity value, as shown in Fig. 13(a). However, as expected, the maximum concentration of holes does not cross unity value, as shown in Fig. 13(b), since $\Delta p(\xi = 0) = \Delta p(\xi = 1) = 0$. In all cases, $l_D = 0.3$ is used, which corresponds to, for instance, $g = 10^{22} cm^{-3} s^{-1}$, $\tau = 2.067\ ns$, $L = 3\ \mu m$, $T = 300\ K$ for Si ($\varepsilon = 11.7$).

To find currents $j(\xi)$ for $k = 0$, the following system of equations, given below, needs to be solved

$$j_n(\xi) = l_{dr,n,0} \Delta n_0(\xi) + l_{di,n}^2 \frac{\partial(\Delta n(\xi))}{\partial \xi}, \tag{31a}$$

$$j_p(\xi) = l_{dr,p,0} \Delta p_0(\xi) + l_{di,p}^2 \frac{\partial(\Delta p(\xi))}{\partial \xi}, \tag{31b}$$

$$j(\xi) = j_n(\xi) + j_p(\xi), \tag{31c}$$

whilst the similar set of equations given below should be solved for $k = 1$ to calculate the corresponding current after $i$ number of iterations

$$j_{n,i}(\xi) = l_{dr,n,0} \left(1 - \frac{l_{di,n}^2}{l_{dr,n,0}} \phi_{i-1}(\xi)\right) \Delta n_i(\xi) + l_{di,n}^2 \frac{\partial(\Delta n_i(\xi))}{\partial \xi}, \tag{32a}$$

$$j_{p,i}(\xi) = l_{dr,p,0} \left(1 - \frac{l_{di,p}^2}{l_{dr,p,0}} \phi_{i-1}(\xi)\right) \Delta p_i(\xi) + l_{di,p}^2 \frac{\partial(\Delta p_i(\xi))}{\partial \xi}, \tag{32b}$$

$$j_i(\xi) = j_{n,i}(\xi) + j_{p,i}(\xi). \tag{32c}$$

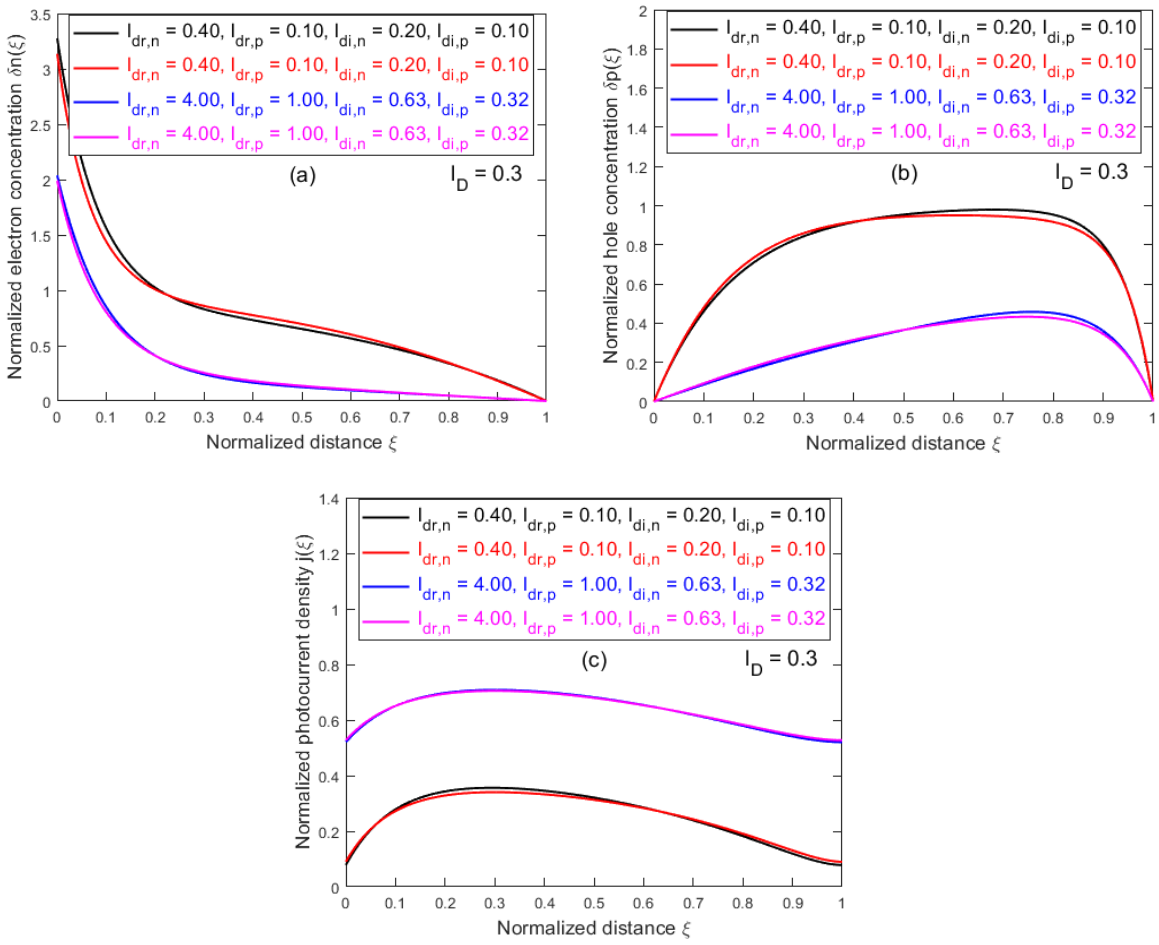


Figure 13: (a) Normalized electron concentration $\delta n(\xi)$ vs. normalized distance $\xi$ for different $(l_{dr}, l_{di})$ combinations; (b) Normalized hole concentration $\delta p(\xi)$ vs. normalized distance $\xi$ for different $(l_{dr}, l_{di})$ combinations; and (c) Normalized photocurrent density $j(\xi)$ vs. normalized distance $\xi$ for different $(l_{dr}, l_{di})$ combinations

Fig. 13(c) plots normalized photocurrent density $j(\xi)$ vs. normalized distance $\xi$, for previous parameters. As expected, $j(\xi = 0) = j(\xi = 1)$, with values of 0.0785, 0.0902, 0.5205, and 0.5274, for black, red, blue, and magenta curves, respectively. When $\mu_n = \mu_p$, the total current is symmetrical and maximizes at the center, as shown in Figs. 12. However, when $\mu_n \neq \mu_p$, the

current distribution becomes asymmetric with respect to the center and tilts up on the side closer to the electrode at which the current is dominated by the larger-mobility species (e.g., when $\mu_n > \mu_p$, the anode side raises relatively to the cathode side).

Another goal of this work is to study the polarization effect in more detail. Since a larger Debye length $l_D$ implies smaller polarization effect, a reasonably large $l_D$ should be set, for instance greater than 0.1, for which the iterative approach for currents could work. Here, it is possible to solve problem iteratively by assuming $\partial \mathrm{E}/\partial\xi \neq 0$, as long as $l_D$ is not too small, e.g., $l_D > 0.1$, but also not too large to avoid $\partial \mathrm{E}/\partial\xi = 0$ and, thus, negligible polarization term. For $k = 0$, $\partial \mathrm{E}/\partial\xi = 0$ results are as those in analytical model. However, to solve for $\Delta n(\xi)$ and $\Delta p(\xi)$ numerically, $k = 1$ includes the polarization term $\partial \mathrm{E}/\partial\xi$. It is interesting to find a normalized photocurrent density $j(\xi)$ by changing $l_D$, at fixed $(l_{dr}, l_{di})$.

Fig. 14(a) shows normalized $j(\xi)$ vs. normalized $\xi$ at $(l_{dr,n}, l_{di,n}) = (l_{dr,p}, l_{di,p}) = (0.2, 0.1)$ for $l_D = 0.1, 0.2, 0.3$ and 0.4. Reducing $l_D$ or increasing carrier generation rate $g$ reduces $QE_{acc}$, calculated as the average of all currents across the normalized distance $\xi$ at particular $l_D$, as shown in Fig. 14(b). However, reducing $l_D$ has an opposite effect on $QE_{app}$, i.e., it increases with reduction of $l_D$, which can be seen from Fig. 14(a) at $\xi = 0$ or $\xi = 1$ or from Fig. 14(c).

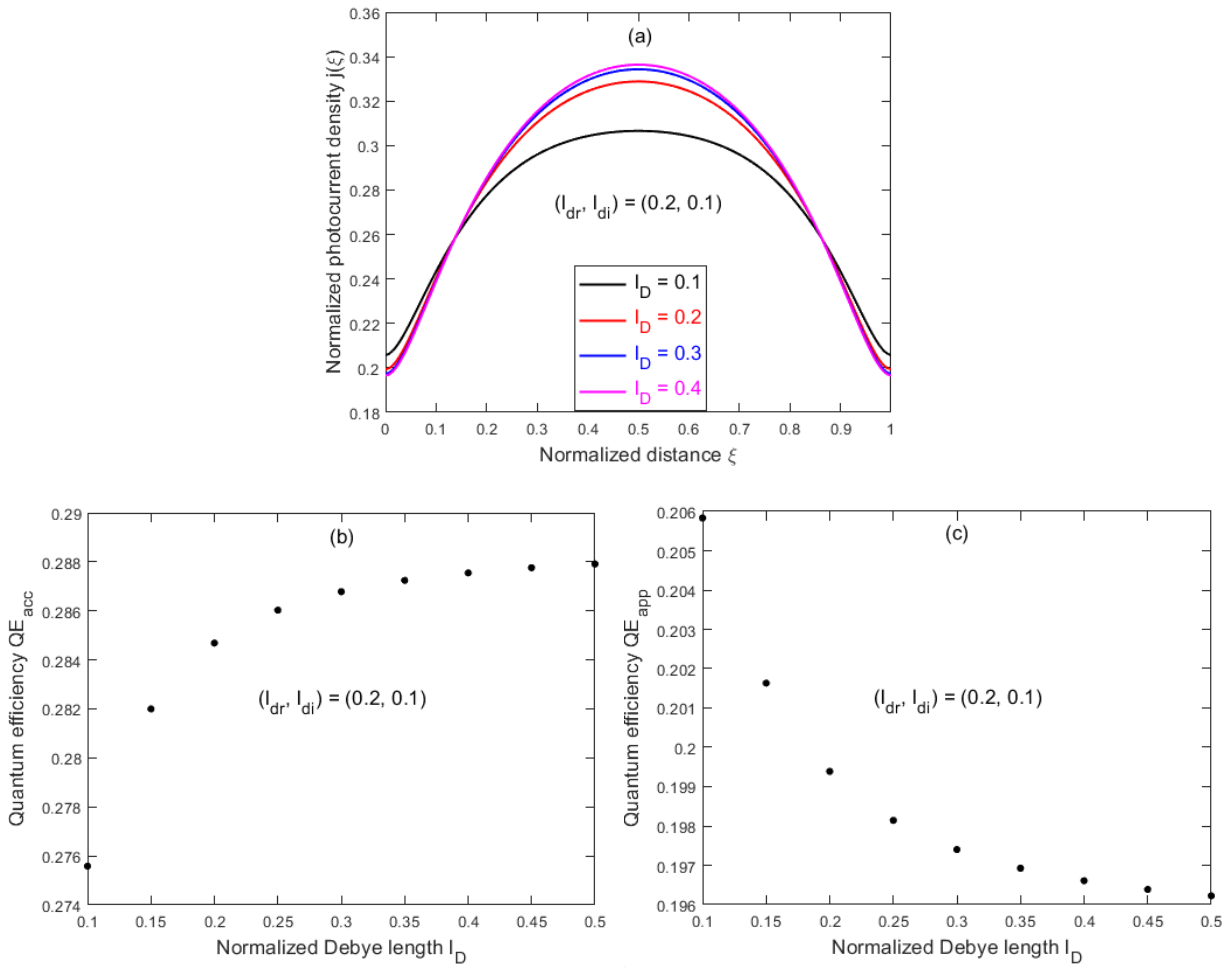


Figure 14: (a) Normalized photocurrent density $j(\xi)$ vs. normalized distance $\xi$ for different normalized Debye lengths $l_D = (0.1, 0.2, 0.3, 0.4)$ and for $(l_{dr}, l_{di}) = (0.2, 0.1)$; (b) $QE_{acc}$ vs. normalized Debye length $l_D$ for $(l_{dr}, l_{di}) = (0.2, 0.1)$; and (c) $QE_{app}$ vs. normalized Debye length $l_D$ for $(l_{dr}, l_{di}) = (0.2, 0.1)$

It should be noted that for $\mu_n \neq \mu_p$, ratio of current at $\xi = 1/2$ and current at one or at another end of device, i.e., $j(\xi = 0)$ or $j(\xi = 1)$, is much larger than that in the case of $\mu_n = \mu_p$. This effect can be explained by the enhanced modulation, which can be understood as result of interplay of the drift and polarization terms. The drift effect tends to drag the electrons and holes,

respectively, to the opposite electrodes, whereas the polarization term makes them attract each other. Therefore, the net effect is to make both types of carriers stay closer to the center compared to the case without the polarization term. The effect is more significant for the weak field, like the effect of diffusion. Although the polarization effect and diffusion have the similar effects on the carrier distributions, their impacts to the $QE_s$ are different: the former affects mostly the internal distribution within the channel, whereas the latter directly affects the current flow to the electrodes.

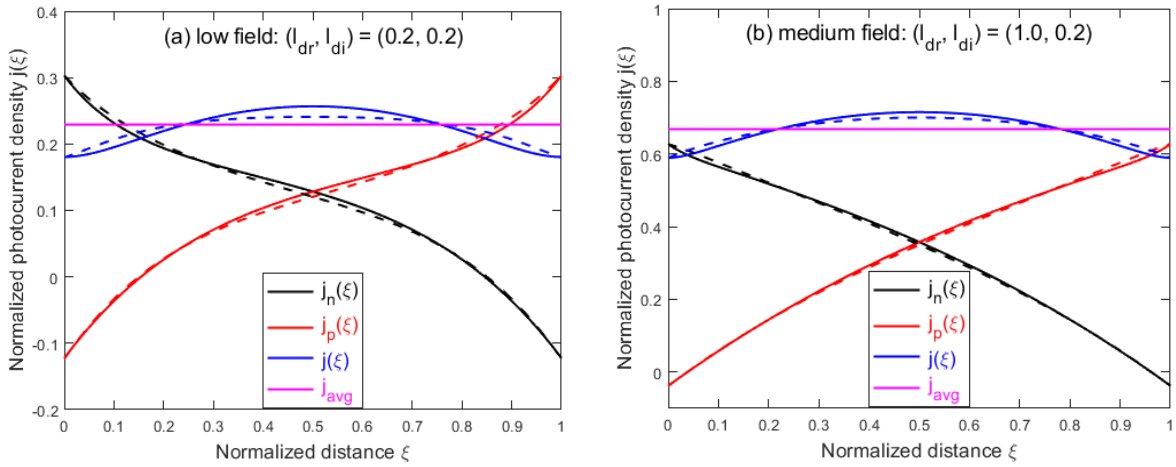


Figure 15: The total normalized photocurrent density $j(\xi)$, electron component $j_n(\xi)$ and hole component $j_p(\xi)$ vs. normalized distance $\xi$, compared to the average photocurrent density $j_{avg}$ for two different $(l_{dr}, l_{di})$ combinations: (a) low field $(0.2, 0.2)$; and (b) medium field $(1.0, 0.2)$. Dashed lines represent $j(\xi)$ for $k = 0$, whilst the solid lines represent $j(\xi)$ for $k = 1$ after 10 iterations.

After introducing possibility of solving problems with the polarization term $\partial \mathrm{E}/\partial\xi$, it is important to compare spatially nonuniform currents without the polarization term $\partial \mathrm{E}/\partial\xi$ included or $k = 0$ and with the polarization term $\partial \mathrm{E}/\partial\xi$ included or $k = 1$ and $n = 10$. The results are

shown in Figs. 15, for two different $(l_{dr}, l_{di})$ combinations. It should be noted from the same figure that with increasing normalized drift length $l_{dr}$, the current with the polarization term $\partial \mathrm{E}/\partial \xi$ approaches the one without the polarization term $\partial \mathrm{E}/\partial \xi$. Thus, it is important to include polarization term $\partial \mathrm{E}/\partial \xi$ at low $l_{dr}$ to get more accurate value of spatial photocurrent density.

# CHAPTER 5: QUANTUM EFFICIENCY OF DRIFT-DIFFUSION CHARGE CARRIERS – SIMULATION RESULTS

In this chapter, numerical simulations by using the Drift-Diffusion Lab simulation tool from NanoHub [53] are performed, to examine the polarization effects and how $\mu_n \neq \mu_p$ may affect the analytic results. Firstly, by assuming $\mu_n = \mu_p$ and $\tau_n = \tau_p$, it is examined how the polarization effect might affect the carrier distributions. Germanium (Ge) is selected as the active material with following parameters: $\mu = 1\ cm^2V^{-1}s^{-1}$ and $\mu = 10\ cm^2V^{-1}s^{-1}$, $\tau = 10\ ns$, $L = 3\ \mu m$, $g = 10^{20}cm^{-3}s^{-1}$, $T = 300\ K$, and $s = 10^{20}cms^{-1}$, which is the largest possible value allowed. Although in the simulator $s$ is meant to be the surface recombination velocity, we take it as the carrier extraction velocity that is assumed to be infinite in the analytic model. Figs. 16(a)-(d) plot $\Delta n(x)$ and $\Delta p(x)$ with $(\mu_n, \mu_p) = (1, 1)\ cm^2V^{-1}s^{-1}$ and $(\mu_n, \mu_p) = (10{,}10)\ cm^2V^{-1}s^{-1}$, respectively. The simulation results (solid curves) are compared to those obtained from the analytic model (dashed curves). As shown in the Figs. 16, for a small applied voltage (e.g., 0.1 V), the impact of $\partial$E/$\partial$x is relatively large, but the effect diminishes for larger applied voltages (e.g., $>$ 1.0 V). From the analytic model, one can find that under a large bias, the carrier density is inversely proportional to the carrier mobility.

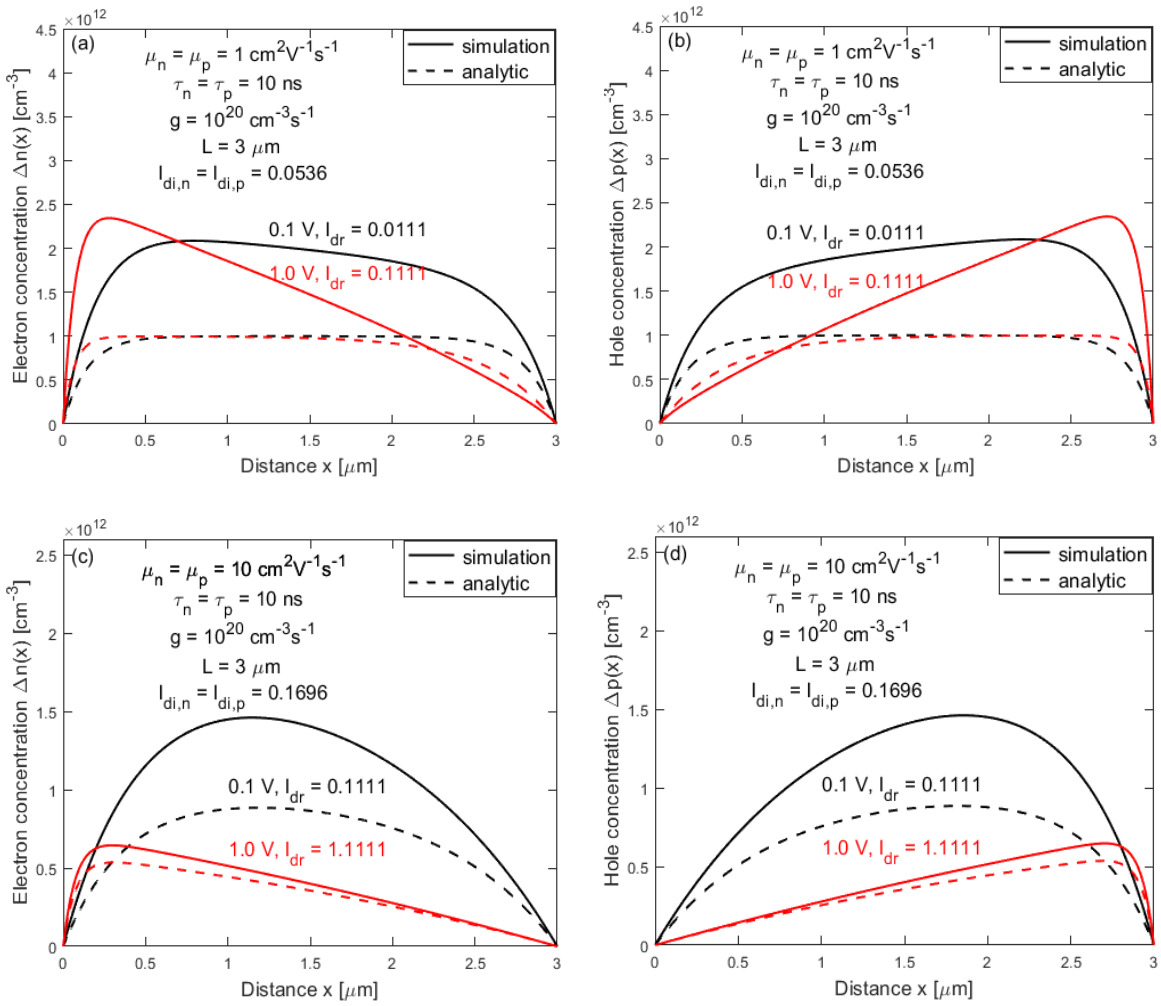


Figure 16: Comparison of spatial distributions of photogenerated carriers $\Delta n(x)$ and $\Delta p(x)$, respectively, for two applied voltages, 0.1 V and 1.0 V: (a) and (b) for $(\mu_n, \mu_p) = (1,1)\ cm^2V^{-1}s^{-1}$; (c) and (d) for $(\mu_n, \mu_p) = (10,10)\ cm^2V^{-1}s^{-1}$

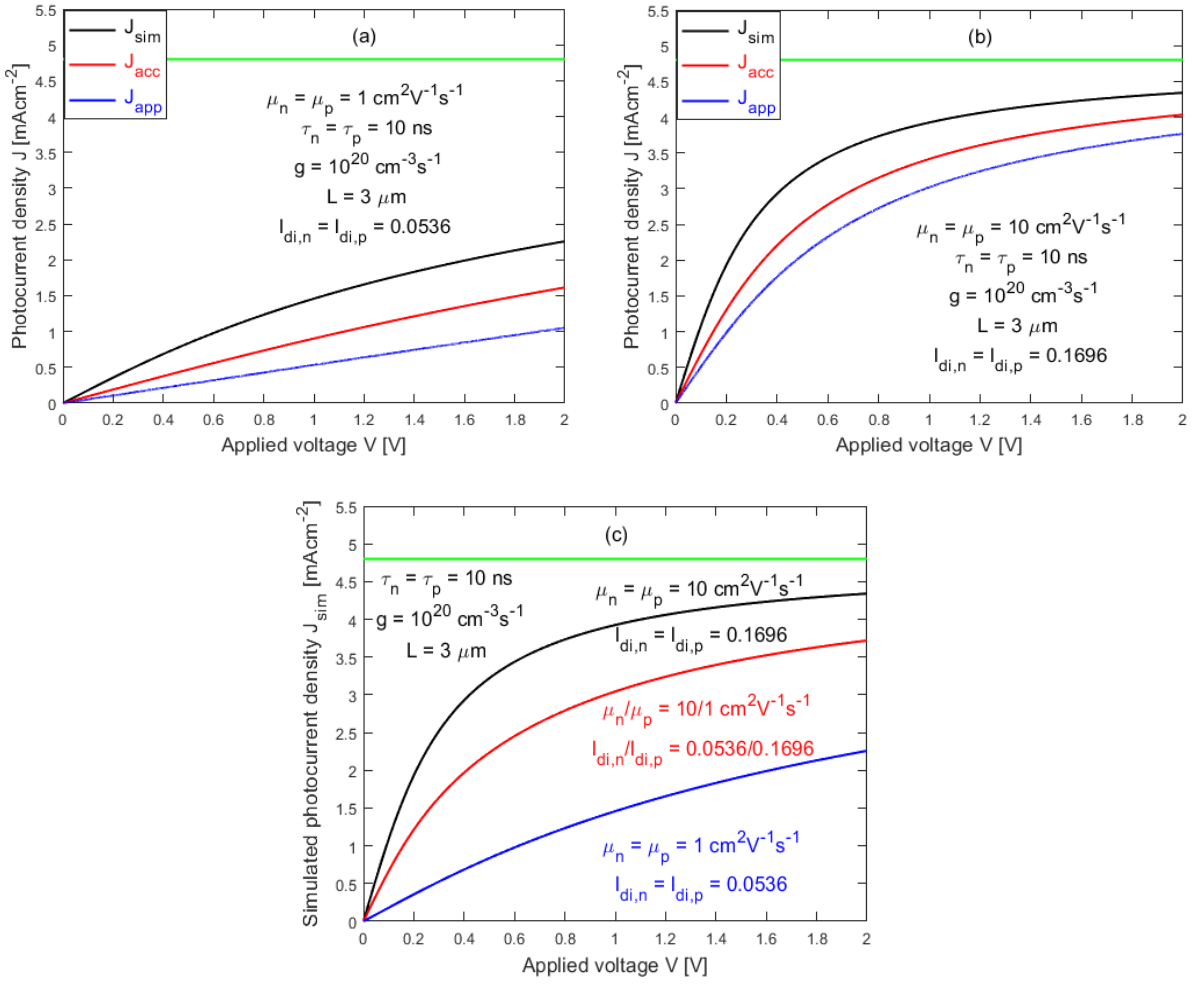


Figure 17: Photocurrent density $J$ vs. applied voltage $V$ for comparison of the simulated results $J_{sim}$ (black curves) and analytic results: $J_{acc}$ (red curves) and $J_{app}$ (blue curves), for different combinations of mobility parameters $(\mu_n, \mu_p)$: (a) $(1,1)\ cm^2V^{-1}s^{-1}$; (b) $(10,10)\ cm^2V^{-1}s^{-1}$; and (c) $J_{sim}$ for $(1,1)\ cm^2V^{-1}s^{-1}$, $(10,1)\ cm^2V^{-1}s^{-1}$, and $(10,10)\ cm^2V^{-1}s^{-1}$, respectively. The green lines represent the maximum photocurrent density $J_{max} = qgL = 4.8\ mAcm^{-2}$.

Secondly, the polarization effect on the *J-V* characteristic is examined. For the same parameters, Figs. 17(a)-(b) plot the *J-V* curves of the simulated results $J_{sim}$ (black curves),

comparing with the analytic results: $J_{acc}$ (red curves), where the average currents correspond to $QE_{acc}$ and $J_{app}$ (blue curves), and where $J(x = 0)$ or $J(x = L)$ correspond to $QE_{app}$. In all cases, it is found $J_{sim} > J_{acc} > J_{app}$, but they all approach the unity limit when $l_{dr}$ is large. Furthermore, as mobilities increases from (1, 1) $cm^2V^{-1}s^{-1}$ to (10, 10) $cm^2V^{-1}s^{-1}$, as shown in Fig. 17(a) and (b), respectively, device enters into the saturation faster, but also $J_{app} \rightarrow J_{acc} \rightarrow J_{sim}$ in low-drift limit, which indicates that analytic model is more accurate for larger $(l_{dr}, l_{di})$ combinations.

Overall, the numerical simulations which include the polarization term do not result in qualitative differences from the analytic model, but do exhibit significant quantitative differences, particularly for the cases of small $l_{dr}$ values, for instance, in Fig. 16 when $l_{dr} \ll 1$. Fig. 17(c) indicates that if $\mu_n \neq \mu_p$, the photocurrent is smaller than that with the equal mobility values of the larger one. Therefore, even without making the $dE/dx = 0$ approximation, the $\mu_n = \mu_p$ case still offers higher $QE$ than $\mu_n \neq \mu_p$ case, yet obeying the unity limit.

Thirdly, the impact of the polarization effect on the spatial variation of the photocurrent is examined. By using the simulated carrier densities in Fig. 16, the spatial variation of the photocurrents is calculated by using Eqs. (14), in which the electric field $E(x)$ is obtained by integrating Eq. (15c), while keeping the same voltage difference between the electrode as the applied voltage. The results are shown in Fig. 18 (solid curves), in comparison with the results of the analytic model (dashed curves). Out of 150 data points, the last two data points closest to the respective electrode are found unreliable due to the singularity in taking derivative using the numerical data, and, thus, they have been omitted in the plots. However, the extrapolated values to the electrodes are close to the direct current outputs of the simulations. Thus, the current values from the *J-V* curves in Fig. 17 are used for the end points at $x = 0$ and $x = L$. Clearly, the total current remains nonuniform, with a maximum at the center, with comparable modulation

amplitudes compared to the analytic results, as shown in Figs. 18(a)-(b). As expected, as the applied voltage increases from 0.1 V to 2.0 V, currents tend to be more uniform, and differences in magnitude between analytic and simulated curves become smaller. For instance, from the analytic model, the ratios between the maximum and minimum point are found to be 1.611, 1.205, and 1.108, compared to 1.382, 1.099, and 1.050 from the simulations, for 0.1 V, 1.0 V, and 2.0 V, respectively. As predicted by the analytic model, from Eq. (26b) and Eq. (28), the modulation amplitude reduces with increasing $l_{dr}$: from 0.111, 1.111, to 2.222, for 0.1 V, 1.0 V, and 2.0 V, with a constant, relatively small $l_{di} = 0.17$. Besides the systematically larger $J_{sim}(x)$ compared to that of the analytic model $J_{app}(x)$, the simulated results show upward bending near the end points. Due to the bending, the difference between $QE_{acc}$ and $QE_{app}$ is reduced compared to the analytic model: for 0.1 V, $QE_{acc} = 0.227$ and $QE_{app} = 0.226$; for 1.0 V, $QE_{acc} = 0.820$ and $QE_{app} = 0.818$, and for 2.0 V, $QE_{acc} = 0.908$ and $QE_{app} = 0.904$. Nonuniform spatial variations of the drift and diffusion components of photocurrent density are also shown in Figs. 18(c)-(d) for $J(x)$ (blue curves), $J_{dr}(x)$ (black curves), and $J_{di}(x)$ (red curves) for mobility parameters $(\mu_n, \mu_p) = (10, 10)\ \ cm^2V^{-1}s^{-1}$ and different voltages and 0.1 V and 1.0 V, respectively. It should be noted that $J_{dr}(x) = 0$ at both ends of device, i.e., at $x = 0$ and $x = L$ whilst $J_{di}(x)$ reaches its maximum, and thus $J(x) = J_{di}(x)$. On the other hand, $J_{dr}(x)$ reaches its maximum at $x = L/2$, whilst $J_{di}(x)$ reaches its minimum. Nonuniformity of photocurrent is a consequence of using a simplified analytic model and is contrast to the continuous currents throughout the circuit. For instance, in p-i-n solar cell structures, it is pointed out that near the interfaces, an increase of the drift current is balanced by an increase of the diffusion current, and thus, the total current is found to be spatially uniform [54].

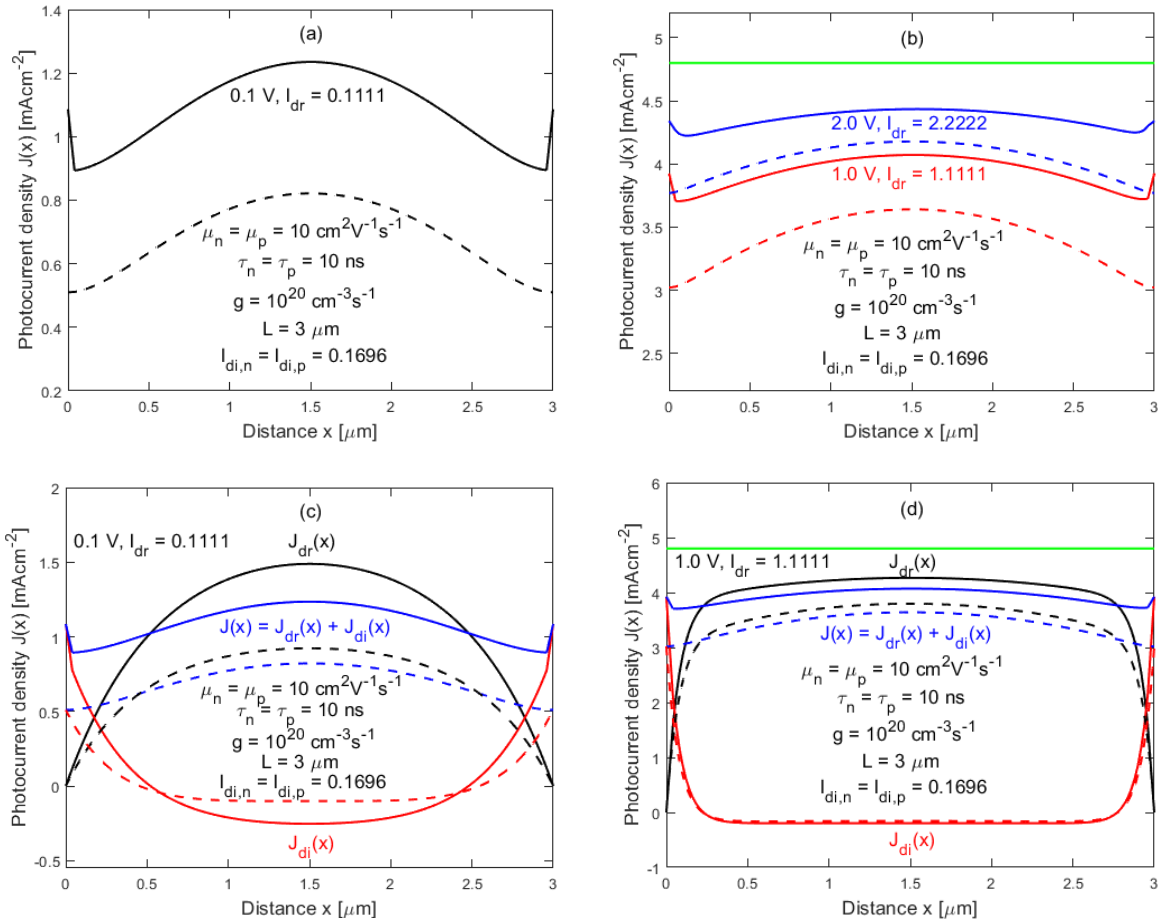


Figure 18: Spatial variations of the photocurrent density $J(x)$ for mobility parameters $(\mu_n, \mu_p) = (10, 10)\ cm^2V^{-1}s^{-1}$ and different voltages: (a) 0.1 V; (b) 1.0 V and 2.0 V. Spatial variations of the photocurrent densities $J(x)$ (blue curves), $J_{dr}(x)$ (black curves), $J_{di}(x)$ (red curves), for mobility parameters $(\mu_n, \mu_p) = (10, 10)\ cm^2V^{-1}s^{-1}$ and for different voltages: (c) 0.1 V; (d) 1.0 V. Solid lines represent simulated results, dashed lines represent analytic results, whilst the green lines represent the maximum photocurrent density $J_{max} = qgL = 4.8\ mAcm^{-2}$.

It should be noted that the differences between analytic and simulation results are not simply due to whether the polarization term is included. The simulator considers other effects, such as the carrier density and field dependence of the mobility, however, it also uses the simplified

assumption of constant carrier lifetime, which as pointed out earlier should be spatially dependent. Therefore, even using same constant mobilities and lifetimes for the electrons and holes, the relationship $\Delta n(\mathrm{x}) = \Delta p(L - x)$, predicted by the analytic model, is often found invalid for the simulated results. Concerted efforts have been made for identifications of parameters which ensure that the charge neutrality condition in the photoconductive channel is nearly satisfied. Furthermore, the use of a constant carrier lifetime as an approximation implies that the carrier density of the trap states is much smaller than that of the free carriers [55]. A more comprehensive model should be developed in the future to explicitly treat the occupation level of the trap states [54, 55]. Additionally, parameters are selected to weaken the polarization effect. For cases considered in Fig. 18, $l_D = 1.604$, thus, the polarization effect is expected to be relatively small.

Carrier trapping is often cited as the reason for increasing the carrier lifetime, and thus, greater-than-unity gain [22]. Typically, the trapping of carriers by defect centers, through which they return to the ground states, shortens $\tau_c$ and has a detrimental effect on $QE$ [43]. Here, it is pointed out that even in the case that the trapped carriers do not deplete from the trapped states, thus, can be released back to the free states with a time delay, only transient gain could potentially be achieved if the trapping time is shorter than the reemission time. However, under continuous illumination, the trapping rate and reemission rate eventually reach a balance [55], thus, no gain should be expected. This case is not too much different from a high-quality, indirect bandgap material that has a long $\tau_c$, but if it is intrinsic, no gain should be expected in the framework of the primary photoconductivity. In fact, although non-recombination traps could increase $\tau_c$, they might also increase $\tau_t$, thus, such traps do not necessarily lead to gain, even by using Eq. (2) [25]. However, for a doped structure, photogenerated carriers might alter the carrier distribution of the dopants, which may result in the change of the depletion region and yield above unity gain [3, 5,

56]. Therefore, to explain the experimentally observed $QE_s$ above unity, it is necessary to consider the possible secondary photoconductivity mechanisms.

# CHAPTER 6: QUANTUM EFFICIENCY OF DOPED PHOTOCONDUCTIVE DEVICE – SIMULATION RESULTS

Often, photoconductive devices involve doped semiconductors [3, 5], where work based on numerical simulations concluded that a doped photoconductive device can only have a modest gain, limited by the ratio of mobilities of majority to minority carriers, i.e., $\mu_{maj}/\mu_{min}$. Again, by using the Drift-Diffusion Lab simulation tool from NanoHub [53], carrier distributions of minority (electron) carrier concentrations under *p*-type doping for Si based semiconductor slab are shown in Figs. 19. Here, four different levels of applied voltages $\mathrm{V} = 0.1, 0.5, 1.0, 2.0\ V$ are used, with a doping level equal to $10^{17} cm^{-3}$, as well as following parameters: $\tau = 200\ ns$, $L = 50\ \mu m$, $g = 10^{22} cm^{-3} s^{-1}$, $s = 10^{20} cms^{-1}$, $T = 300\ K$, and $\mu_n = 875\ cm^2 V^{-1} s^{-1}$, for four different mobility values of holes: $\mu_p = (337, 875, 1700, 2700)\ cm^2 V^{-1} s^{-1}$. It should be noted that the carrier distributions of the majority carrier concentrations (holes) are the same and follow distributions of minority carrier concentrations (electrons), i.e., $\Delta n(x) = \Delta p(x)$. The results show that there is a better agreement between analytic and simulation results for a larger ratio of majority to minority carrier concentrations.

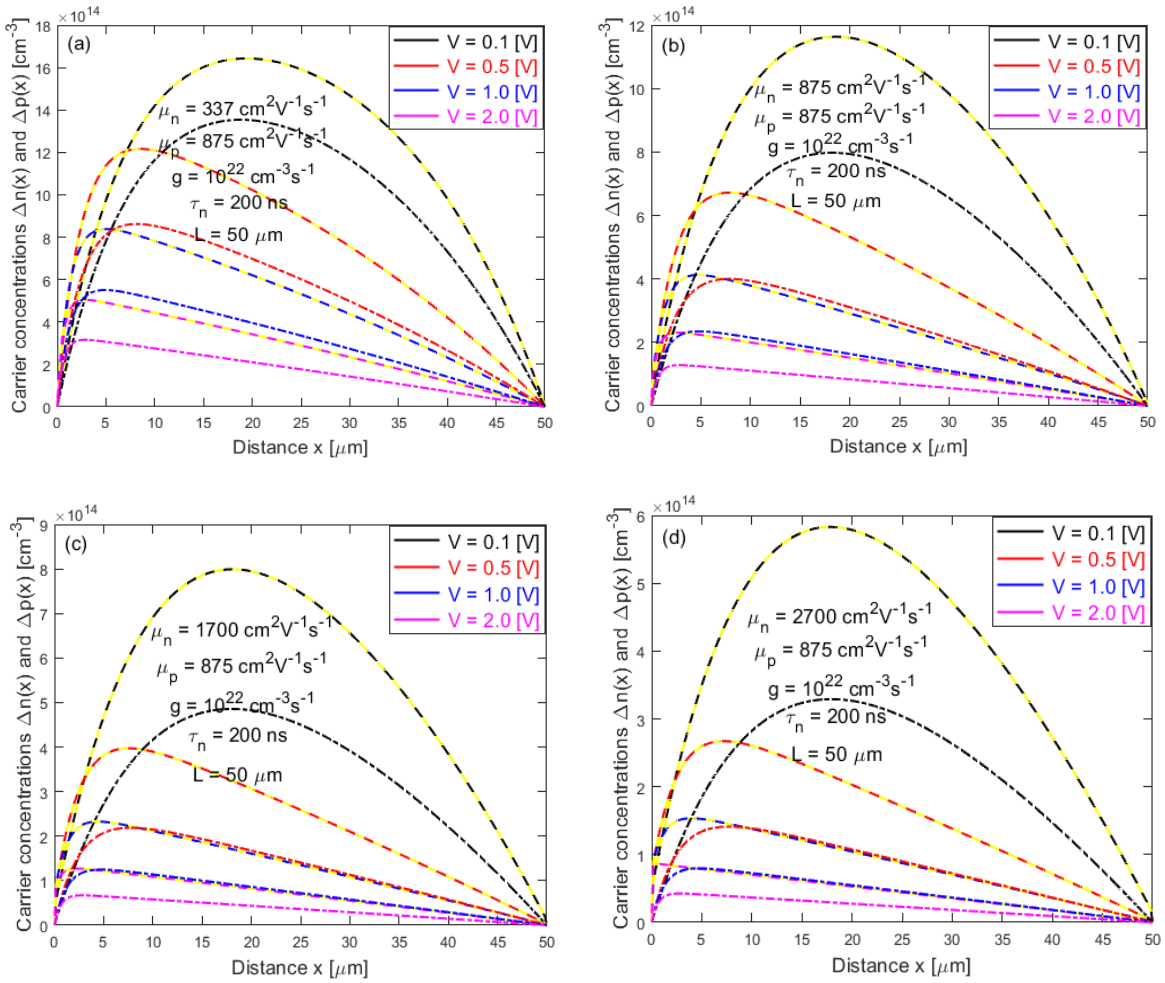


Figure 19: Spatial distributions of photogenerated minority (electron) carrier concentrations $\Delta n(x)$ under $p$-type doping concentration of $10^{17} cm^{-3}$, for different levels of applied voltages $0.1\ V, 0.5\ V, 1.0\ V, 2.0\ V$ and for different combinations of mobility parameters: (a) $(\mu_n, \mu_p) = (337, 875)\ cm^2V^{-1}s^{-1}$ ; (b) $(\mu_n, \mu_p) = (875, 875)\ cm^2V^{-1}s^{-1}$ ; (c) $(\mu_n, \mu_p) = (1700, 875)\ cm^2V^{-1}s^{-1}$; and (d) $(\mu_n, \mu_p) = (2700, 875)\ cm^2V^{-1}s^{-1}$. Simulated results of minority carriers (electrons) are represented by solid lines, simulated results of majority carriers (holes) are represented by yellow dashed lines, whilst analytic results are represented by dash-dotted lines.

When doping is used, it is indeed possible to achieve small gains [3, 5], limited by the ratio of majority to minority carrier mobilities, as shown by magenta and blue *J*-*V* curves in Fig 20. Furthermore, if mobilities are the same for the minority and majority carriers, the maximum gain is limited to unity even with doping, as shown by the red curve in Fig. 20. Finally, if the mobility of majority carriers is smaller than the mobility of minority carriers, the photocurrent saturates below the maximum value and the gain is smaller than unity, as shown by the black curve in Fig. 20. The upper limit of the gain with doping is suggested to be given by [3]

$$G_{max,p} = \frac{1}{2}\left(1 + \frac{\mu_p}{\mu_n}\right), \tag{33a}$$

and

$$G_{max,n} = \frac{1}{2}\left(1 + \frac{\mu_n}{\mu_p}\right), \tag{33b}$$

for *p*-type and *n*-type doping, respectively.

Since the upper limit of gain under high electric field is given in [3], it would be interesting to find if it is possible to obtain the analytic solution for gain over the whole drift region, as well as in the low drift region. In case of $J_{acc}$, by using Eq. (20a), it is possible to introduce effective carrier lifetime of minority carrier concentrations, for instance electrons in case of *p*-type of doping, as given below

$$\tau_{n,eff} = \tau_n \left\{1 - \frac{1}{L}\left[\frac{1}{\lambda_1} - \frac{1}{\lambda_2}\right]\frac{[1-exp(-L\lambda_1)][1-exp(-L\lambda_2)]}{exp(-L\lambda_2)-exp(-L\lambda_1)}\right\}. \tag{34}$$

From Eq. (34), it can be noted that the effective carrier lifetime of minority carriers is not constant. It considers not only minority carrier lifetime, but also device length $L$, as well as $\lambda_1$ and $\lambda_2$, which further depend on drift and diffusion lengths, $L_{dr,n}$ and $L_{di,n}$, respectively.

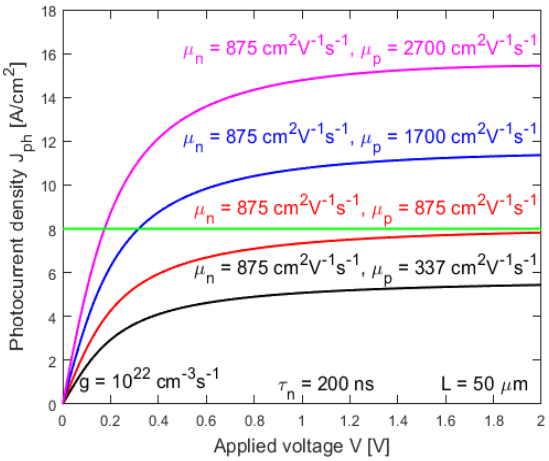


Figure 20: Photocurrent density $J_{ph}$ vs. applied voltage $V$ for $\mu_n > \mu_p$ (black curve), $\mu_n = \mu_p$ (red curve), and $\mu_n < \mu_p$ (blue and magenta curves) for *p*-type doping concentration of $10^{17} cm^{-3}$. The green line represents the maximum photocurrent density $J_{max} = qgL = 8\ Acm^{-2}$ for $\mu_n = \mu_p$.

By keeping in mind that effective lifetime of both type of carriers are same and that they differ only in their mobilities, the total current of doped device can be written as sum of majority and minority carrier concentrations, given as

$$J_{acc} = J_{acc,n} + J_{acc,p} = qgE\tau_{n,eff}(\mu_n + \mu_p) = qgE\mu_n\tau_{n,eff}\left(1 + \frac{\mu_p}{\mu_n}\right), \quad (35)$$

which is the same result as if the analytic result of $J_{acc,n}$ would be multiplied by $\left(1 + \frac{\mu_p}{\mu_n}\right)$. By dividing $J_{acc}$ given by Eq. (35) with $J_{max} = qgL$, the total $QE_{acc}$ can be expressed as [5]

$$QE_{acc} = \frac{E\tau_{n,eff}\mu_n}{L}\left(1 + \frac{\mu_p}{\mu_n}\right) = l_{dr,n}\left(1 + \frac{\mu_p}{\mu_n}\right) = \frac{\tau_{n,eff}}{\tau_{t,n}}\left(1 + \frac{\mu_p}{\mu_n}\right). \quad (36)$$

Similarly, multiplying $QE_{app}$ given by Eq. (26b), by Eq. (33a) yields the analytic result given below as

$$QE_{app} = \frac{1}{2}\left(1 + \frac{\mu_p}{\mu_n}\right) l_{dr,n}[1 - \alpha csch(\alpha\beta)sinh(\beta)]. \quad (37)$$

If *n*-type doping is the concern, then doped results for $J_{acc}$ and $J_{app}$ can be found by multiplying analytic results of $J_{acc}$ and $J_{app}$ respectively by $2G_{max,n}$ and $G_{max,n}$ given by Eq. (33b). In the low drift region, i.e., $l_{dr,n} \ll ½$, the respective $QE_{acc}$ and $QE_{app}$ for *p*-type doped devices are given as below

$$QE_{acc} \approx \left(1 + \frac{\mu_p}{\mu_n}\right) l_{dr,n} \left[1 - 2l_{di,n}\, tanh\left(\frac{1}{2l_{di,n}}\right)\right], \tag{38}$$

$$QE_{app} \approx \frac{1}{2}\left(1 + \frac{\mu_p}{\mu_n}\right) l_{dr,n} \left[1 - \frac{1}{l_{di,n}} csch\left(\frac{1}{l_{di,n}}\right)\right]. \tag{39}$$

Thus, by using the analytic results of $J_{acc}$ and $J_{app}$ it is possible to determine analytic solutions for doped curves, which closely follow simulated results. Figs. 21 plot the photocurrent density $J_{ph}$ vs. applied voltage *V* for *p*-type doping concentration of $10^{17}cm^{-3}$, to compare simulated and analytic results for different combinations of mobility parameters $(\mu_n, \mu_p)$. It can be noted that there is an excellent agreement between analytic and simulation results. It should be also pointed out that the different doping concentrations produce the different *J-V* characteristics. For instance, Figs. 22 plot the analytic photocurrent densities $J_{acc}$ and $J_{app}$, as well as three simulated photocurrent densities $J_{sim}$ under *n*-type doping concentrations $10^{15}cm^{-3}$, $10^{16}cm^{-3}$ and $10^{17}cm^{-3}$ for different combinations of mobility parameters $(\mu_n, \mu_p)$ and three cases: $\mu_n < \mu_p$, $\mu_n = \mu_p$ and $\mu_n > \mu_p$. However, obtained results still give a decent agreement between analytic and simulated results.

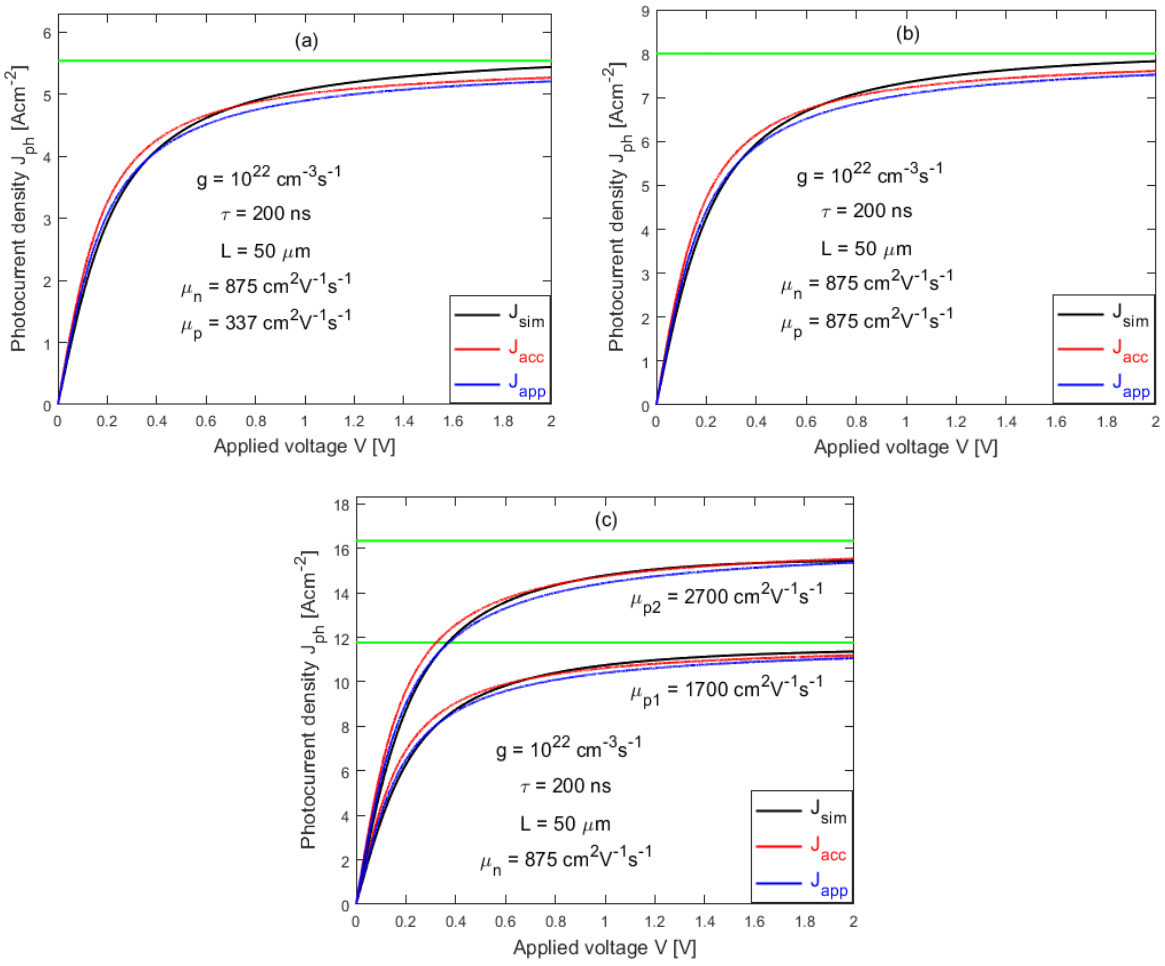


Figure 21: Photocurrent density $J_{acc}$ vs. applied voltage $V$ curves under $p$-type doping concentration of $10^{17}cm^{-3}$ for comparison of the simulated results $J_{sim}$ (black curves) and analytic results: $J_{acc}$ (red curves) and $J_{app}$ (blue curves), for different combinations of mobility parameters $(\mu_n, \mu_p)$: (a) $\mu_n > \mu_p$; (b) $\mu_n = \mu_p$; (c) and (d) $\mu_n < \mu_p$. The green lines represent the maximum photocurrent densities $J_{max} = qgL$ for different combinations of mobility parameters $(\mu_n, \mu_p)$.

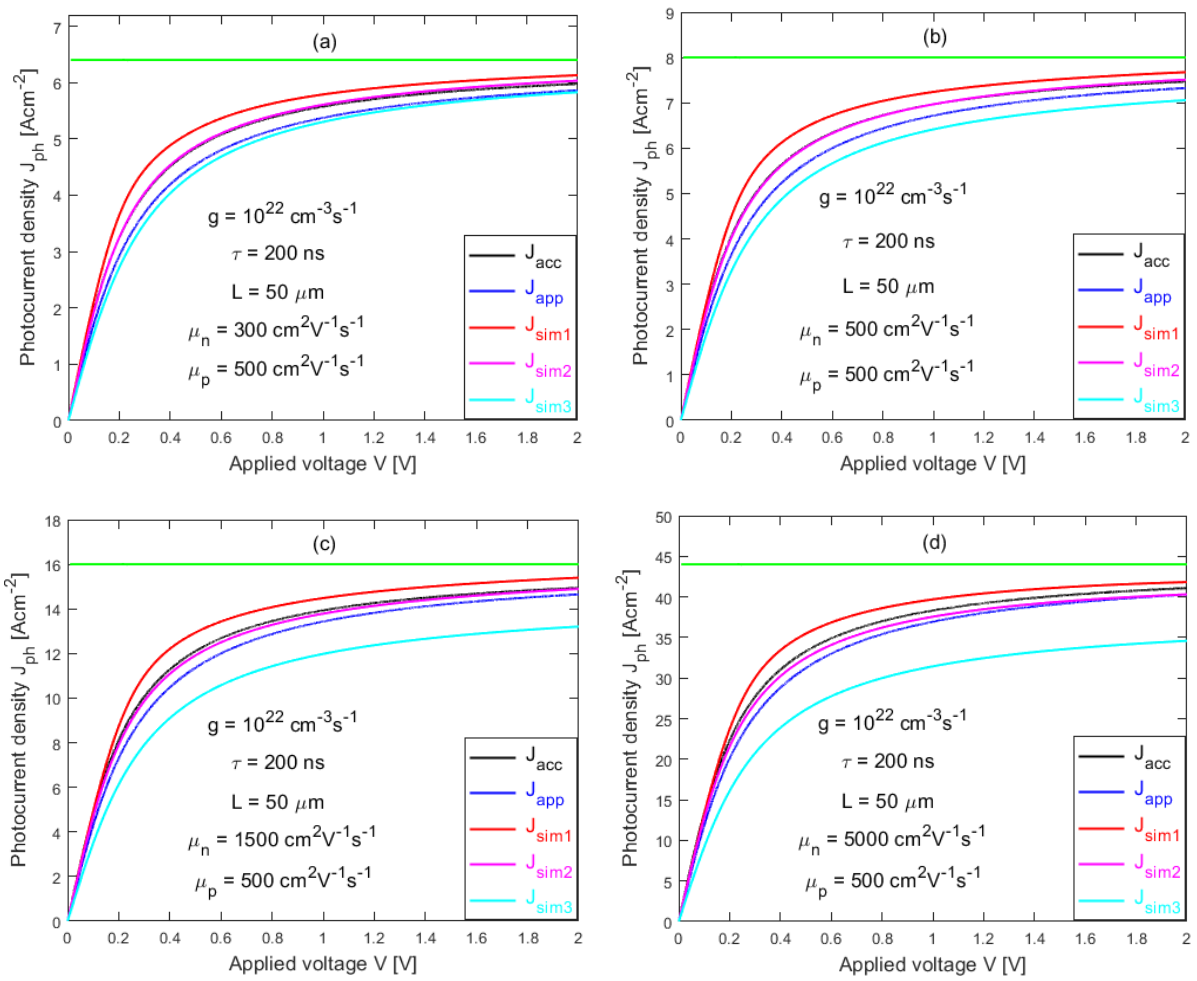


Figure 22: Analytic photocurrent densities $J_{acc}$ and $J_{app}$, and three simulated photocurrent densities $J_{sim}$ under *n*-type of doping for different levels of *n*-type doping concentrations $10^{15}cm^{-3}$ (red curves), $10^{16}cm^{-3}$ (magenta curves), and $10^{17}cm^{-3}$ (cyan curves) vs. applied voltage $V$: (a) $\mu_n < \mu_p$; (b) $\mu_n = \mu_p$; (c) and (d) $\mu_n > \mu_p$. The green lines represent the maximum photocurrent densities $J_{max} = qgL$ for different combinations of mobility parameters $(\mu_n, \mu_p)$.

# CHAPTER 7: CONCLUSIONS

## 7.1. Summary

This work reexamines the photoconductive gain theory of intrinsic (undoped) semiconductor devices, when primary photoconductivity is considered. Under numerous assumptions, the drift-diffusion equations for the photocurrent density and gain are solved analytically and two non-equivalent quantum efficiencies $QE_s$: accumulative quantum efficiency ($QE_{acc}$) vs. apparent quantum efficiency ($QE_{app}$) are obtained, as well as their approximations in the low-drift limit. The underlying physics of both $QE_s$ is discussed, and it was pointed out that these two non-equivalent $QE_s$, used in literature but not explicitly distinguished, should be equivalent if spatially dependent carrier lifetimes are used instead of constant carrier lifetimes. These results, while capable of recovering the drift-only results in the early literature, lead to the conclusion that the photoconductive gain or $QE$ is limited to unity for arbitrary strength of drift and diffusion. Furthermore, it is concluded that in general, the presence of diffusion tends to reduce the photocurrent. Additionally, it is found that in the absence of diffusion, the ratio of $QE_{acc}$ and $QE_{app}$ in the low drift limit is 2:1, but they approach the same unity limit under the strong drift. Moreover, it is shown that the commonly adopted definition of photoconductive gain, as the ratio of the lifetime $\tau_c$ to the transit time $\tau_t$, is only applicable in the low-drift limit, when diffusion is neglected.

By performing numerical simulations in Drift-Diffusion Lab it is concluded that the presence or absence of polarization term does not lead to the qualitative changes of the above findings. Furthermore, numerical simulations have revealed that in general $QE_{app} < QE_{acc} < QE_{sim}$. However, it is shown that in the low-drift limit $QE_{app} \rightarrow QE_{acc} \rightarrow QE_{sim}$ for large values of mobilities and lifetimes, which leads to fast saturation of photoconductive devices. On the other

hand, in high-drift limit $QE_{app} \rightarrow QE_{acc} \rightarrow QE_{sim} \rightarrow 1$. Thus, it is confirmed analytically and by simulations that the existing "recycling gain mechanism theory" cannot explain above unity photoconductive gains, at least not in the case of intrinsic photoconductive devices, when only the primary photocurrents considered.

Furthermore, it is examined to what degree the spatial nonuniformity of the photocurrent can vary with the material and device parameters. Under numerous assumptions typically used in literature, it is found that the total photocurrent in the photoconductive channel is spatially nonuniform, which is in stark contrast with results in literature where the photoconductive current is considered as uniform. However, it is pointed out that nonuniformity of the photocurrent is consequence of using constant carrier lifetimes instead of spatially dependent carrier lifetimes. Additionally, since most photoconductive devices have different mobility-lifetime products for electrons and holes, the new set of boundary conditions (BCs) is suggested for solving drift-diffusion equations, which can be solved only numerically when polarization term is included in analysis. It is further pointed out that within the framework of the primary conductivity, the carrier trapping does not lead to gain. In fact, assuming no loss, the carrier trapping effect only prolongs the carrier lifetime, just like in a high-quality indirect bandgap material, however, it does not result in a gain. By performing numerical simulations using Drift-Diffusion Lab, *n*-type and *p*-type doped photoconductors are examined. As one form of secondary photoconductivity, it is confirmed that the photoconductive gain can be above unity, but the gain is limited by the ratio of mobilities of majority and minority carriers, as earlier reported in the literature. Based on simulated results, analytic solutions for doped photoconductive devices are suggested.

This work should lay the ground for understanding the mechanisms of experimentally observed, above-unity photoconductivity gains. Moreover, these findings should offer new

insights into photoconductivity and semiconductor device physics and may potentially lead to novel applications.

## 7.2. Further work

Since an intrinsic photoconductor under the assumption of primary photoconductivity is not itself enough to produce photoconductive gain larger than unity, the natural question would be from where the gain larger than unity comes. There are various possible secondary photoconductive effects that can affect the $QE$ and even lead to gain, such as carrier injection from electrodes, caused either by thermal injection (i.e., SCLC) [1] or by light induced changes in the MS interface [57], carrier recycling or replenishing [1, 4, 15, 27, 47], and other mechanisms [43, 58]. In fact, doping in the photoconductive channel bears some similarity with the SCLC effect, except that the charges that induce the dark current are from the internal dopants for the former and injected from the electrode for the latter. In both cases, the presence of the pre-existing charges may alter the distributions of the photogenerated carriers, thus, the quantum yield. For instance, since the light induced change in the channel conductivity, more carriers could be injected into the semiconductor from the electrodes, enhancing the photocurrent. Therefore, the assumption that only the photogenerated carriers contribute to the photocurrent should be reexamined.

As pointed out in the introductory part, there were many attempts toward explanation of high photoconductive gain. However, all these explanations omit the effect of SCLC. Furthermore, if SCLC, as one form of secondary photoconductivity is not considered, it is likely not possible to properly explain experimentally obtained photoconductive gains significantly above unity, because high voltages will inevitably build up space-charge. Mott and Gurney [1] introduced the SCLC model to describe the conductivity of a trap-free insulating semiconductor with free carriers injected from the electrode. Over time this theory has been further developed and besides trap-free

devices, it also describes insulators and semiconductors with traps [2, 6-9, 16-18, 25, 30, 59-69]. Therefore, to find the upper limit of photoconductive gain it is necessary to use the concept of SCLC and carrier localization, as pointed out in numerous textbooks [1, 2, 6-8, 19, 30, 70] and papers [16-18, 25, 60, 68].

Hilsch and Pohl were the first that made a distinction between the primary and the secondary photocurrent [1, 2, 31, 47, 71]. They considered the primary photocurrent as the direct result of the absorption of energy, whereas the secondary photocurrent is considered as the result of the passage of the primary current. The reason for the appearance of the secondary photocurrent in some crystals is that the continuous passage of the primary current can break down the resistance of the crystal, thus, electrons can enter the crystal from the cathode and pass through it, as it is often the case with the semiconductor photoconductive devices. Besides the primary photocurrents, they found many photoconductive effects of comparatively mysterious origin which they attributed to the secondary photocurrents. Until recently, the secondary photocurrents were generally considered as an undesirable superposition on the primary photocurrents, and therefore, received a little recognition as being important in the understanding of the photoconductivity. Hilsch and Pohl further argued that as a straightforward electronic process and under conditions where electrons could enter the crystal from the cathode to replenish those leaving the crystal at the anode, one absorbed photon could produce more than one charge-carrying electron, and thus, $QE$ can be much larger than unity. This contradicts with the primary photoconductivity, where one absorbed photon could produce at most one electron-hole pair, which limits $QE$ to unity. However, over the many decades thereafter, more attention has been paid to the question of the nature of secondary photocurrents. It is found that the secondary photocurrents are more prominent at high applied electric fields. In addition, it is also found that

their behavior violates all the criteria previously set forth for the primary photocurrent. The main characteristics of the secondary photocurrents are: 1) a nonlinear variation of photocurrent with the light intensity; 2) a dependence of spectral response curve on voltage; and 3) a slow response in rise or decay of the photocurrent with the change in the illumination. Secondary photoconductivity involves replenishment of carriers from electrodes and the imposed condition for observing secondary photoconduction is at least one injecting Ohmic contact at the electrode. By using approach based on accumulated photocurrent $J_{acc}$, but without considering a diffusion effect, Hilsch, Pohl and Stockmann [31, 47, 71-73] experimentally measured and found analytic expression for $QE > 1$, based on the ratio of electronic (secondary) and ionic (primary) currents. Stockmann [74] confirmed these experimental observations for conventional semiconductor materials such as Ge and CdS. Thus, after reexamination of primary photoconductive gain theory for intrinsic devices with unity limit gain, the next step is exploring the secondary photoconductivity and SCLC in more detail to explain experimentally obtained photoconductive gains significantly larger than unity.

REFERENCES

[1] N. F. Mott and R. W. Gurney, “Electronic Processes in Ionic Crystals”, Oxford: Oxford University Press (1940).

[2] R. H. Bube, “Photoconductivity of Solids”, John Wiley & Sons, Inc. (1960).

[3] H. Beneking, “On the Response Behavior of Fast Photoconductive Optical Planar and Coaxial Semiconductor Detectors”, IEEE Transactions on Electron Devices, Volume: 29 Issue: 9, pp. 1431-1441, (1982). https://doi.org/10.1109/t-ed.1982.20893

[4] R. S. Quimby, “Photonics and Lasers-An Introduction”, John Wiley & Sons, Inc. (2006). http://doi.org/10.1002/0471791598

[5] Y. Dan, X. Zhao, K. Chen, and A. Mesli, ACS Photonics, “A Photoconductor Intrinsically Has No Gain”, Vol. 5, No. 10, pp. 4111–4116, (2018). https://doi.org/10.1021/acsphotonics.8b00805

[6] M. A. Lampert, “Current Injection in Solids”, Academic Press (1970).

[7] R. H. Bube, “Photoelectronic Properties of Semiconductors”, Cambridge University Press. (1992).

[8] K. C. Kao, “Dielectric Phenomena in Solids”, Elsevier, (2004).

[9] A. Ruzin, “Scaling effects in ohmic contacts on semiconductors”, Journal of Applied Physics 117, 164502, (2015). https://doi.org/10.1063/1.4918901

[10] J. G. Simmons, Elsevier, “Theory of metallic contacts on high resistivity solids (II) deep traps”, Journal of Physics and Chemistry of Solids, Volume 32, Issue 11, pp. 2581-2591, (1971). https://doi.org/10.1016/S0022-3697(71)80104-X

[11] B. Gudden, R. Pohl, “Das Quantenäquivalent bei der lichtelektrischen Leitung”, Springer Nature, Zeitschrift für Physik, 17, pp. 331-346, (1923). https://doi.org/10.1007/bf01328691

[12] B. Gudden, R. Pohl, “Zum Mechanismus des lichtelektrischen Primärstromes in Kristallen”, Springer Nature, Z. Physik 30, pp. 14-23, (1924). https://doi.org/10.1007/bf01331819

[13] B. Gudden, R. Pohl, “Zum Nachweis des selektiven Photoeffekts”, Z. Physik 34, pp. 245-248, Springer Nature, (1925). https://doi.org/10.1007/bf01328470

[14] K. Hecht,“Zum Mechanismus des lichtelektrischen Primärstromes in isolierenden Kristallen, Zeitschrift für Physik”, 77, pp. 235-245, Springer Nature, (1932). https://doi.org/10.1007/bf01338917

[15] A. Many, “High-field effects in photoconducting cadmium sulphide”, Elsevier, J. Phys. Chem. Solids Pergamon Press, Vol. 26, pp. 575-585, (1965). https://doi.org/10.1016/0022-3697(65)90133-2

[16] R. W. Smith, “Properties of Ohmic Contacts to Cadmium Sulfide Single Crystals”, Phys. Rev. 97, 1525, (1955). https://doi.org/10.1103/PhysRev.97.1525

[17] R. W. Smith, A. Rose, “Space-Charge-Limited Currents in Single Crystals of Cadmium Sulfide”, Phys. Rev. 97, 1531, (1955). https://doi.org/10.1103/PhysRev.97.1531

[18] A. Rose, “Space-Charge-Limited Currents in Solids“, Phys. Rev. 97, 1538, (1955). https://doi.org/10.1103/PhysRev.97.1538

[19] S. O. Kasap, “Photoconductivity and Photoconductive Materials-Fundamentals, Techniques and Applications”, Wiley, (2022). https://doi.org/10.1002/9781119579182

[20] W. Smith, “Effect of Light on Selenium During the Passage of An Electric Current”, Nature volume 7, 303, (1873). https://doi.org/10.1038/007303e0

[21] R. W. Smith, “Some Aspects of the Photoconductivity of Cadmium Sulfide”, RCA Rev. 12:350-361, (1951).

[22] C. Soci, A. Zhang, B. Xiang, S. A. Dayeh, D. P. R. Aplin, J. Park, X. Y. Bao, Y. H. Lo, and D. Wang, “ZnO Nanowire UV Photodetectors with High Internal Gain”, Nano Letters, Vol. 7, No. 4, pp. 1003-1009, (2007). https://doi.org/10.1021/nl070111x

[23] R. Dong, Y. Fang, J. Chae, J. Dai, Z. Xiao, Q. Dong, Y. Yuan, A. Centrone, X. Cheng Zeng, and J. Huang, “High-Gain and Low-Driving-Voltage Photodetectors Based on Organolead Triiodide Perovskites”, Adv. Mater. 27, pp. 1912-1918, (2015). https://doi.org/10.1002/adma.201405116

[24] Q. Guo, A. Pospischil, M. Bhuiyan, H. Jiang, H. Tian, D. Farmer, B. Deng, C. Li, S.-J. Han, H. Wang, Q. Xia, T.-P. Ma, T. Mueller, and F. Xia, “Black Phosphorus Mid-Infrared Photodetectors with High Gain”, Nano Lett., 16, pp. 4648-4655, (2016). https://doi.org/10.1021/acs.nanolett.6b01977

[25] A. Rose, “An outline of some photoconductive processes”, RCA Rev. 12:362-414, (1951).

[26] S. M. Sze and K. K. Ng, “Physics of Semiconductor Devices”, 3rd ed.; John Wiley & Sons, Inc. (2007). http://doi.org/10.1002/0470068329

[27] D. A. Neamen, “Semiconductor Physics and Devices: Basic Principles”, 4th ed.; McGraw-Hill (2012).

[28] M. Grundmann, “The Physics of Semiconductors-An Introduction Including Nanophysics and Applications”, 4th ed.; Springer, (2021). http://doi.org/10.1007/978-3-030-51569-0

[29] O. Lopez-Sanchez, D. Lembke, M. Kayci, A. Radenovic, and A. Kis, “Ultrasensitive photodetectors based on monolayer MoS2”, Nature Nanotechnology 8, pp. 497−501, (2013). https://doi.org/10.1038/nnano.2013.100

[30] A. Rose, “Concepts in Photoconductivity and Allied Problems”, Interscience Publishers, (1963).

[31] R. Hilsch, R. W. Pohl, and H. L. Jackson, “Photochemical processes. New investigations of photochemical processes in crystals and measurements by electrical means”, Transactions of the Faraday Society 34, pp. 883-888, (1938). https://pubs.rsc.org/en/content/articlepdf/1938/tf/tf9383400883

[32] C. H. Chu, M. H. Mao, C.W. Yang and H.H. Lin, “A New Analytic Formula for Minority Carrier Decay Length Extraction from Scanning Photocurrent Profiles in Ohmic-Contact Nanowire Devices”, Scientific Reports 9, Article number: 9426, (2019). https://doi.org/10.1038/s41598-019-46020-2

[33] N. Matsuo, H. Ohno, H. Hasegawa, “Mechanism of High Gain in GaAs Photoconductive Detectors under Low Excitation”, Japanese Journal of Applied Physics 23, pp. 299-301, (1984). https://doi.org/10.1143/jjap.23.L299

[34] G. J. Papaioannou, “A study of the gain and noise mechanisms in Gab planar photoconductive detectors”, Journal of Applied Physics 72, 5269, (1992). https://doi.org/10.1063/1.352010

[35] G. E. Zardas, C. J. Aidinis, E. A. Anagnostakis, and C. I. Symeonides, “On a Predictive Scheme of Slow Photoconductive Gain Evolution in Epitaxial Layer/Substrate Optoelectronic Nanodevices”, Open Journal of Microphysics, 1, pp. 32-34, (2011). http://doi.org/10.4236/ojm.2011.12006

[36] G. Konstantatos, M. Badioli, L. Gaudreau, J. Osmond, M. Bernechea, F. P. Garcia de Arquer, F. Gatti, and F. H. L. Koppens, “Hybrid graphene–quantum dot phototransistors with ultrahigh gain”, Nature Nanotechnology 7, pp. 363-368, (2012). http://doi.org/10.1038/nnano.2012.60

[37] T. Grünwald and M. Schreck, “Photoconductive gain in single crystal diamond detectors”, J. Appl. Phys. 129, 124502, (2021). http://doi.org/10.1063/5.0044649

[38] E. S. Rittner, R. G. Breekenridge, Ed., B. R. Russell, in Photoconductivity Conference. pp. 215-268, New York: Wiley (1956).

[39] R. S. Van Heyningen, Frederick C. Brown, “Transient Photoconductivity in Silver Chloride at Low Temperatures”, Phys. Rev. 111, Vol. 111, Iss. 2, pp. 462-470, (1958).

[40] D. Z.-Y. Ting, C. J. Hill, A. Soibel, S. A. Keo, J. M. Mumolo, J. Nguyen, and S. D. Gunapala, “A high-performance long wavelength superlattice complementary barrier infrared detector”, Appl. Phys. Lett. 95, 023508, (2009). https://doi.org/10.1063/1.3177333

[41] D. R. Rhiger and E. P. Smith, “Carrier Transport in the Valence Band of nBn III–V Superlattice Infrared Detectors”, U.S. Workshop on Physics and Chemistry of II-VI Materials 2018, June 2019, Volume 48, pages 6053–6062, (2019). https://doi.org/10.1007/s11664-019-07319-y

[42] G. Wang, C. Zhang, H. Sun, Z. Huang, and S. Zhong, “Understanding and design of efficient carrier-selective contacts for solar cells”, AIP Advances 11, 115026, (2021). https://doi.org/10.1063/5.0063915

[43] M. Karimi, X. Zeng, B. Witzigmann, L. Samuelson, M. T. Borgström, and H. Pettersson, “High Responsivity of InP/InAsP Nanowire Array Broadband Photodetectors Enhanced by Optical Gating”, Nano Lett. 19, pp. 8424-8430, (2019). https://doi.org/10.1021/acs.nanolett.9b02494

[44] B. Gudden, R. Pohl, “Über lichtelektrische Wirkung und Leitung in Kristallen”, Z. Physik 16, pp. 170-182, (1923). https://doi.org/10.1007/BF01327388

[45] W. Lehfeldt, “Zur Elektronenleitung in Silber-und Thalliumhalogenidkristallen”, Nachr. Ges. Wiss. Gottingen, 171, (1935).

[46] P. J. van Heerden, “Primary Photocurrent in Cadmium Sulfide”, Phys. Rev., Vol. 106, Iss. 3, pp. 468-473, (1957). https://doi.org/10.1103/PhysRev.106.468

[47] R. Hilsch, R. W. Pohl, “Eine quantitative Behandlung der stationären lichtelektrischen Primär- und Sekundärströme in Kristallen, erläutert am KH-KBr-Mischkristall als Halbleitermodell”, Zeitschrift für Physik, 108, pp. 55-84, Springer, (1938). https://doi.org/10.1007/bf01375000

[48] R. N. Hall, “Electron-Hole Recombination in Germanium”, Phys. Rev. 87, Vol. 87, Iss. 2, pp. 387, (1952). https://doi.org/10.1103/PhysRev.87.387

[49] W. Shockley, W. T. Read, Jr., “Statistics of the Recombinations of Holes and Electrons”, Phys. Rev. 87, Vol. 87, Iss. 5, pp. 835-842, (1952). https://doi.org/10.1103/PhysRev.87.835-843

[50] C. Sah, R N. Noyce, and W. Shockley, “Carrier Generation and Recombination in P-N Junctions and P-N Junction Characteristics”, Proceedings of the IRE, Vol. 45, Iss. 9, pp. 1228-1243, (1957). https://doi.org/10.1109/JRPROC.1957.278528

[51] J. E. Pedersen, V. G. Lyssenko, J. M. Hvam, P. Uhd Jepsen, S. R. Keiding, C. B. Sorensen, and P. E. Lindelof, “Ultrafast local field dynamics in photoconductive THz antennas”, Appl. Phys. Lett. 62, pp. 1265-1267, (1993). https://doi.org/10.1063/1.108702

[52] W. Shockley, H. J. Queisser, “Journal of Applied Physics, Detailed Balance Limit of Efficiency of p-n Junction Solar Cells”, Vol. 32, No. 3, pp. 510-519, (1961). https://doi.org/10.1063/1.1736034

[53] S. R. Mehrotra, A. Paul, G. Klimeck, and G. W. Budiman, “Drift-Diffusion Lab”, (2021). https://doi.org/10.21981/G0QV-VD57

[54] M. Hack and M. Shur, “Physics of amorphous silicon alloy p-i-n solar cells”, J. Appl. Phys. 58 (2), (1985). http://dx.doi.org/10.1063/1.336148

[55] F. Zhang, J. F. Castaneda, T. H. Gfroerer, D. Friedman, Y.-H. Zhang, M. W. Wanlass, and Y. Zhang, “An all-optical approach for comprehensive in-operando analysis of radiative and nonradiative recombination processes in GaAs double heterostructures”, Nature, Light: Science & Applications 11, Article Number: 137, (2022). https://doi.org/10.1038/s41377-022-00833-5

[56] J. He, K. Chen, C. Huang, X. Wang, Y. He, and Y. Dan, “Explicit Gain Equations for Single Crystalline Photoconductors”, ACS Nano, 14, pp. 3405-3413, (2020). https://doi.org/10.1021/acsnano.9b09406

[57] M. Hiramoto, T. Imahigashi, and M. Yokoyama, “Photocurrent multiplication in organic pigment films”, Appl. Phys. Lett. 64, pp. 187-189, (1994). https://doi.org/10.1063/1.111527

[58] R. L. Petritz, “Theory of Photoconductivity in Semiconductor Films”, Phys. Rev. 104, pp. 1508-1516, (1956). https://doi.org/10.1103/PhysRev.104.1508

[59] M. A. Lampert, “Simplified Theory of Space-Charge-Limited Currents in an Insulator with Traps”, Phys. Rev. (Series I), Vol. 103 iss. 6, (1956). https://doi.org/10.1103/PhysRev.103.1648

[60] A. Rose, M. A. Lampert, “Photoconductor Performance, Space-Charge Currents, and the Steady-State Fermi Level”, Phys. Rev, Vol. 113, Number 5, (1959). https://doi.org/10.1103/PhysRev.113.1227

[61] F. C. Chiu, H.W. Chou, J.Y Lee, “Electrical conduction mechanisms of metal/La2O3/Si structure”, Journal of Applied Physics, 97, 103503, (2005). https://doi.org/10.1063/1.1896435

[62] F. C. Chiu, “Electrical characterization and current transportation in metal/ Dy2O3/Si structure”, Journal of Applied Physics, 102, 044116, (2007). https://doi.org/10.1063/1.2767380

[63] F. C. Chiu, “A Review on Conduction Mechanisms in Dielectric Films”, Advances in Materials Science and Engineering, Volume 2014, Article ID 578168, (2014). http://doi.org/10.1155/2014/578168

[64] G. Gupta, S. Banerjee, S. Dutta, A. A. I. Aarnink, J. Schmitz, A. Y. Kovalgin, R. J. E. Hueting, “Charge carrier transport and electroluminescence in atomic layer deposited poly-GaN/c-Si heterojunction diodes”, Journal of Applied Physics, 124, 084503, (2018). https://doi.org/10.1063/1.5041089

[65] E. A. Duijnstee, J.M. Ball, V.M. Le Corre, L.J.A. Koster, H.J. Snaith, and J. Lim, “Toward Understanding Space-Charge Limited Current Measurements on Metal Halide Perovskites”, ACS Energy Lett., 5, pp. 376-384, (2020). https://doi.org/10.1021/acsenergylett.9b02720

[66] V. M. Le Corre, E. A. Duijnstee, O. El Tambouli, J. M. Ball, H. J. Snaith, J. Lim, and L. J.A. Koster, “Revealing Charge Carrier Mobility and Defect Densities in Metal Halide Perovskites via Space-Charge-Limited Current Measurements”, ACS Energy Lett., 6, pp. 1087-1094, (2021). https://doi.org/10.1021/acsenergylett.0c02599

[67] A. Rose, “Maximum Performance of Photoconductors”, Helv. Phys. Acta, Vol. 30, p. 242, (1957).

[68] M. A. Lampert, “The Role of Injecting Contacts in Photoconductors”, J. Phys. Chem. Solids, Vol. 22, pp. 189-197, Pergamon Press, (1961). https://doi.org/10.1016/0022-3697(61)90261-X

[69] K. Sivula, “Improving Charge Carrier Mobility Estimations When Using Space-Charge-Limited Current Measurements”, ACS Energy Lett., 7, pp. 2102-2104, (2022). https://doi.org/10.1021/acsenergylett.2c01154

[70] E. L. Dereniak, G. D. Boreman, “Infrared Detectors and Systems”, John Wiley & Sons, Inc. (1996).

[71] R. Hilsch, R.W. Pohl, “Zur quantitativen Behandlung der lichtelektrischen Primär-und Sekundärströme”, Springer Nature, Zeitschrift für Physik, 112, pp. 252-255, (1939). https://doi.org/10.1007/bf01340069

[72] R. W. Pohl, F. Stöckmann, “Die Rolle sekundärer Elektronen bei der lichtelektrischen Leitung”, Annalen der Physik, 6. Folge, Band 1, Heft 6, pp. 275-284, (1947). https://doi.org/10.1002/andp.19474360603

[73] F. Stöckmann, “Theorie der lichtelektrischen Leitung in Mischleitern”, Springer Nature, Zeitschrift für Physik, 128, pp. 185-211, (1950). https://doi.org/10.1007/bf01333069

[74] F. Stöckmann, “Lichtelektrische Sättigungsströme in Halbleitern”, Springer Nature, Zeitschrift für Physik, 138, pp. 404-410, (1954). https://doi.org/10.1007/bf01340686